

Utah State University

DigitalCommons@USU

All Graduate Theses and Dissertations

Graduate Studies

5-2014

Advancing Digital Soil Mapping and Assessment in Arid Landscapes

Colby W. Brungard
Utah State University

Follow this and additional works at: <https://digitalcommons.usu.edu/etd>



Part of the [Plant Sciences Commons](#)

Recommended Citation

Brungard, Colby W., "Advancing Digital Soil Mapping and Assessment in Arid Landscapes" (2014). *All Graduate Theses and Dissertations*. 3305.
<https://digitalcommons.usu.edu/etd/3305>

This Dissertation is brought to you for free and open access by the Graduate Studies at DigitalCommons@USU. It has been accepted for inclusion in All Graduate Theses and Dissertations by an authorized administrator of DigitalCommons@USU. For more information, please contact digitalcommons@usu.edu.



ADVANCING DIGITAL SOIL MAPPING AND ASSESSMENT IN ARID LANDSCAPES

by

Colby W. Brungard

A dissertation submitted in partial fulfillment
of the requirements for the degree

of

DOCTOR OF PHILOSOPHY

in

Soil Science

Approved:

Dr. Janis L. Boettinger
Major Professor

Dr. Astrid R. Jacobson
Committee Member

Dr. Lawrence E. Hipps
Committee Member

Dr. Thomas C. Edwards Jr.
Committee Member

Dr. Jürgen Symanzik
Committee Member

Dr. Mark R. McLellan
Vice President for Research and
Dean of the School of Graduate Studies

UTAH STATE UNIVERSITY
Logan, Utah

2014

ABSTRACT

Advancing Digital Soil Mapping and Assessment in Arid Landscapes

by

Colby W. Brungard, Doctor of Philosophy

Utah State University, 2014

Major Professor: Dr. Janis L. Boettinger
Department: Plants, Soils and Climate

There is a need to understand the spatial distribution of soil taxonomic classes, the spatial distribution of potential biological soil crust, and soil properties related to wind erosion to address land use and management decisions in arid and semi-arid areas of the western USA. Digital soil mapping (DSM) can provide this information.

Chapter 2 compared multiple DSM functions and environmental covariate sets at three geographically distinct semi-arid study areas to identify combinations that would best predict soil taxonomic classes. No single model or type of model was consistently the most accurate classifier for all three areas. The use of the “most important” variables consistently resulted in the highest model accuracies for all study areas. Overall classification accuracy was largely dependent upon the number of taxonomic classes and the distribution of pedons between taxonomic classes. Individual class accuracy was dependent upon the distribution of pedons in each class. Model accuracy could be increased by increasing the number of pedon observations or decreasing the number of taxonomic classes.

Potential biological soil crust level of development (LOD) classes were predicted over a large area surrounding Canyonlands National Park in Chapter 3. The moderate LOD class was

modeled with reasonable accuracy. The low and high LOD classes were modeled with poor accuracy. Prediction accuracy could likely be improved through the use of additional covariates. Spatial predictions of LOD classes may be useful for assessing the impact of past land uses on biological soil crusts.

Threshold friction velocity (TFV) was measured and then correlated with other, easier-to-measure soil properties in Chapter 4. Only soils with alluvial surficial rocks or weak physical crusts reached TFV in undisturbed conditions. All soil surfaces reached TFV after disturbance. Soils with weak physical crusts produced the most sediment. Future work on wind erosion in the eastern Great Basin should focus on non-crusted/weakly crusted soils and soils formed in alluvium overlying lacustrine materials. Soils with other crust types are likely not susceptible to wind erosion. Threshold friction velocity in undisturbed soils with weak physical crusts and undisturbed soils with surficial rocks was predicted using a combination of penetrometer, rock cover, and silt measurements.

(170 pages)

PUBLIC ABSTRACT

Advancing Digital Soil Mapping and Assessment in Arid Landscapes

Colby W. Brungard

Soil information is required for arid and semi-arid land management decisions such as permitting livestock grazing or planning vegetation restoration projects. However, traditional soil mapping methods may not provide adequate soil information, because the scale of mapping often requires dissimilar soils to be grouped together and there are no estimates of map uncertainty. Traditional methods are also often too costly or impractical to implement in large, remote, public arid and semi-arid rangelands. Digital soil mapping (DSM) may be able to overcome these limitations. Digital soil mapping is the creation of pixel-based soil maps using quantitative statistical models that relate easily measured biophysical environmental variables derived from geospatial data (e.g., slope and aspect from a digital elevation model) with more difficult to measure soil observations.

We investigated DSM for producing soil information useful for land management decisions. Specifically we: 1) compared multiple DSM methods for predicting soil taxonomic classes, 2) predicted the spatial distribution of potential biological soil crust classes, and 3) measured threshold friction velocity, a necessary input for wind erosion modeling.

Many existing soil use and management decisions are based on soil taxonomic classes; thus digital soil taxonomic class maps are useful for quantitative decision making. However, there are a large number of available DSM methods to produce such maps. Understanding which DSM method produces the most accurate soil taxonomic maps would contribute to robust management decisions. Comparison of DSM methods revealed that prediction accuracy

was more dependent upon the number of taxonomic classes and the number of observations of each taxonomic class, than the specific method chosen.

Biological soil crusts (BSC) are important organisms in arid lands, but are highly susceptible to surface disturbance. Maps of BSC potential (BSC in the absence of disturbance) would be useful for understanding the impact of different land uses on BSC distribution. Digital soil mapping can be used to make such maps. We produced maps of low, moderate, and high potential BSC level-of-development classes. Accuracy assessment revealed that only the moderate level-of-development class was reliable. The map of the moderate BSC level-of-development class is anticipated to be useful for assessing the impact of land use practices on BSC distribution.

Proposed pumping in western Utah could reduce groundwater, thus reducing vegetation cover and exposing more soil surface area to wind erosion. Evaluating the potential impacts of proposed pumping requires the use of wind erosion models. Such models require inputs of threshold friction velocity (TFV), which is the minimum turbulence required to initiate wind erosion. However, TFV is difficult to measure, and we sought to predict TFV from easier to measure soil surface properties. We found TFV to be dependent upon soil surface type. Only undisturbed soils with weak physical crusts and some undisturbed soils with surficial rock fragments reached TFV. All soil surfaces reached TFV when disturbed. On average, soils with weak physical crusts were more susceptible to wind erosion, but great variability between surface types was found. Threshold friction velocity in undisturbed soils with weak physical crusts and undisturbed soils with surficial rock fragments was predicted using a combination of penetrometer force, percent rock cover, and silt concentration.

DEDICATION

I dedicate this dissertation to my dear wife, Tanzi, my daughters Lilly and Rose, and my son Sam. They have supported me through many long nights and challenging days and have been a great blessing. I also dedicate this dissertation my parents and grandparents who placed such great emphasis on education and set an example of honesty, integrity, dedication, and hard work.

ACKNOWLEDGMENTS

The successful completion of this work has not been accomplished on my own. This research was supported in large part by the United States Department of the Interior- Bureau of Land Management (BLM) via Cooperative Ecosystem Study Unit (CESU) Agreement number L09AC15757 and the Utah Agricultural Experiment Station (UAES), Utah State University. I would like to thank Lisa Bryant and Jeremy Jarneke for helping to define project objectives and for providing knowledgeable guidance.

I would like to thank Jeremiah Armentrout, Brook Fannesbeck, and the Fort Bliss military base for providing the NM dataset used in Chapter 2. Brook Fannesbeck, Mike Leno, Zamir Libohova, Shawn Nield and Amanda Preddice collected the WY data used in Chapter 2. We would also like to thank Rob Gentilion for assisting with variable development in Chapter 2. I would like to thank Dan Pittenger, USGS, for operating the wind tunnel used in Chapter 4 and Xin Dai, USU Agricultural Experiment Station statistician, for help in calculating TFV uncertainty used in Chapter 4. Mention of any product by name does not constitute endorsement by the U.S. Geological Survey.

Julie Baker, Chad Clay, Kyle Hollingshead, Dan Horne, Jon Jones, Jerimiah Lamb, John Lawley, Ingrid Merrill, Leanna Reynolds-Hayes, and Angela Swainston provided invaluable assistance in collecting field data and performing laboratory analysis. My good friends Xystus Amakor, Jeremiah Armentrout, Suzann Kienast-Brown, Charles Delaney, Brook Fannesbeck, Davey Olsen, and Chod Stephens provided camaraderie and an intellectually stimulating atmosphere. I also acknowledge God-given help to perform beyond my own abilities.

I would like to thank Dr. Astrid Jacobsen for assistance with understanding and performing laboratory analysis, Dr. Tom Edwards for predictive modeling guidance, Dr. Larry

Hipps for patiently explaining fluid dynamics and threshold friction velocity equations, and Dr. Jürgen Symanzik for statistical visualization and data exploration help.

Most especially I would like to thank Dr. Janis Boettinger. Janis has been an exceptional major professor. She has mentored me, answered endless questions, given me the freedom to explore many ideas and topics, and provided a world-class education.

Colby W. Brungard

CONTENTS

| | Page |
|---|------|
| ABSTRACT..... | ii |
| PUBLIC ABSTRACT | iv |
| DEDICATION | vi |
| ACKNOWLEDGMENTS..... | vii |
| LIST OF TABLES..... | xii |
| LIST OF FIGURES..... | xiii |
| CHAPTER | |
| 1. INTRODUCTION..... | 1 |
| 2. MACHINE LEARNING FOR PREDICTING SOIL CLASSES IN THREE SEMI-ARID LANDSCAPES | 7 |
| Abstract | 7 |
| Introduction..... | 8 |
| Methods | 11 |
| Study Areas..... | 11 |
| Sampling | 12 |
| Additional variables..... | 16 |
| Variable selection | 18 |
| Modeling..... | 18 |
| Model validation and comparison..... | 20 |
| Results | 21 |
| Discussion | 21 |
| Model performance..... | 21 |
| Variable set comparison | 26 |
| Spatial predictions | 28 |
| Conclusions..... | 29 |
| References | 30 |
| 3. SPATIAL PREDICTIONS OF POTENTIAL BIOLOGICAL SOIL CRUST LEVEL OF DEVELOPMENT CLASSES AROUND CANYONLANDS NATIONAL PARK..... | 51 |
| Abstract | 51 |

| | |
|--|------------|
| Introduction..... | 52 |
| Methods | 54 |
| Study area..... | 54 |
| Biological soil crust observations | 56 |
| Environmental covariates..... | 57 |
| Model building and analysis | 58 |
| Results and discussion | 63 |
| Modeling..... | 63 |
| Spatial prediction..... | 65 |
| Variable importance | 67 |
| Conclusions..... | 68 |
| References | 68 |
| 4. THRESHOLD FRICTION VELOCITY OF LACUSTRINE AND ALLUVIAL SOILS BEFORE AND AFTER DISTURBANCE IN THE EASTERN GREAT BASIN, USA..... | 85 |
| Abstract | 85 |
| Introduction..... | 86 |
| Methods | 89 |
| Study area..... | 89 |
| Threshold friction velocity and mobilized sediment measurement..... | 89 |
| Soil surface properties..... | 93 |
| Soil surface classes | 95 |
| Statistical analysis..... | 96 |
| Results and discussion | 96 |
| Threshold friction velocity and sediment production | 96 |
| Predicting TFV from soil properties..... | 99 |
| Conclusions..... | 100 |
| References | 101 |
| 5. CONCLUSIONS..... | 116 |
| APPENDICES | 120 |
| Appendix A. Threshold friction velocity measurement error estimation | 120 |
| Rational for estimating TFV measurement uncertainty..... | 121 |
| TFV measurement uncertainty estimation methods | 121 |
| TFV measurement uncertainty | 122 |
| TFV measurement uncertainty conclusions..... | 124 |

References..... 124

Appendix B. Permission and release letters 146

CURRICULUM VITAE..... 149

LIST OF TABLES

| Table | Page |
|---|------|
| 2-1 Distribution of soil observations in each subgroup class for the three study areas..... | 37 |
| 2-2 Classification models used to predict soil subgroup classes in each study area by variable set..... | 38 |
| 2-3 "Most important" variables as selected by random forests for each study area..... | 39 |
| 3-1 The number of observations per combined LOD class in the training, testing and validation datasets | 73 |
| 3-2 Covariates, the source of the covariate, and the rational for inclusion | 74 |
| 3-3 Optimal model parameters for SGB and RF, and area under the receiver operator characteristic curve (AUC) for each LOD class | 75 |
| 3-4 Accuracy metrics for each model by LOD class..... | 76 |
| 4-1 Threshold friction velocity of undisturbed and disturbed soil surfaces | 106 |
| 4-2 Multiple linear regressions that best predict undisturbed TFV for soils with surficial rock fragments and weak physical crusts..... | 108 |

LIST OF FIGURES

Figure

| | |
|--|----|
| 2-1 Study area locations in western USA. | 40 |
| 2-2 Spatial distribution of pedon observation locations in the NM study area..... | 41 |
| 2-3 Spatial distribution of pedon observation locations in the UT study area | 42 |
| 2-4 Spatial distribution of pedon observation locations in the WY study area | 43 |
| 2-5 Kappa for the NM study area..... | 44 |
| 2-6 Kappa for the UT study area. | 45 |
| 2-7 Kappa for the WY study area. | 46 |
| 2-8 Variable importance | 47 |
| 2-9 Spatial predictions of subgroup classes for the NM study area using radial basis support vector machines..... | 48 |
| 2-10 Spatial predictions of subgroup classes for the UT study area made using a bagging classification tree | 49 |
| 2-11 Spatial predictions of subgroup classes for the WY study area made using random forests | 50 |
| 3-1 The project area location in southeastern Utah..... | 77 |
| 3-2 Biological soil crust LOD classes used by soil surveyors in Canyonlands National Park. | 78 |
| 3-3 Low LOD class predicted probability..... | 79 |
| 3-4 Moderate LOD class predicted probability | 80 |
| 3-5 High LOD class predicted probability..... | 81 |
| 3-6 Final LOD classification | 82 |
| 3-7 Final LOD classification confidence..... | 83 |
| 3-8 Covariate importance for each LOD class..... | 84 |

| | |
|---|-----|
| 4-1 Study area location in Snake Valley, Utah, adjacent to the Nevada border..... | 109 |
| 4-2 Portable wind tunnel used to measure TFV | 110 |
| 4-3 Threshold friction velocity measurement procedure..... | 111 |
| 4-4 Photos of representative sites from each soil surface type | 112 |
| 4-5 Dot-boxplots of threshold friction velocity and the amount of sediment produced by surface type for undisturbed and disturbed soil surfaces..... | 113 |
| 4-6 Plot of measured vs. predicted TFV for undisturbed soils with surficial rock fragments.... | 114 |
| 4-7 Plot of measured vs. predicted TFV for undisturbed soils with weak physical crusts..... | 115 |
| A-1 Measured wind speed profiles of the undisturbed soil surfaces at TFV for sampling sites 1-4 | 126 |
| A-2 Measured wind speed profiles of the undisturbed soil surfaces at TFV for sampling sites 5-8..... | 127 |
| A-3 Measured wind speed profiles of the undisturbed soil surfaces at TFV for sampling sites 9- 12 | 128 |
| A-4 Measured wind speed profiles of the undisturbed soil surfaces at TFV for sampling sites 13- 16 | 129 |
| A-5 Measured wind speed profiles of the undisturbed soil surfaces at TFV for sampling sites 17- 20 | 130 |
| A-6 Measured wind speed profiles of the undisturbed soil surfaces at TFV for sampling sites 21- 24 | 131 |
| A-7 Measured wind speed profiles of the undisturbed soil surfaces at TFV for sampling sites 25- 28 | 132 |
| A-8 Measured wind speed profiles of the undisturbed soil surfaces at TFV for sampling sites 29- 32 | 133 |
| A-9 The measured wind speed profile of the undisturbed soil surface at TFV for sampling site 33..... | 134 |

| | |
|--|-----|
| A-10 Measured wind speed profiles of the disturbed soil surfaces at TFV for sampling sites 1-4..... | 135 |
| A-11 Measured wind speed profiles of the disturbed soil surfaces at TFV for sampling sites 5-8..... | 136 |
| A-12 Measured wind speed profiles of the disturbed soil surfaces at TFV for sampling sites 9-12..... | 137 |
| A-13 Measured wind speed profiles of the disturbed soil surfaces at TFV for sampling sites 13-16 | 138 |
| A-14 Measured wind speed profiles of the disturbed soil surfaces at TFV for sampling sites 17-20 | 139 |
| A-15 Measured wind speed profiles of the disturbed soil surfaces at TFV for sampling sites 21-24 | 140 |
| A-16 Measured wind speed profiles of the disturbed soil surfaces at TFV for sampling sites 25-28 | 141 |
| A-17 Measured wind speed profiles of the disturbed soil surfaces at TFV for sampling sites 29-32 | 142 |
| A-18 The measured wind speed profile of the disturbed soil surface at TFV for sampling site 33..... | 143 |
| A-19 Sources of uncertainty in TFV measurement for undisturbed and disturbed soils..... | 144 |
| A-20 Percent decrease in TFV uncertainty with added simulated observations..... | 145 |

CHAPTER 1

INTRODUCTION

Soil information is critical to address social, economic and environmental issues because soils exert fundamental influences on ecosystem properties and processes (Baveye et al., 2011; Grunwald et al., 2011). In arid and semi-arid rangelands, soil information is required for land use and management decisions such as permitting livestock grazing or planning vegetation restoration projects. Traditionally, soil information is produced using manual air photo interpretation to identify areas of a landscape that share similar soil types. However, in arid and semi-arid rangelands traditional soil mapping methods may not provide the information necessary to assess land management decisions because the scale of mapping often requires dissimilar soils to be grouped together (Zhu et al., 2001). Additionally traditional soil mapping methods do not provide estimates of map uncertainty and are often too costly or impractical to implement in large, remote, public arid and semi-arid rangelands. Digital soil mapping (DSM) may be able to overcome these limitations.

Digital soil mapping is the creation of spatially explicit soil information with estimated error from quantitative relationships between easily measured environmental covariates and more difficult to measure soil observations (Lagacherie, 2008; McBratney et al., 2003; Omuto et al., 2013). Environmental covariates are spatially explicit biogeophysical properties derived from remote sensing (e.g., surface reflectance from Landsat ETM+ imagery), digital elevation models (e.g., slope and aspect), and other geospatial information (e.g., geology maps). Soil observations are soil measurements obtained by field sampling and/or laboratory analysis.

Digital soil mapping builds upon the fundamental soil state-factor equation:

$$s = f(cl, o, r, p, t) \quad (1-1)$$

which states that soil (s) is a function of climate (cl), organisms (o), relief (r), parent material (p) and time (t) (Jenny, 1941). Digital soil mapping adapts Equation 1-1 for quantitative spatial prediction to:

$$s_a|s_c = f(s, c, o, r, p, a, n) + \varepsilon \quad (1-2)$$

where $s_a|s_c$ are soil attributes (s_a , e.g. percent clay) or classes (s_c , e.g. soil depth classes), f is an empirical function, (s, c, o, r, p, a, n) are soil forming factors (soil (s), climate (cl), organisms (o), relief (r), parent material (p), age (a) and spatial location (n)) represented by environmental covariates, and ε is estimated error (McBratney et al., 2003). Soil is included on the right hand side of the equation as existing soil information (i.e., soil maps) can be used to predict other soil classes or properties (McBratney et al., 2003).

The objectives of this dissertation were to investigate the application of DSM techniques to produce spatially explicit soil information in arid and semi-arid rangelands in the western United States, with a particular focus on semi-arid rangelands in Utah. Digital soil mapping was used to predict soil taxonomic classes in three distinct semi-arid landscapes in the western USA (Chapter 2). Based on earlier work predicting the level of development of biological soil crusts in Canyonlands National Park (Brungard and Boettinger, 2012), DSM was applied to predict the spatial distribution of potential biological soil crust in an area surrounding the park (Chapter 3). The measurement and prediction of threshold friction velocity, a necessary input for spatially explicit wind erosion modeling (Okin and Gillette, 2004), was also investigated (Chapter 4).

Chapter 2 compares multiple DSM functions (f , Equation 1-2) and environmental covariate sets representative of s, c, o, r, p, a, n factors (Equation 1-2) for predicting soil taxonomic class distribution at three geographically distinct semi-arid study areas in the western USA (southern New Mexico, southwestern Utah, and northeastern Wyoming). Key components of DSM are the function and environmental covariates used to predict soil classes. Many different

environmental covariates and functions are available (McBratney et al., 2003), but there is a lack of information as to which sets of covariates and functions may be optimal in specific landscapes. Thus, the objectives of Chapter 2 were to compare multiple functions and environmental covariate sets to identify combinations that would best predict soil taxonomic classes in semi-arid rangelands.

Chapter 3 investigates the application of DSM to predicting potential biological soil crust (BSC) level of development classes. Biological soil crusts are communities of cyanobacteria, microfungi, lichens, and mosses that form at the soil surface (Belnap et al., 2001). In arid and semi-arid areas they stabilize soil, reduce wind and water erosion, and are important sources of soil N and organic C (Belnap, 2002; Belnap and Gillette, 1998; Bowker and Belnap, 2008). Because BSCs occur at the soil surface, BSCs are susceptible to surface disturbance (Belnap and Eldridge, 2003; Belnap et al., 2001; Kuske et al., 2012). As soil surface disturbance is often a direct result of land use practices and because recovery of BSCs from surface disturbance can be a lengthy process (Belnap, 1993), it would be useful to understand how past disturbance has affected BSC distribution. Such understanding requires knowledge of actual (existing) and potential BSC distribution. Actual BSC can be observed by field sampling. Potential BSC (BSC in the absence of major soil surface disturbance) must either be observed before soil surface disturbance occurs or inferred from an undisturbed area. Lack of pre-disturbance BSC observation on the Colorado Plateau in eastern Utah requires potential BSC be inferred from undisturbed areas. Canyonlands National Park has been protected from livestock grazing and mineral exploration for about 50 years (1964 - 2014), making it one of the best available areas on the Colorado Plateau to assess potential BSC development in the absence of major soil surface disturbance. Biological soil crust observations from Canyonlands National Park and environmental covariates representative of the factors controlling BSC distribution were

combined to predict potential BSC distribution over approximately 8300 km² surrounding Canyonlands National Park.

In contrast to Chapters 2 and 3, Chapter 4 investigates the measurement of threshold friction velocity (the minimum turbulence required for wind erosion to occur) and soil attributes (S_a , Equation 1-2) related to threshold friction velocity, as a first step towards spatially explicit wind erosion modeling. Wind erosion is a natural phenomenon in drylands worldwide. Anthropogenic surface disturbance and groundwater withdrawal can exacerbate wind erosion (Gill, 1996). Proposed groundwater pumping in the eastern Great Basin (Southern Nevada Water Authority Water Resource Plan 2009, http://www.snwa.com/assets/pdf/wr_plan.pdf) could influence soil wind erosion. To understand the spatial variability of soil wind erosion and to assess both, the impacts of anthropogenic soil surface disturbance, and the potential influences of ground water withdrawal on wind erosion in the eastern Great Basin, a spatially explicit wind erosion model could be used (Okin, 2008; Okin and Gillette, 2004). This model requires spatially explicit inputs of threshold friction velocity (TFV). Spatially explicit estimates of TFV could likely be produced using a DSM approach. Digital soil mapping of TFV requires multiple measurements of TFV, especially for large and heterogeneous areas, but TFV is time consuming and difficult to accurately measure. A method to estimate TFV from alternate measurements would be useful. Thus the objectives of Chapter 4 were to measure TFV in eastern Great Basin soils and to develop relationships between TFV and other easy-to-measure soil surface properties as a first step towards modeling wind erosion in the eastern Great Basin.

References

Baveye, P.C., Rangel, D., Jacobson, A.R., Laba, M., Darnault, C., Otten, W., Radulovich, R., Camargo, F.A.O., 2011. From dust bowl to dust bowl: soils are still very much a frontier of science. *Soil Sci. Soc. Am. J.* 75, 2037. doi:10.2136/sssaj2011.0145

- Belnap, J., 1993. Recovery rates of cryptobiotic crusts: inoculant use and assessment methods. *Gt. Basin Nat.* 53, 89–95.
- Belnap, J., 2002. Nitrogen fixation in biological soil crusts from southeast Utah, USA. *Biol. Fertil. Soils* 35, 128–135. doi:10.1007/s00374-002-0452-x
- Belnap, J., Eldridge, D., 2003. Disturbance and recovery of biological soil crusts, in: Belnap, J., Lange, O.L. (Eds.), *Biological Soil Crusts: Structure, Function, and Management*. Springer, Berlin, pp. 363–383.
- Belnap, J., Gillette, D.A., 1998. Vulnerability of desert biological soil crusts to wind erosion: the influences of crust development, soil texture, and disturbance. *J. Arid Environ.* 39, 133–142. doi:10.1006/jare.1998.0388
- Belnap, J., Kaltenecker, J.H., Rosentreter, R., Williams, J., Leonard, S., Eldridge, D., 2001. *Biological soil crusts: ecology and management*, Technical Reference No. 1730-2. U.S. Department of the Interior, Bureau of Land Management, U.S. Geological Survey, Forest and Rangeland Ecosystem Science Center, Denver.
- Bowker, M.A., Belnap, J., 2008. A simple classification of soil types as habitats of biological soil crusts on the Colorado Plateau, USA. *J. Veg. Sci.* 19, 831–840. doi:10.3170/2008-8-18454
- Brungard, C.B., Boettinger, J.L., 2012. Spatial prediction of biological soil crust classes; value added DSM from soil survey, in: Minasny, B., Malone, B.P., McBratney, A. (Eds.), *Digital Soil Assessments and Beyond: Proceedings of the 5th Global Workshop on Digital Soil Mapping*. CRC Press, Sydney, pp. 57–60.
- Gill, T.E., 1996. Eolian sediments generated by anthropogenic disturbance of playas: human impacts on the geomorphic system and geomorphic impacts on the human system. *Geomorphology, Response of Aeolian Processes to Global Change* 17, 207–228. doi:10.1016/0169-555X(95)00104-D
- Grunwald, S., Thompson, J.A., Boettinger, J.L., 2011. Digital soil mapping and modeling at continental scales: finding solutions for global issues. *Soil Sci. Soc. Am. J.* 75, 1201. doi:10.2136/sssaj2011.0025
- Jenny, H., 1941. *Factors of soil formation: a system of quantitative pedology*. McGraw-Hill, New York.
- Kuske, C.R., Yeager, C.M., Johnson, S., Ticknor, L.O., Belnap, J., 2012. Response and resilience of soil biocrust bacterial communities to chronic physical disturbance in arid shrublands. *ISME J.* 6, 886–897. doi:10.1038/ismej.2011.153
- Lagacherie, P., 2008. Digital soil mapping: a state of the art, in: Hartemink, A.E., McBratney, A.B., Mendonça-Santos, M.D. L. (Eds.), *Digital Soil Mapping with Limited Data*. Springer, Netherlands, pp. 3–14.
- McBratney, A.B., Mendonça Santos, M.D.L., Minasny, B., 2003. On digital soil mapping. *Geoderma* 117, 3–52. doi:10.1016/S0016-7061(03)00223-4

- Okin, G.S., 2008. A new model of wind erosion in the presence of vegetation. *J. Geophys. Res. Earth Surf.* 113, F02S10. doi:10.1029/2007JF000758
- Okin, G.S., Gillette, D.A., 2004. Modelling wind erosion and dust emission on vegetated surfaces, in: Kelly, R.E.J., Drake, N.A., Barr, S.L. (Eds.), *Spatial Modelling of the Terrestrial Environment*. John Wiley & Sons, Chichester. pp. 137–156.
- Omuto, C.T., Nachtergaele, F., Rojas, R.V., 2013. State of the art report on global and regional soil information: where are we? Where to go? Global Soil Partnership Tech. Report. United Nations (UN) Food and Agriculture Organization (FAO), Rome Italy. <http://www.fao.org/docrep/017/i3161e/i3161e.pdf> (last accessed: 7/7/2014).
- Zhu, A.X., Hudson, B., Burt, J., Lubich, K., Simonson, D., 2001. Soil mapping using GIS, expert knowledge, and fuzzy logic. *Soil Sci. Soc. Am. J.* 65, 1463. doi:10.2136/sssaj2001.6551463x

CHAPTER 2

MACHINE LEARNING FOR PREDICTING SOIL CLASSES IN THREE SEMI-ARID LANDSCAPES¹**Abstract**

Mapping the spatial distribution of soil taxonomic classes is important for informing soil use and management decisions. Digital soil mapping (DSM) can quantitatively predict the spatial distribution of soil taxonomic classes. Key components of DSM are the method and the set of variables, or environmental covariates, used to predict soil classes. Machine learning is a general term for a broad set of statistical models and algorithms. Many different machine learning models have been applied in the literature and there are different approaches for selecting variables for DSM. However, there is little guidance as to which, if any, machine learning model and variable set might be optimal for predicting soil classes across different landscapes.

Our objective was to compare multiple machine learning methods and variable sets for predicting soil taxonomic classes at three geographically distinct areas in the semi-arid western United States of America (southern New Mexico, southwestern Utah, and northeastern Wyoming). All three areas were the focus of digital soil mapping studies. Sampling sites at each study area were selected using conditioned Latin hypercube sampling (cLHS). Tested models included clustering algorithms, linear models, neural networks, tree based methods and support vector machine classifiers. Tested predictive variables were derived from digital elevation models and Landsat imagery, and were divided into three different sets: 1) variables selected *a priori* by soil scientists familiar with each area for input into cLHS, 2) the variables in set 1 plus

¹ Co-authored by Colby W. Brungard and Janis L. Boettinger. Utah State University 4820 Old Main Hill, Logan, UT, 8432-4820. Michael C. Duniway. U.S. Geological Survey, Southwest Biological Science Center, 2290 SW Resource Blvd, Moab, UT 84532. Skye A. Wills. National Soil Survey Center, Natural Resources Conservation Service – United States Department of Agriculture. 100 Centennial Mall North, Lincoln, NE 68508. Thomas C. Edwards, Jr. U.S. Geological Survey, Utah Cooperative Fish and Wildlife Research Unit and Department of Wildland Resources, Utah State University, Logan, UT 84322.

113 additional variables, and 3) variables selected by the classification method random forests as the “most important”.

We were unable to identify a single model or type of model which was consistently the most accurate classifier for all three areas. However, random forests and bagged classification trees were among the three most accurate models for two of the three study areas. The use of the “most important” variables (variable set 3) consistently resulted in the highest model accuracies for all study areas. Overall classification accuracy in each area was largely dependent upon the number of soil taxonomic classes and the frequency distribution of pedon observations between taxonomic classes. Individual subgroup class accuracy was dependent upon the frequency distribution of soil pedon observations in each taxonomic class.

Results suggest that several machine learning models are applicable for DSM, and that the model that returns the highest classification accuracy be used for subsequent spatial prediction. Results also indicate that variables selected by soil scientists as cLHS input variables may not be optimal for modeling soil classes and that some form of statistical variable selection should be applied. The number of soil classes is related to the inherent variability of a given area. The imbalance of soil pedon observations between classes is likely related to cLHS. Imbalanced frequency distributions of soil pedon observations between classes must be addressed to improve model accuracy. Solutions include increasing the number of soil pedon observations in classes with few observations or decreasing the number of classes.

1. Introduction

Maps that predict the spatial distribution of soil taxonomic classes are of interest in many countries because they inform soil use and management decisions. Digital soil mapping (DSM) of soil taxonomic classes has many advantages over conventional soil mapping approaches as it is better able to capture observed spatial variability and can reduce the need to

aggregate soil types based on a set mapping scale (Zhu et al., 2001). A key component of any DSM activity is the method used to define the relationship between soil observations and environmental variables. Many such methods have been investigated including expert systems (Smith et al., 2012, Van Zijl et al., 2012, Zhu et al., 2001), unsupervised classification (Boruvka et al., 2008; Triantifilis et al., 2012) and machine learning (Behrens and Scholten, 2006; Bui and Moran, 2003; Kim et al., 2012; Stum et al., 2010).

Machine learning is a general term for a broad set of models and algorithms used to discover patterns in data and to make predictions (Witten et al., 2011). Although machine learning is most often applied to large databases, it is an attractive tool for learning about and making spatial predictions of soil classes because knowledge about relationships between soil classes and environmental variables is often poorly understood (Grunwald, 2006). Machine learning techniques have been used to model soil depth classes (Boer et al., 1996), biological soil crust classes (Brungard and Boettinger, 2012), soil drainage classes (Campling et al., 2002; Liu et al., 2008) and the presence/absence of diagnostic soil horizons (Jafari et al., 2012).

Two general approaches have been applied to predicting soil taxonomic classes using machine learning. The first approach attempts to find and extract soil class-landscape relationships from existing digitized soil polygon maps when the exact locations (GPS coordinates) of soil pedon observations are unknown (Behrens et al., 2005; Grinand et al., 2008; Subburayalu and Slater, 2013). The second approach attempts to construct soil class-landscape relationships from soil pedon observations made by field sampling at known locations (Hengl et al., 2007; Kim et al., 2012; Stum et al., 2010). The choice of approach largely depends on the availability of soil pedon observations with known locations.

There are a large number of available machine learning techniques (Kuhn and Johnson, 2013), but there is a lack of information as to which machine learning technique may be optimal

in specific landscapes. Of the available peer-reviewed literature that used soil pedon observations to construct soil class-landscape relationships (Barthold et al., 2013; Jafari et al., 2012; Kempen et al., 2012) few compared more than two machine learning models and none compared multiple machine learning models at more than one study area. The objective of this study was thus to compare multiple machine learning techniques for predicting subgroup classes in Soil Taxonomy (Soil Survey Staff, 1999) using soil pedon observations at three geographically distinct areas in the western United States of America (southern New Mexico, southwestern Utah, and northeastern Wyoming; Fig. 2-1). Each area was the focus of a digital soil mapping study and represents a broad range of semi-arid landscapes that have different soil-landscape relationships. Machine learning techniques were selected to represent several classes of machine learning methods, including discriminant analysis, classification trees, multinomial logistic regression, neural networks, and clustering methods.

Recognizing that model performance depends on the variables used to represent soil-landscape relationships, we also tested the influence of three groups of variables: 1) variables selected *a priori* by soil scientists familiar with each area (expert knowledge; Zhu et al., 2001), 2) the variables in set 1 plus 113 additional variables derived from digital elevation models and Landsat imagery at several resolutions that represented a large suite of potentially useful variables, and 3) a subset of variables identified as “most important” by the classification method random forests from sets 1 and 2.

Formally, we had two objectives: 1) test multiple machine learning methods to identify accurate classifiers; 2) compare multiple variable sets to identify those which resulted in the most accurate classification.

2. Methods

2.1. Study Areas

2.1.1 New Mexico (NM)

The New Mexico (NM) study area is located on Otero Mesa in the northern reaches of the Chihuahuan Desert, approximately 130 km northeast of El Paso, TX, USA. Centered at 105.6° W longitude, 32.5° N latitude (Fig. 2-1) the area is approximately 190 km². The underlying geology is primarily limestone and sandstone (Green and Jones, 1997). Soil parent material is primarily calcareous alluvium but also includes eolian sands and residuum. Vegetation is a mix of shrublands (primarily creosote bush [*Larrea tridentata*] and tar bush [*Florenxia cernua*]) and grasslands (primarily black grama [*Boutalua eriopoda*] and tobosa [*Pleuraphis mutica Buckley*]). Elevation ranges from 1430 to 1915 m. The soil moisture regime is aridic bordering on ustic. Mean annual precipitation is 354 mm, the majority of the precipitation arrives between June and December, and mean annual temperature is approximately 15 °C (PRISM Climate Group, Oregon State University, <http://prism.oregonstate.edu/>, accessed 4 March 2014).

2.1.2 Utah (UT)

The Utah (UT) study area is located in the eastern Great Basin physiographic province, approximately 14 km southwest of Milford, UT, USA. Centered at 113° W longitude and 38° N latitude the area is approximately 300 km² of mountainous terrain and associated alluvial fans formed from a complex mix of limestone, dolomite, quartzite, basalt, quartz monzonite, quartz latite, shale, sandstone, andesite, rhyolite, granite, and ash flows (Best et al., 1989). Elevation ranges from 1540 to 2100 m. Vegetation consists of shrubs (primarily Wyoming big sagebrush [*Artemisia tridentata*] and black sagebrush [*Artemisia nova*]) and bunch grasses (Indian ricegrass [*Achnatherum hymenoides*]) at lower elevations, while trees (primarily Utah Juniper [*Juniperus osteosperma*] and Singleleaf Pinyon [*Pinus monophylla*]) dominate higher elevations. The soil

moisture regime is aridic bordering on xeric in lower elevations and xeric in higher elevations. Mean annual temperature and precipitation for the nearest weather station (Milford, UT) is 11°C and 200 mm, respectively, the majority of the precipitation arrives in April and October (Western Regional Climate Center, 2013).

2.1.3 Wyoming (WY)

The Wyoming (WY) study area is located in the Powder River Basin of Wyoming, USA, part of the Northern Rolling High Plains (United States Department of Agriculture, 2006), approximately 43 km southwest from Gillette, WY. Centered at approximately 106° W longitude and 44° N latitude the area is approximately 296 km². Geology in the area consists of variegated mudstone, sandstone, conglomerate, limestone, shale and coal (Cole and Boettinger, 2006; Green and Drouillard, 1994). Topography is a mix of bedrock-controlled, low rolling hills and badlands (locally known as the “Powder River Breaks”) a system of steep, bedrock-controlled hills and gullies (gullies commonly > 6 m deep) with extremely high rates of erosion and low vegetation cover (Cole, 2004). Vegetation is characterized by a mixture of mid-stature cool season grasslands (bluebunch wheatgrass [*Pseudoroegneria spicata*] and needle-and-thread [*Hesperostipa comata*]) and sagebrush shrublands (Wyoming big sagebrush [*Artemisia tridentata*]) (United States Department of Agriculture, 2006). Elevation ranges from 1220 and 1600 m. The soil moisture regime is aridic bordering on ustic. Mean annual temperature and precipitation is 8°C and 310 mm, respectively, with the majority of the precipitation falling between April and October (Western Regional Climate Center, 2013).

2.2 Sampling

Sampling locations for each study area were selected using conditioned Latin hypercube sampling (cLHS) (Minasny and McBratney, 2006). Variables used for input into cLHS were chosen

by soil scientists familiar with each study area and assumed to best represent soil-landscape relationships and anticipated soil forming processes in each area (variable set 1). The soil scientists who selected cLHS input variables for the NM study area had worked inside the study area and in similar landscapes for approximately ten years. The soil scientist who selected cLHS input variables for the UT study area had visited the area, performed three months of field sampling in a nearby area, and conducted a literature review to identify important variables in similar landscapes. The soil scientists who selected cLHS input variables for the WY area were Natural Resource Conservation Service (NRCS) soil scientists who were conducting traditional soil surveys in similar landscapes around the study area.

In each area, soils were manually excavated to a depth of at least 100 cm, or root limiting layer if shallower, and were sampled and described according to Schoeneberger et al. (2003). Soil Taxonomy (Soil Survey Staff, 1999) defines the following hierarchical levels of classification: order, suborder, great group, subgroup, and family. We chose to model at the subgroup class as this level of classification existed for the soils described in each study area. Rock outcrop and Badland were also included at the subgroup level. For each area, subgroup classes with only 1 observation were grouped with the most similar subgroup class.

2.2.1 New Mexico cLHS

Variables used for cLHS were derived from an October 2006 Landsat 5 TM image and a 5-m Lidar digital elevation model (DEM). Imagery variables from Landsat were band 5 (short wave infrared) plus band 2 (green), band 5 minus band 2, and a normalized band 5/2 ratio ($[(\text{Band 5} - \text{Band 2}) / (\text{Band 5} + \text{Band 2})]$). Terrain attributes were aspect in degrees, elevation, slope, and a multipath wetness index (Shi, 2013) calculated at four slope resolutions (5, 10, 25, 35 m) from the DEM. A categorical terrain classification was also used. Imagery variables were chosen for use in cLHS because they had been shown to correlate with soil surface properties. Slope and

the multipath wetness index, were chosen to represent potential soil moisture distribution. Aspect and elevation were chosen to represent microclimate and potential soil moisture (higher elevation, north-facing areas often have more potential soil moisture than lower elevation, south-facing areas). The terrain classification consisted of seven classes related to elevation and slope.

Initially 200 potential sampling sites were identified, but because of logistical constraints it was impossible to visit all 200 sites. To select a smaller set of representative sampling locations cLHS was used to produce a hierarchical nested set of 175, 150, 125 and 100 potential sampling sites from the original 200 sites. All sites in the 100 subset were visited, plus an additional three sites. In total 103 soil sampling locations were observed (Fig. 2-2). Each soil observation was classified to family level in Soil Taxonomy. Ten subgroup classes were extracted from family names (Table 2-1).

2.2.2 Utah cLHS

Variables used for cLHS were derived from an atmospherically corrected (Chavez, 1996) July 31st 2000 Landsat 7 ETM+ image and a 10-m hydrologically correct DEM. A soil adjusted vegetation index (SAVI) was derived from the imagery using an L value of 0.5 (Heute, 1988). Terrain attributes were slope, inverse wetness index (Tarboton, 2013) and transformed aspect (a measure of northness vs. southness). Land cover and geologic type were also used. Land cover type was obtained from the Southwest Regional Gap Analysis Program (Lowry et al., 2007). Geology was obtained from a United States Geological Survey 1:50,000 geology map (Best et al., 1989). Land cover and SAVI were chosen because it was anticipated that vegetation type and density was correlated with soil properties such as soil depth. Geologic type was chosen because the highly complex geology in this area was anticipated to exert a strong control

on potential pedogenesis. Terrain variables were chosen to represent microclimate, because microclimate heavily influences soil moisture, which in turn influences pedogenesis.

Three hundred locations were visited. Soils were excavated, described, and classified to family level. Subgroup classes were extracted from family names. Three soil observations were excluded from modeling as they were located in highly disturbed areas. This resulted in 297 soil observations in 15 subgroup classes (Fig. 2-3, Table 2-1).

2.2.3 Wyoming cLHS

Variables used for cLHS were derived from a Landsat 5 TM image and a 2-m Lidar DEM. Imagery variables were Normalized Difference Vegetation Index (NDVI) and band ratios 5/2 and 5/7. Terrain derivatives were topographic wetness index, topographic position index, stream power index (Wilson and Gallant, 2000) and distance to the nearest road. All variables for cLHS, except distance to the nearest road, were selected using the Optimum Index Factor (OIF). OIF identifies the combination of input variables that maximize variability, with the lowest correlation among variables (Kienast-Brown and Boettinger, 2010). Distance to the nearest road was included for a vegetation sampling project not directly related to soil mapping.

Similar to the NM study area, cLHS was used to select hierarchical nested sets of 150, 100, and 50 potential sampling sites from 200 original sampling sites. Fifty-seven soil pedon observations were made: the set of 50 nested cLHS samples plus an additional seven pedon observations (Fig. 2-4). Each soil was excavated, described, and assigned to a soil series. Subgroup classes were extracted from each series using official soil series descriptions (<https://soilseries.sc.egov.usda.gov/osdname.asp>). This resulted in 5 subgroup classes (Table 2-1).

2.3 Additional variables

Additional terrain variables were created from a 5-m Lidar derived DEM for the NM study area, a 5-m auto-correlated DEM (Utah Automated Geographic Reference Center, 2013) for the UT study area and resampling the 2-m WY Lidar DEM to 5-m. Terrain variables were created in R (R Core Team, 2012) with the RSAGA package (Brenning, 2008). For each area the following terrain variables were created: slope, total curvature, plan and profile curvature, SAGA wetness index, catchment area, catchment slope, modified catchment area, convergence index, morphometric protection index (Yokoyama et al., 2002), multi-resolution index of valley bottom flatness and multi-resolution index of ridge top flatness (Gallant and Dowling, 2003), topographic position index, and terrain ruggedness index. Plan and profile curvature represent the rate of change parallel and perpendicular to the slope, respectively (Wilson and Gallant 2000). Total curvature is the curvature of the surface itself (Wilson and Gallant 2000). Definitions of individual terrain variables can be found in Wilson and Gallant (2000) and Hengl and Reuter (2008).

Estimated potential direct, diffuse, total, and the duration of incoming solar radiation of the approximate growing season in each area were also calculated. All potential incoming solar radiation was calculated for clear sky and standard atmosphere conditions, and represent potential solar radiation in the absence of clouds or significant amounts of atmospheric aerosols. All terrain and potential solar radiation variables were calculated at 5, 10, 30, 50, and 100 m cell sizes. Digital elevation models with 10, 30, 50, and 100 m cell sizes were created from the 5-m DEMs by averaging over blocks of cells at these resolutions. The morphometric protection index calculated at 100-m cell size was not used because at this resolution there was no variance in the variable. This resulted in 89 terrain variables for each area.

For each area, we selected Landsat 5 TM imagery from 2 different dates. Each image pair consisted of an image acquired during a season of peak vegetation growth and a season of dormant vegetation. Each image was atmospherically corrected using the “Cost without Tau” method (Chavez, 1996) in the R Landsat package (Goslee, 2011). From each image the following variables were created: normalized band ratios 5/2, 5/7, 3/1, and 1/7; NDVI; six bands of the tasseled cap transformation (Crist and Kauth, 1986); and greenness above bare soil (GRABS) index (Jensen, 2005). This resulted in 24 imagery variables for each area. Total additional terrain and imagery variables for each area were 113 (variable set 2).

These variables represent a wide range of topographic and spectral derivatives commonly used for DSM in the western USA (Boettinger, 2010), but the selected variables are not exhaustive of the potentially available variables. For example, in other DSM studies, Heung et al. (2014) included distance to the nearest stream/river and relative hydrological slope position. Behrens et al. (2010) used elevation differences from the center pixel of a DEM as predictor variables. Xiong et al. (2012) used variables such as LANDFIRE (Landscape fire and resource management tools project) vegetation maps and geospatial land cover maps as vegetation related variables. Poggio et al. (2013) used multi-temporal MODIS (Moderate Resolution Imaging Spectroradiometer) vegetation and drought indices. Taylor et al. (2013) used potential evapotranspiration from ASTER (Advanced Spaceborne Thermal Emission and Reflection Radiometer) imagery. Although a wide range of potential covariates does exist, we chose to incorporate the specific terrain and imagery variables in variable set 1+2, because they were easily calculated with the available software and imagery with which we were familiar, and because we anticipated these variables to adequately characterize soil distribution in these areas.

2.4 Variable selection

For each study area we used random forests models (Liaw and Wiener, 2002; parameters $mtry = \text{default}$ and $ntree = 1000$) to identify the most important variables from the set of all available variables (variable set 2). Random forests identifies important variables by generating multiple classification trees (a forest) using bootstrap sampling, randomly scrambling the variables in each bootstrap sample and reclassifying the bootstrap sample. The misclassification error of the bootstrap sample (termed the “out-of-bag” error) using the scrambled variable is compared to the misclassification error using the original variable and the percent difference is used as a measure of variable importance (Peters et al., 2007). Variables that are important will have a large increase in “out-of-bag” error.

Using a similar approach to Xiong et al. (2012), we selected the “most important” variables by recursively eliminating the variable with the lowest importance until the random forests model reached a threshold after which model error significantly increased (Fig. 2-8). For the UT study area, although a set of 12 variables returned the lowest misclassification error, we selected a set of 6 variables as the “most important” for a more parsimonious model. Selected variables ranked by importance (variable set 3) are listed in Table 2-3.

2.4 Modeling

All modeling was performed using the caret package (Kuhn et al., 2013) in R (R Core Team, 2012). We tested 20 classification models for each area (Table 2-2). An accessible explanation of all tested models can be found in Kuhn and Johnson (2013). For each study area, 70% of the soil pedon observations were used for model training (the training set) and 30% for model testing (the testing set; Table 2-1). Splitting observations into training and testing sets in such a manner is a standard approach taken in other DSM studies (e.g., Henderson et al., 2005; Tesfa et al., 2009). For the UT study area 18 additional validation pedons were added to the

testing set. These additional pedon observations consisted of both soil observations made during initial field work but, which were not part of the initial 300 cLHS locations, and several soil pedon observations collected specifically for validation after initial field work was completed.

The goal of machine learning is to find a useful approximation of the function that underlies the predictive relationship between input variables and desired outcomes (Hastie et al., 2001). In this study input variables were derived from DEM's and Landsat imagery and the desired outcomes were subgroup classes. Each type of model (e.g., support vector machines, neural networks) has specific and different required parameters (referred to as tuning parameters) that control how the relationship between input variables and outcomes is defined. These parameters must be optimized to generate the best "fit" possible between variables and outcomes. For each model we used 50-fold cross-validation to select optimal tuning parameters (Kuhn, 2014). Briefly, for each required model parameter (the number of required model parameters ranged between 0 and 4) ten potential candidate values were defined. This resulted in an $n \times 10$ matrix of potential model tuning parameters, where n = the number of required parameters. Models were built using each set of tuning parameters and the average classification accuracy over the 50 folds was calculated. Optimal parameters were chosen as the set of tuning values that resulted in the highest classification accuracy (Kuhn, 2008). For those models that did not require tuning parameters (bagged classification tree, linear discriminant analysis) the model was built only once and no optimization was possible. For several models final tuning parameters could not be determined (Table 2-2).

We tested three sets of variables for each area: the soil scientist selected variables used as input into cLHS (variable set 1), the variables in set 1 plus the 113 additional terrain and imagery variables that we created (variable sets 1 + 2) and those variables that were identified

by random forests as the “most important” (variable set 3). Because some models required variables to have similar ranges (e.g., partial least squares), all environmental variables were centered and scaled to have mean = 0 and standard deviation = 1 before use.

When using variable sets 1+2, any cLHS variable that was duplicated by the additional terrain and imagery variables (e.g., slope) was removed. Additionally, geologic type and distance to roads were removed from the UT and WY study areas, respectively; because the geology variable did not cover the entire study area, and distance to roads was included for another purpose not thought to be related to soil taxonomic classes (impact of disturbance on vegetation) in the initial cLHS.

2.5 Model validation and comparison

Models were validated by classifying the testing set (predicted vs. observed class). We used the percent correctly classified to assess model accuracy for each class. The percent correctly classified is the percent of the validation observations that were correctly classified for each subgroup type. Kappa analysis was also used for model comparison, where the kappa statistic (κ) (Congalton, 1991) is a measure of classification accuracy accounting for chance agreement (Congalton and Green, 1998). Accounting for change agreement is an important consideration when dealing with highly imbalanced classes as high classification accuracy could result from classifying all observations as the largest class (Congalton and Green, 1998). The κ of a random classifier would be 0 whereas a κ of 1 would indicate perfect classification (Congalton, 1991). Kappa values greater than 0.80 represents strong agreement, values between 0.4 and 0.8 represent moderate agreement, and values below 0.4 represent poor agreement (Congalton and Green, 1998).

3. Results

The most accurate model for all three study areas was constructed using variable set 3 (Figs. 2-5, 2-6, & 2-7); although there was little difference in maximum κ between variable sets for the UT study area (Fig. 2-6). The most accurate model (highest κ) for the NM study area ($\kappa = 0.55$) was support vector machines using a radial basis function (SVMR) (Fig. 2-5). Bagging classification tree (BCT) was the most accurate model for the UT study area ($\kappa = 0.13$) (Fig. 2-6), whereas random forests (RF) was the most accurate model for the WY study area ($\kappa = 0.69$) (Fig. 2-7). Several models had $\kappa < 0$ indicating they performed worse than a random classifier. The percent of correctly classified test set observations for each subgroup class (i.e. individual class accuracy) ranged between 0 and 100 percent (Table 2-1). The number of “most important” variables as determined by random forests for each study area ranged between six and ten and included terrain derivatives at multiple cell sizes as well as several Landsat derivatives (Table 2-3). Spatial predictions using the most accurate model for each study area are shown in Figs. 2-9, 2-10 and 2-11.

4. Discussion

4.1 Model performance

No single model was consistently the most accurate classifier (had the highest κ) between study areas or between variable sets within an area (Figs. 2-5, 2-6, & 2-7); however, some model types were more often among the top performers. At the UT and WY study areas, both bagging trees and random forests were among the three models with the highest κ . If multiple model comparisons are not possible, these results suggest that bagging based tree models be investigated for soil type classification in landscapes that are characterized by complex geology and topography.

Maximum κ values for the NM and WY study areas, 0.55 and 0.69, respectively, were similar to other published studies. For example, Hengl et al. (2007) had a κ of 54.2% (0.542) when modeling 15 World Resource Base (WRB) soil groups across Iran, and Kim et al. (2012) had a κ of 78.9% (0.789) when modeling five soil series across 418 km² in Florida, USA. Maximum κ for the UT study area (0.12) was significantly lower than for the other two study areas even though this area had the largest number of soil pedon observations (section 2.2.2; Table 2-1).

As the model with the highest classification accuracy (maximum κ) for each study area is of most interest for predicting soil subgroup types we restrict further discussion to the models which resulted in the highest κ when discussing differences in classification accuracy between study areas.

Differences in classification accuracy between study areas can be partially attributed to the number of soil subgroup classes and the frequency distribution (the balance of observations between subgroup classes) of soil pedon observations. The UT study area was the least accurately classified, had the most soil subgroup classes ($n = 15$), and the most skewed frequency distribution of soil pedon observations between subgroup classes. Two subgroup classes for the UT study area contained almost 70% of the total soil pedon observations (Table 2-1). In contrast, the WY study area, the most accurately classified, had the fewest soil subgroup classes ($n = 5$) and a somewhat more balanced soil pedon observation distribution frequency. The classification accuracy, number of soil subgroup classes ($n = 10$) and soil pedon observation distribution frequency for the NM study area was between those of the UT and WY study areas. This suggests that overall classification accuracy will be highest when there are many soil observations, few soil classes, and the frequency distribution of soil observations between classes is approximately equal.

The frequency distribution of soil pedon observations heavily influenced individual soil subgroup class accuracies (Table 2-1). Classes with lower sampling frequencies were modeled less accurately. This finding is consistent with data presented by others (Barthold et al., 2013; Hengl et al., 2007; Kim et al., 2012; Marchetti et al., 2011; Stum et al., 2010; Taghizadeh-Mehrjard et al., 2012) and is likely because there are simply not enough observations to separate such classes in feature space.

The number of soil subgroup classes per study area appears related to the inherent variability of the given landscape. Areas with high geological and topographical complexity likely experience complex relationships between soil forming factors that lead to increased diversity in soil types. For example, the geologically and topographically complex UT study area had more subgroup classes than did the less complex NM or WY sites (Table 2-1).

The frequency distribution of soil pedon observations between subgroup types in a study area is likely a result of the sampling strategy used to select sites. Conditioned Latin hypercube sampling is a stratified random sampling method designed to identify sampling sites which represent the multivariate distribution of input environmental variables and assumes that the input environmental variables are related to the variable of interest (Minasny and McBratney, 2006). Environmental variables used as input to cLHS for each study area were selected to represent broad soil-landscape relationships. Our results suggest that in complex landscapes where likely many different soil types exist, such input environmental variables result in adequate sampling of the most frequent soil types, but not of rare soil types (e.g., the UT study area).

As accurate modeling of soil classes depends on the number of classes and the frequency distribution of soil pedon observations between classes (many classes with few observations = poor model performance) such imbalance must be addressed for accurate

modeling. There are two options to address such challenges: 1) increase observation number in classes with few observations and 2) decrease the number of classes.

Increasing the number of observations in classes with few observations may be difficult given financial and logistical constraints, and because it is likely difficult to identify *a priori* which classes will need to be more intensively sampled. However, this might be addressed using a combination of cLHS and targeted sampling or case-based reasoning (Shi et al., 2009), where the soil surveyor could manually identify likely locations of rare soil types. This may be especially useful in arid and semi-arid regions where small localized areas often contain significant diversity when compared to the majority landscape.

The second option is to decrease the number of taxonomic classes. This could be accomplished by: 1) combining similar classes and 2) modeling separate sub-areas. Combining similar subgroup classes could be accomplished by using higher taxonomic levels such as great group or suborder. Modeling higher taxonomic levels would likely increase model accuracy (Jafari et al., 2013), but a trade-off between taxonomic level and soil information usefulness exists. Many decisions about soil use and management are based on soil differences not captured by higher taxonomic levels (i.e., order, suborder, and great group), so combining subgroup classes into higher taxonomic levels may miss important differences in soil function and likely not provide useful information for soil management decisions.

Ideally, DSM would be able to accurately model all levels of Soil Taxonomy including soil series. Soil series are the finest level of Soil Taxonomy (Soil Survey Staff, 1999) and two levels finer than what was predicted in this study. However, accurate predictions of soil series may not be possible, because soil series are often defined by soil morphological diagnostic criteria which may not be well represented by DEM and remote sensing variables.

Similar classes could also be combined based on a particular soil property (e.g., bedrock contact). This would result in a focus on the specific property while excluding other potentially important soil properties. Likely any such decision to group classes by soil property types would best be made by the user of the soil information. A further option may be to combine classes with few observations into a single class denoted as “other soil classes.” This approach has been taken by others (Pahlavan Rad et al., 2014), but we decided against doing so, because we suspected that classes with few observations might be topographically and spectrally distinct and thus be accurately predicted. However; individual class accuracies (Table 2-1) do not indicate this to be the case, and so in retrospect such a pragmatic approach is probably wise.

Modeling separate sub-areas might also decrease the number of taxonomic classes by reducing the area and thus the number of soil types considered in a model. For example, it is likely that the number of subgroup classes in one model would have been fewer had the UT study area been segregated into uplands and alluvial fan sub-areas. Although such an approach would increase the number of required models in proportion to the number of chosen sub-areas, this is theoretically appealing as different pedo-geomorphic sub-areas are likely to have different relationships between subgroup classes and environmental variables (McBratney et al., 2003).

Another option to increase model accuracy could be to apply a weighting scheme to soil classes with few observations during model construction. This might improve classification accuracy, but for highly imbalanced datasets weighting can severely decrease the accuracy of the majority classes and result in apparent over prediction of the small classes (Stum et al., 2010). Overall, increasing model accuracy is likely to require several of these options (increasing observation numbers, reducing class numbers, or the use of a weighting scheme), and that applicable options will best be identified on a project by project basis.

4.2 Variable set comparison

Perhaps unsurprisingly, using all variables (set 1+2) resulted in the lowest maximum k for all study areas (Figs. 2-5, 2-6 & 2-7). This is probably because many of the variables were unrelated to the factors that drove soil development in these areas, or were not at the correct scale.

As variable set 1 was selected by soil scientists anticipating how soil-landscape relationships would be best represented for modeling, the fact that this variable set did not result in the most accurate models suggests that soil scientists may be unable to *a priori* identify optimal variables for predicting taxonomic classes. In hindsight, this is not entirely surprising given the complexity of soil taxonomic classes and the disparate kinds of knowledge needed to predict these relationships *a priori*. Soil taxonomic classes represent multiple soil forming factors operating over long periods of time (likely decades to millennia) at several scales. Thus choosing optimal predictive variables for modeling requires knowing both 1) how, and the scale at which, multiple soil forming factors vary across the landscape to produce soil taxonomic classes and 2) how those factors are best distinguished using spectral and topographic variables. Being able to do both requires extensive familiarity with the local landscape and an understanding of terrain modeling and remote sensing. This suggests a pressing need for further investigation into relationships between specific environmental variables and soil forming processes.

In addition to producing models with the highest accuracy, variable set 3 may also provide information about the processes controlling soil type distribution across each study area landscape. The NM area mostly consists of broad, gently sloping, southward facing alluvial surfaces. More than half of the “most important” variables for this study area were related to catchment-scale patterns of potential soil moisture (multipath wetness index, catchment area and catchment slope; Table 2-3). We attribute this to the correlation of run-on/run-off

relationships, landscape stability, and soil formation observed in this region (Gile et al., 1981). Vegetation related variables (tasseled cap greenness band and the GRABS index) selected in variable set 3, were likely related to the strong control of soils in determining vegetation cover and composition in the study area (Bestelmeyer et al., 2006, Duniway et al., 2010). Thus variables related to catchment scale patterns of potential soil moisture and vegetation indices may be the best predictors in similar landscape settings. Similar settings include the large alluvial fans and bajadas (coalesced alluvial fans) that extend from mountain fronts into the valleys of many semi-arid and arid landscapes. Interestingly, topographic shading is an important variable for both the UT and WY areas, but not the NM area. This is likely because landforms in the NM area are mostly southward facing with little vertical relief.

The most important variables for the UT study area were related to topographic shading (diffuse insolation), slope, slope position, and terrain ruggedness (Table 2-3). The UT area was highly variable in topographic relief. This local topography strongly influences soil erosion and deposition as well as the amount of incoming solar radiation, which in turn influences soil distribution (Beaudette and O'Geen, 2009). As the UT area had the greatest geologic complexity between the three study areas, it is surprising that variables related to geology (Landsat band ratios 5/2, 5/7) were not among those identified as "most important". This may be because the influence of local topography exerted a stronger effect on soil development than did the relatively larger scale influence of geology. In semi-arid steeply sloping uplands and mountainous erosional landscapes, variables related to soil erosion/deposition processes and solar radiation may be the most useful for predicting soil distribution.

The WY area is generally composed of rounded hills which have been dissected by numerous small drainages and lacks the topographic relief of the UT area or the broad alluvial slopes of the NM area. The most important variables for this area were plan and total curvature,

topographic shading (diffuse insolation), catchment slope and Landsat band ratio 5/2 (Table 2-3). As three of the seven “most important” variables were related to slope curvature which approximates flow convergence/divergence (Wilson and Gallant, 2000) and as topographic shading was also an important variable, it is likely that differences in soil moisture control soil development in this area. Landsat band ratio 5/7 is useful for distinguishing differences in geologic parent material (Inzana et al., 2003) and likely helps distinguish differences in inter-bedded geologic types. For much of the northern rolling high plains and possibly for other areas with rolling hills, curvature, potential solar radiation and geological type are likely useful for modeling soil distribution.

4.3 Spatial predictions

Spatial predictions of subgroup classes using the most accurate model visually appear to represent expected soil distribution patterns for each study area (Figs. 2-9, 2-10, & 2-11). For the NM and WY study areas spatial predictions generally agree with published soil surveys although our predictions show much finer spatial detail. For the NM study area, soils with a bedrock contact (Lithic Ustic Haplocambids and Lithic Ustic Haplocalcids) were predicted on steeply sloping uplands. Calcic Petrocalcids (subsurface cemented CaCO_3) were predicted on older, stable alluvial surfaces. Ustic Haplocambids (little soil development) were predicted on younger land surfaces (e.g. inset fans). Petronodic Ustic Haplocalcids (subsurface CaCO_3 concretions, maybe approaching cementation) were predicted on landforms intermediate between where Calcic Petrocalcids and Ustic Haplocambids were predicted. Ustic Haplargids (subsurface clay accumulation) were predicted on lower elevation run-in areas, where finer particles can accumulate. Also at lower elevations, on what are likely more active and recent geomorphic surfaces, Ustic Haplocalcids (subsurface CaCO_3 accumulation) were predicted. For the WY study area both Ustic Torriorthents (minimal development) and Badlands (steep hills

and gullies) were predicted on steeply sloping, dissected landforms near a stream channel where active erosion may be occurring. Ustic Haplargids (subsurface clay accumulation) were predicted on flatter, more stable upland surfaces that likely had enough time for clay to form and/or translocate in the subsoil.

Although these results must be treated with caution given the low kappa value, the spatial patterns of predicted subgroup classes for the UT study area corresponded to our understanding of soil-landscape relationships. Lithic Xeric Haplocalcids (soils with a bedrock contact and subsurface accumulation of CaCO_3) were predicted on steeply sloping uplands. Lithic Calciargids (bedrock contact and subsurface accumulation of CaCO_3 and clay) were predicted on many concave areas of these steeply sloping uplands where potential soil moisture accumulation is higher, resulting in greater development of subsurface clay. Rock Outcrops were predicted on the steepest mountain faces where many cliffs and talus fields were observed. Xeric Haplocalcids (subsurface CaCO_3) were predicted to occur on alluvial surfaces. Xeric Calciargids (subsurface CaCO_3 and clay) were predicted on older more stable alluvial surfaces. Xeric Torriorthents (minimal development) were predicted on the youngest, most active alluvial surfaces.

5. Conclusions

This study provides insight into the use of machine learning for mapping the spatial distribution of soil taxonomic classes. We applied multiple machine learning models to three separate semi-arid study areas using three different sets of environmental variables, but no model was consistently the most accurate classifier. However, bagging classification trees and random forests were among the most accurate classifiers for two of the three areas, suggesting the utility of these models. To use machine learning for spatial prediction of soil classes several machine learning models should be applied and the most accurate selected.

Models built using variables identified as “most important” by random forests were more accurate than models built using either variables selected by soil scientists familiar with each area, or a large suite of available variables. Thus some form of variable selection should be incorporated as an explicit part of digital soil mapping activities. Variable selection also gives insight into the soil forming factors operating across a landscape.

Machine learning models are most accurate when there are few soil classes and when the frequency distribution of soil pedon observations are approximately equal between classes. The number of soil subgroup classes depends on the inherent variability of each landscape. The frequency distribution of soil pedon observations depends on the sampling method. The use of cLHS results in many soil pedon observations in common soil classes and few observations in “rare” soil classes. One solution to this problem could include increasing the number of samples in rare classes by targeted sampling or case-based reasoning.

6. References

- Barthold, F.K., Wiesmeier, M., Breuer, L., Frede, H.-G., Wu, J., Blank, F.B., 2013. Land use and climate control the spatial distribution of soil types in the grasslands of Inner Mongolia. *J. Arid Environ.* 88, 194–205. doi:10.1016/j.jaridenv.2012.08.004
- Beaudette, D.E., O’Geen, A.T., 2009. Quantifying the aspect effect: an application of solar radiation modeling for soil survey. *Soil Sci. Soc. Am. J.* 73, 1345–1352. doi:10.2136/sssaj2008.0229
- Behrens, T., Förster, H., Scholten, T., Steinrücken, U., Spies, E.-D., Goldschmitt, M., 2005. Digital soil mapping using artificial neural networks. *J. Plant Nutr. Soil Sci.* 168, 21–33. doi:10.1002/jpln.200421414
- Behrens, T., Scholten, T., 2006. A Comparison of Data-Mining Techniques in Predictive Soil Mapping, in: Lagacherie, P., McBratney, A.B., Voltz, M. (Eds.), *Digital Soil Mapping: An Introductory Perspective*. Elsevier, Amsterdam, pp. 353 – 617.
- Behrens, T., Schmidt, K., Zhu, A.X., Scholten, T., 2010. The ConMap approach for terrain-based digital soil mapping. *Eur. J. Soil Sci.* 61, 133–143. doi:10.1111/j.1365-2389.2009.01205.x

- Best, M.G., Lemmon, D.M., Morris, H.T., 1989. Geologic map of the Milford quadrangle and east half of the Frisco quadrangle, Beaver county, Utah. Miscellaneous Investigations Series Map I-1904. U.S. Geological Survey. Reston.
- Bestelmeyer, B.T., Ward, J.P., Havstad, K.M., 2006. Soil-geomorphic heterogeneity governs patchy vegetation dynamics at an arid ecotone. *Ecology* 87, 963–973. doi:10.1890/0012-9658(2006)87[963:SHGPVD]2.0.CO;2
- Boer, M., DelBarrio, G., Puigdefabregas, J., 1996. Mapping soil depth classes in dry Mediterranean areas using terrain attributes derived from a digital elevation model. *Geoderma* 72, 99–118. doi:10.1016/0016-7061(96)00024-9
- Boettinger, J.L., 2010. Environmental covariates for digital soil mapping in the western USA, in: Boettinger, J.L., Howell, D.W., Moore, A.C., Hartemink, A.E., Kienast-Brown, S. (Eds.), *Digital Soil Mapping: Bridging Research, Environmental Application, and Operation*. Springer, Dordrecht, pp. 17–27.
- Boruvka, L., Pavlu, L., Vasat, R., Penizek, V., Drabek, O., 2008. Delineating acidified soils in the Jizera mountains region using fuzzy classification, in: Hartemink, A.E., McBratney, A., Mendonça-Santos, M. de L. (Eds.), *Digital Soil Mapping with Limited Data*. Springer, Netherlands, pp. 303–309.
- Brenning, A., 2008. Statistical geocomputing combining R and SAGA: The example of landslide susceptibility analysis with generalized additive models, in: *SAGA – Seconds Out (= Hamburger Beitrage zur Physischen Geographie und Landschaftsoekologie, Vol. 19)*. J. Boehner, T. Blaschke, L. Montanarella, pp. 23–32.
- Brungard, C.B., Boettinger, J.L., 2012. Spatial prediction of biological soil crust classes; value added DSM from soil survey, in: Minasny, B., Malone, B.P., McBratney, A. (Eds.), *Digital Soil Assessments and Beyond Proceedings of the 5th Global Workshop on Digital Soil Mapping*. CRC Press, Sydney, pp. 57–60.
- Bui, E.N., Moran, C.J., 2003. A strategy to fill gaps in soil survey over large spatial extents: an example from the Murray-Darling basin of Australia. *Geoderma* 111, 21–44. doi:10.1016/S0016-7061(02)00238-0
- Campling, P., Gobin, A., Feyen, J., 2002. Logistic Modeling to spatially predict the probability of soil drainage classes. *Soil Sci. Soc. Am. J.* 66, 1390–1401.
- Chavez Jr, P.S., 1996. Image-Based Atmospheric Corrections - Revisited and Improved. *Photogramm. Eng. Remote Sens.* 62, 1025–1036.
- Cole, N.J., 2004. A pedogenic understanding raster classification model for mapping soils, Powder River Basin, Wyoming (MS Thesis). Utah State University, Logan, USA.
- Cole, N.J., Boettinger, J.L., 2006. Pedogenic understanding raster classification methodology for mapping soils, Powder River Basin, Wyoming, USA, in: Lagacherie, P., McBratney, A.B.,

- Voltz, M. (Eds.), *Digital Soil Mapping: An Introductory Perspective*. Elsevier, Amsterdam, pp. 377–619.
- Congalton, R., 1991. A review of assessing the accuracy of classifications of remotely sensed data. *Remote Sens. Environ.* 37, 35–46. doi:10.1016/0034-4257(91)90048-B
- Congalton, R.G., Green, K., 1998. *Assessing the Accuracy of Remotely Sensed Data: Principles and Practices*. CRC/Taylor & Francis, Boca Raton.
- Crist, E., Kauth, R., 1986. The tasseled cap de-mystified. *Photogramm. Eng. Remote Sens.* 52, 81–86.
- Duniway, M.C., Herrick, J.E., Monger, H.C., 2010. Spatial and temporal variability of plant-available water in calcium carbonate-cemented soils and consequences for arid ecosystem resilience. *Oecologia* 163, 215–226. doi:10.1007/s00442-009-1530-7
- Gile, L.H., Hawley, J.W., Grossman, R.B., 1981. Memoir 39—Soils and geomorphology in the Basin and Range area of southern New Mexico: Guidebook to the Desert Project. New Mexico Bureau of Mines and Mineral Resources, Socorro.
- Gallant, J.C., Dowling, T.I., 2003. A multiresolution index of valley bottom flatness for mapping depositional areas. *Water Resour. Res.* 39. doi:10.1029/2002WR001426
- Goslee, S.C., 2011. Analyzing remote sensing data in R: the landsat package. *J. Stat. Softw.* 43, 1–25.
- Green, G.N., Drouillard, P.H., 1994. The Digital Geologic Map of Wyoming in ARC/INFO Format. U.S. Geological Survey Open-File Report 94-0425. <http://geo-nsdi.er.usgs.gov/metadata/open-file/94-425/> (last accessed: 7/5/2014).
- Green, G.N., Jones, G.E., 1997. The Digital Geologic Map of New Mexico in ARC/INFO Format. U.S. Geological Survey Open File Report 97-0052. http://pubs.usgs.gov/of/1997/ofr-97-0052/new_mex.htm (last accessed: 7/5/2014).
- Grinand, C., Arrouays, D., Laroche, B., Martin, M.P., 2008. Extrapolating regional soil landscapes from an existing soil map: sampling intensity, validation procedures, and integration of spatial context. *Geoderma* 143, 180–190. doi:10.1016/j.geoderma.2007.11.004
- Grunwald, S., 2006. *Environmental Soil-Landscape Modeling: Geographic Information Technologies and Pedometrics*. CRC/Taylor & Francis, Boca Raton.
- Hastie, T., Tibshirani, R., Friedman, J.H., 2001. *The Elements of Statistical Learning: Data Mining, Inference, and Prediction*. Springer, New York.
- Henderson, B.L., Bui, E.N., Moran, C.J., Simon, D.A.P., 2005. Australia-wide predictions of soil properties using decision trees. *Geoderma* 124, 383–398. doi:10.1016/j.geoderma.2004.06.007

- Hengl, T., Toomanian, N., Reuter, H.I., Malakouti, M.J., 2007. Methods to interpolate soil categorical variables from profile observations: lessons from Iran. *Geoderma* 140, 417–427. doi:10.1016/j.geoderma.2007.04.022
- Hengl, T., Reuter, H.I., 2008. *Geomorphometry. Concepts, Software, Applications. Developments in Soil Science.* Elsevier, Amsterdam.
- Heute, A.R., 1988. A Soil-Adjusted Vegetation Index (SAVI). *Remote Sens. Environ.* 25, 295–309.
- Heung, B., Bulmer, C.E., Schmidt, M.G., 2014. Predictive soil parent material mapping at a regional-scale: A Random Forest approach. *Geoderma* 214–215, 141–154. doi:10.1016/j.geoderma.2013.09.016
- Inzana, J., Kusky, T., Higgs, G., Tucker, R., 2003. Supervised classifications of Landsat TM band ratio images and Landsat. *J. Afr. Earth Sci.* 37, 59–72. doi:10.1016/S0899-5362(03)00071-X
- Jafari, A., Finke, P.A., Van de Wauw, J., Ayoubi, S., Khademi, H., 2012. Spatial prediction of USDA-great soil groups in the arid Zarand region, Iran: comparing logistic regression approaches to predict diagnostic horizons and soil types. *Eur. J. Soil Sci.* 63, 284–298. doi:10.1111/j.1365-2389.2012.01425.x
- Jafari, A., Ayoubi, S., Khademi, H., Finke, P.A., Toomanian, N., 2013. Selection of a taxonomic level for soil mapping using diversity and map purity indices: a case study from an Iranian arid region. *Geomorphology* 201, 86–97. doi:10.1016/j.geomorph.2013.06.010
- Jensen, J.R., 2005. *Introductory Digital Image Processing: A Remote Sensing Perspective.* Pearson Prentice Hall, Upper Saddle River.
- Kempen, B., Brus, D.J., Heuvelink, G.B.M., 2012. Soil type mapping using the generalised linear geostatistical model: A case study in a Dutch cultivated peatland. *Geoderma* 189, 540–553. doi:10.1016/j.geoderma.2012.05.028
- Kienast-Brown, S., Boettinger, J.L., 2010. Applying the optimum index factor to multiple data types in soil survey, in: Boettinger, J.L., Howell, D.W., Moore, A.C., Hartemink, A.E., Kienast-Brown, S. (Eds.), *Digital Soil Mapping: Bridging Research, Environmental Application, and Operation.* Springer, Dordrecht, pp. 385–398.
- Kim, J., Grunwald, S., Rivero, R.G., Robbins, R., 2012. Multi-scale modeling of soil series using remote sensing in a wetland ecosystem. *Soil Sci. Soc. Am. J.* 76, 2327–2341. doi:10.2136/sssaj2012.0043
- Kuhn, M., 2008. Building predictive models in R using the caret package. *J. Stat. Softw.* 28, 1–26.
- Kuhn, M., Wing, J., Weston, S., Williams, A., Keefer, C., A. Engelhardt. 2012. caret: Classification and Regression Training. R package version 5.17-7. <http://CRAN.R-project.org/package=caret>

- Kuhn, M., Johnson, K., 2013. *Applied Predictive Modeling*. Springer, New York.
- Kuhn, M., 2014. A short introduction to the caret package. <http://cran.r-project.org/web/packages/caret/vignettes/caret.pdf> (last accessed: 7/5/2014).
- Liaw, A., Wiener, M., 2002. Classification and regression by randomForest. *R News* 2, 18–22.
- Liu, J., Pattey, E., Nolin, M.C., Miller, J.R., Ka, O., 2008. Mapping within-field soil drainage using remote sensing, DEM and apparent soil electrical conductivity. *Geoderma* 143, 261 – 272. doi:<http://dx.doi.org/10.1016/j.geoderma.2007.11.011>
- Lowry, J., Ramsey, R.D., Thomas, K., Schrupp, D., Sajwaj, T., Kirby, J., Waller, E., Schrader, S., Falzarano, S., Langa, L., Manis, G., Wallace, C., Schulz, K., Comer, P., Pohs, K., Rieth, W., Velasquez, C., Wolk, B., Kepner, W., Boykin, K., O'Brien, L., Bradford, D., Thompson, B., Prior-Magee, J., 2007. Mapping moderate-scale land-cover over very large geographic areas within a collaborative framework: a case study of the Southwest Regional Gap Analysis Project (SWReGAP). *Remote Sens. Environ.* 108, 59 – 73. doi:<http://dx.doi.org/10.1016/j.rse.2006.11.008>
- Marchetti, A., Piccini, C., Santucci, S., Chiuchiarelli, I., Francaviglia, R., 2011. Simulation of soil types in Teramo province (Central Italy) with terrain parameters and remote sensing data. *CATENA* 85, 267–273. doi:[10.1016/j.catena.2011.01.012](http://dx.doi.org/10.1016/j.catena.2011.01.012)
- McBratney, A.B., Mendonça Santos, M.D.L., Minasny, B., 2003. On digital soil mapping. *Geoderma* 117, 3–52. doi:[10.1016/S0016-7061\(03\)00223-4](http://dx.doi.org/10.1016/S0016-7061(03)00223-4)
- Minasny, B., McBratney, A.B., 2006. A conditioned Latin hypercube method for sampling in the presence of ancillary information. *Comput. Geosci.* 32, 1378–1388. doi:[10.1016/j.cageo.2005.12.009](http://dx.doi.org/10.1016/j.cageo.2005.12.009)
- Pahlavan Rad, M.R., Toomanian, N., Khormali, F., Brungard, C.W., Komaki, C.B., Bogaert, P., 2014. Updating soil survey maps using random forest and conditioned Latin hypercube sampling in the loess derived soils of northern Iran. *Geoderma* 232–234, 97–106. doi:[10.1016/j.geoderma.2014.04.036](http://dx.doi.org/10.1016/j.geoderma.2014.04.036)
- Peters, J., Baets, B.D., Verhoest, N.E.C., Samson, R., Degroeve, S., Becker, P.D., Huybrechts, W., 2007. Random forests as a tool for ecohydrological distribution modelling. *Ecol. Model.* 207, 304–318. doi:[10.1016/j.ecolmodel.2007.05.011](http://dx.doi.org/10.1016/j.ecolmodel.2007.05.011)
- Poggio, L., Gimona, A., Brewer, M.J., 2013. Regional scale mapping of soil properties and their uncertainty with a large number of satellite-derived covariates. *Geoderma* 209–210, 1–14. doi:[10.1016/j.geoderma.2013.05.029](http://dx.doi.org/10.1016/j.geoderma.2013.05.029)
- R Core Team, 2012. *R: A language and environment for statistical computing*. R Foundation for Statistical Computing, Vienna, Austria. <http://www.R-project.org/>.

- Schoeneberger, P.J., Wysocki, D.A., Benham, E.C., Broderson, W.D. (Eds.), 2003. Field Book for Describing and Sampling Soils, Version 2.0. Natural Resources Conservation Service. National Soil Survey Center, Lincoln.
- Shi, X., Long, R., Dekett, R., Philippe, J., 2009. Integrating different types of knowledge for digital soil mapping. *Soil Sci. Soc. Am. J.* 73, 1682. doi:10.2136/sssaj2007.0158
- Shi, X., 2013. ArcSIE user's guide. http://www.arcsie.com/Download/ArcSIE_UsersGuide_130319.pdf (last accessed: 7/5/2014).
- Smith, C.A.S., Daneshfar, B., Frank, G., 2012. Use of weights of evidence statistics to define inference rules to disaggregate soil survey maps, in: Minasny, B., Malone, B.P., McBratney, A. (Eds.), *Digital Soil Assessments and Beyond: Proceedings of the 5th Global Workshop on Digital Soil Mapping*. CRC Press, Sydney, pp. 215–220.
- Soil Survey Staff, 1999. *Soil taxonomy: a basic system of soil classification for making and interpreting soil surveys*, 2nd ed. U.S. Department of Agriculture Handbook 436. Natural Resources Conservation Service, Lincoln.
- Stum, A.K., Boettinger, J.L., White, M.A., Ramsey, R.D., 2010. Random Forests Applied as a Soil Spatial Predictive Model in Arid Utah, in: Boettinger, J.L., Howell, D.W., Moore, A.C., Hartemink, A.E., Kienast-Brown, S. (Eds.), *Digital Soil Mapping: Bridging Research, Environmental Application, and Operation*, Springer, Dordrecht, pp. 179–190.
- Subburayalu, S.K., Slater, B.K., 2013. Soil series mapping by knowledge discovery from an Ohio county soil map. *Soil Sci. Soc. Am. J.* 77, 1254–1268. doi:10.2136/sssaj2012.0321
- Taghizadeh-Mehrjard, R., Minasny, B., McBratney, A.B., Triantafilis, J., Sarmadian, F., Toomanian, N., 2012. Digital soil mapping of soil classes using decision trees in central Iran, in: Minasny, B., Malone, B.P., McBratney, A. (Eds.), *Digital Soil Assessments and Beyond: Proceedings of the 5th Global Workshop on Digital Soil Mapping*. CRC Press, Sydney, pp. 197–202.
- Tarboton, D., 2013. *Terrain Analysis Using Digital Elevation Models (TauDEM)*. <http://hydrology.usu.edu/taudem/taudem5/index.html> (last accessed: 7/5/2014).
- Taylor, J.A., Jacob, F., Galleguillos, M., Prévot, L., Guix, N., Lagacherie, P., 2013. The utility of remotely-sensed vegetative and terrain covariates at different spatial resolutions in modelling soil and watertable depth (for digital soil mapping). *Geoderma* 193–194, 83–93. doi:10.1016/j.geoderma.2012.09.009
- Tesfa, T.K., Tarboton, D.G., Chandler, D.G., McNamara, J.P., 2009. Modeling soil depth from topographic and land cover attributes. *Water Resour. Res.* 45, W10438. doi:10.1029/2008WR007474
- Triantafilis, J., Earl, N.Y., Gibbs, I.D., 2012. Digital soil-class mapping across the Edgeroi district using numerical clustering and gamma-ray spectrometry data, in: Minasny, B., Malone,

- B.P., McBratney, A. (Eds.), Digital Soil Assessments and Beyond: Proceedings of the 5th Global Workshop on Digital Soil Mapping. CRC Press, Sydney, pp. 187–191.
- United States Department of Agriculture, 2006. Land Resource Regions and Major Land Resource Areas of the United States, the Caribbean, and the Pacific Basin. ftp://ftp-fc.sc.egov.usda.gov/NSSC/Ag_Handbook_296/Handbook_296_low.pdf (last accessed: 7/5/2014).
- Utah Automated Geographic Reference Center, 2013. 5 Meter Auto-Correlated Elevation Models. <http://gis.utah.gov/data/elevation-terrain-data/5-meter-auto-correlated-elevation-models/> (last accessed: 7/5/2014).
- Van Zijl, G.M., le Roux, P.A.L., Smith, A.B., 2012. Rapid soil mapping under restrictive conditions in Tete, Mozambique, in: Minasny, B., Malone, B.P., McBratney, A. (Eds.), Digital Soil Assessments and Beyond: Proceedings of the 5th Global Workshop on Digital Soil Mapping. CRC Press, Sydney, pp. 335–339.
- Western Regional Climate Center, 2013. Cooperative Climatological Data Summaries. <http://www.wrcc.dri.edu/climatedata/climsum/> (last accessed: 7/5/2014).
- Wilson, J.P., Gallant, J.C., 2000. Terrain Analysis: Principles and Applications. John Wiley & Sons, New York.
- Witten, I.H., Frank, E., Hall, M.A., 2011. Data mining: Practical Machine Learning Tools and Techniques. Morgan Kaufmann, Burlington.
- Xiong, X., Grunwald, S., Myers, D.B., Kim, J., Harris, W.G., Comerford, N.B., 2012. Which soil, environmental and anthropogenic covariates for soil carbon models in Florida are needed? In: Minasny, B., Malone, B.P., McBratney, A. (Eds.), Digital Soil Assessments and Beyond: Proceedings of the 5th Global Workshop on Digital Soil Mapping. CRC Press, Sydney, pp. 335–339.
- Yokoyama, R., Shirasawa, M., Pike, R.J., 2002. Visualizing topography by openness: a new application of image processing to digital elevation models. *Photogramm. Eng. Remote Sens.* 68, 257–266.
- Zhu, A.X., Hudson, B., Burt, J., Lubich, K., Simonson, D., 2001. Soil mapping using GIS, expert knowledge, and fuzzy logic. *Soil Sci. Soc. Am. J.* 65, 1463–1472.

Table 2-1. Distribution of soil observations in each subgroup class for the three study areas.

| Subgroup Classes | Pedons ^a | % of total ^b | training set ^c | testing set ^d | % Correctly Classified ^e |
|------------------------------|---------------------|-------------------------|---------------------------|--------------------------|-------------------------------------|
| NM | | | | | |
| Ustic Haplocambid | 27 | 26 | 19 | 8 | 100 |
| Petronodic Ustic Haplocalcid | 22 | 21 | 16 | 6 | 67 |
| Calcic Petrocalcid | 21 | 20 | 15 | 6 | 83 |
| Ustic Haplocalcid | 13 | 13 | 10 | 3 | 67 |
| Ustic Haplargid | 5 | 5 | 4 | 1 | 0 |
| Lithic Ustic Haplocalcid | 4 | 4 | 3 | 1 | 0 |
| Ustic Petrocalcid | 4 | 4 | 3 | 1 | 0 |
| Lithic Ustic Haplocambid | 3 | 3 | 2 | 1 | 0 |
| Petronodic Ustic Calciargid | 2 | 2 | 1 | 1 | 0 |
| Ustic Calciargid | 2 | 2 | 1 | 1 | 0 |
| Total | 103 | 100 | 74 | 29 | |
| UT | | | | | |
| Xeric Haplocalcid | 123 | 41 | 87 | 44 | 73 |
| Xeric Calciargid | 85 | 29 | 60 | 28 | 43 |
| Lithic Xeric Haplocalcid | 18 | 6 | 13 | 6 | 0 |
| Lithic Xeric Torriorthent | 14 | 5 | 10 | 6 | 0 |
| Calcic Petrocalcid | 13 | 4 | 10 | 4 | 0 |
| Lithic Calciargid | 10 | 3 | 7 | 4 | 0 |
| Lithic Xeric Haplargid | 6 | 2 | 5 | 2 | 0 |
| Xeric Torriorthent | 6 | 2 | 5 | 1 | 0 |
| Durinodic Xeric Haplocalcid | 4 | 1 | 3 | 2 | 0 |
| Xeric Haplodurid | 4 | 1 | 3 | 1 | 0 |
| Lithic Xeric Calciargid | 3 | 1 | 2 | 1 | 0 |
| Rock Outcrop | 3 | 1 | 2 | 1 | 0 |
| Xeric Argidurid | 3 | 1 | 2 | 1 | 0 |
| Xeric Haplargid | 3 | 1 | 2 | 1 | 0 |
| Durinodic Xeric Calciargid | 2 | 1 | 1 | 1 | 0 |
| Total | 297 | 100 | 212 | 103 | |
| WY | | | | | |
| Ustic Haplargid | 26 | 46 | 19 | 7 | 100 |
| Ustic Torriorthent | 21 | 37 | 15 | 6 | 83 |
| Badland | 6 | 10 | 5 | 1 | 100 |
| Ustic Paleargid | 2 | 4 | 1 | 1 | 0 |
| Ustic Torrifluent | 2 | 4 | 1 | 1 | 0 |
| Total | 57 | 100 | 41 | 16 | |

^a Total number of pedons per subgroup class.

^b Percent of total observations represented by each subgroup class.

^c Number of pedons in training set per subgroup class.

^d Number of pedons in testing set per subgroup class.

^e Percent of testing set observations correctly classified using the model with highest kappa.

Table 2-2. Classification models used to predict soil subgroup classes in each study area by variable set. An “x” indicates that optimal model parameters were able to be determined from a set of 10 candidate parameters.

| Model | NM | | | | UT | | | WY | |
|--|----|-----|---|---|-----|---|---|-----|---|
| | 1 | 1+2 | 3 | 1 | 1+2 | 3 | 1 | 1+2 | 3 |
| Bagged Classification Tree (BCT) | x | x | x | x | x | x | x | x | x |
| Bi-Directional Self-Organizing Map (BDSOM) | x | x | x | x | x | x | | | |
| Classification Tree (CT) | x | x | x | x | x | x | x | x | x |
| Flexible Discriminant Analysis (FDA) | x | x | x | x | x | x | x | x | x |
| Flexible discriminant analysis using MARS functions (BFDA) | | | | x | x | x | x | x | |
| K Nearest Neighbors (KNN) | x | x | x | x | x | x | x | x | x |
| Learned Vector Quantization (LVQ) | x | | x | x | | x | x | | x |
| Linear Discriminant Analysis (LDA) | x | x | x | x | x | x | x | x | x |
| Linear Discriminant Analysis tuned by number of functions (LDA2) | x | x | x | x | x | x | x | x | x |
| Linear Support Vector Machines (SVML) | x | x | x | x | x | x | x | x | x |
| Multinomial Logistic Regression (MLR) | x | | x | x | | x | x | x | x |
| Nearest Shrunken Centroids (NSC) | x | x | x | x | x | x | x | x | x |
| Neural Networks using Model Averaging (ANNET) | x | x | x | x | x | x | x | x | x |
| Oblique Random Forests based on Linear Support Vector Machines (ORF) | x | x | x | x | x | x | x | x | x |
| Partial Least Squares (PLS) | x | x | x | x | x | x | x | x | x |
| Radial Basis Support Vector Machines (SVMR) | x | x | x | x | x | x | x | x | x |
| Random Forests (RF) | x | x | x | x | x | x | x | x | x |
| Shrinkage Discriminant Analysis (SDA) | | | x | x | | x | x | | x |
| Single-Hidden-Layer Neural Networks (NNET) | x | x | x | x | x | x | x | x | x |
| X-Y Fused Self-Organizing Map (XYSOM) | x | x | x | x | x | x | | | |

Table 2-3. “Most important” variables as selected by random forests for each study area. Numbers in parentheses indicate cell size if variable was derived from a digital elevation model.

| NM | UT | WY |
|---|--|---|
| Multipath wetness index - slope calculated at 35 m ^a | Diffuse insolation (100) | Plan curvature (50) |
| September tasseled cap greenness band | Multi-resolution ridge top flatness (10) | Total curvature (50) |
| Catchment slope (100) | Slope (30) | Diffuse insolation (5) |
| Multi-resolution valley bottom flatness (50) | SAGA wetness index (5) | Diffuse insolation (10) |
| Catchment area (10) | Modified catchment area (5) | Plan curvature (5) |
| September Landsat band ratio 5/7 | Topographic ruggedness index (30) | Catchment slope (10) |
| September GRABS index | | October Landsat band ratio 5/2 ^a |
| Catchment slope (5) | | |
| Catchment area (100) | | |
| Catchment slope (50) | | |

^a variable was part of original cLHS variable set

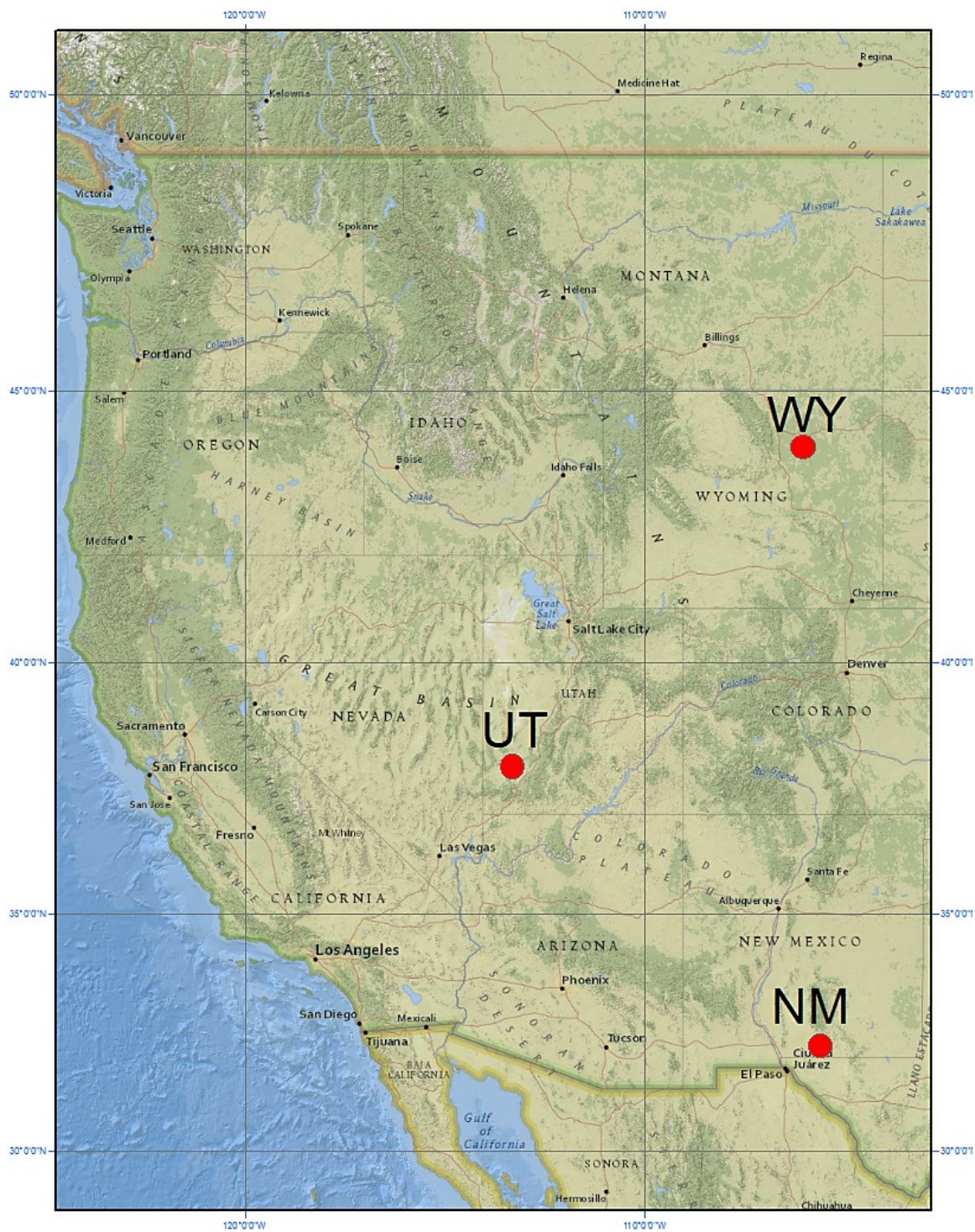


Fig. 2-1. Study area locations in western USA.

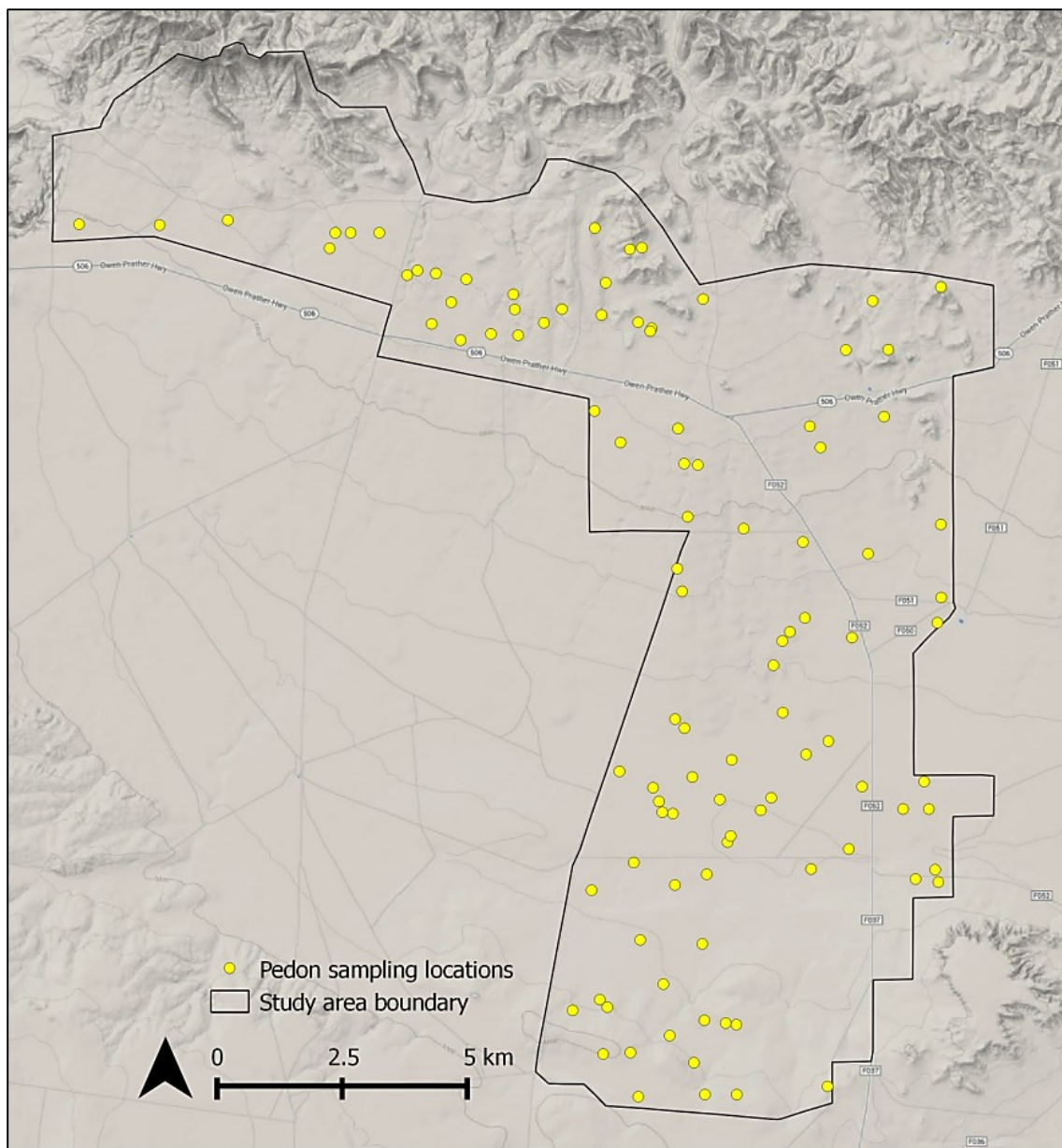


Fig. 2-2. Spatial distribution of pedon observation locations in the NM study area overlain on google physical map. Total number of pedon observations was 103.

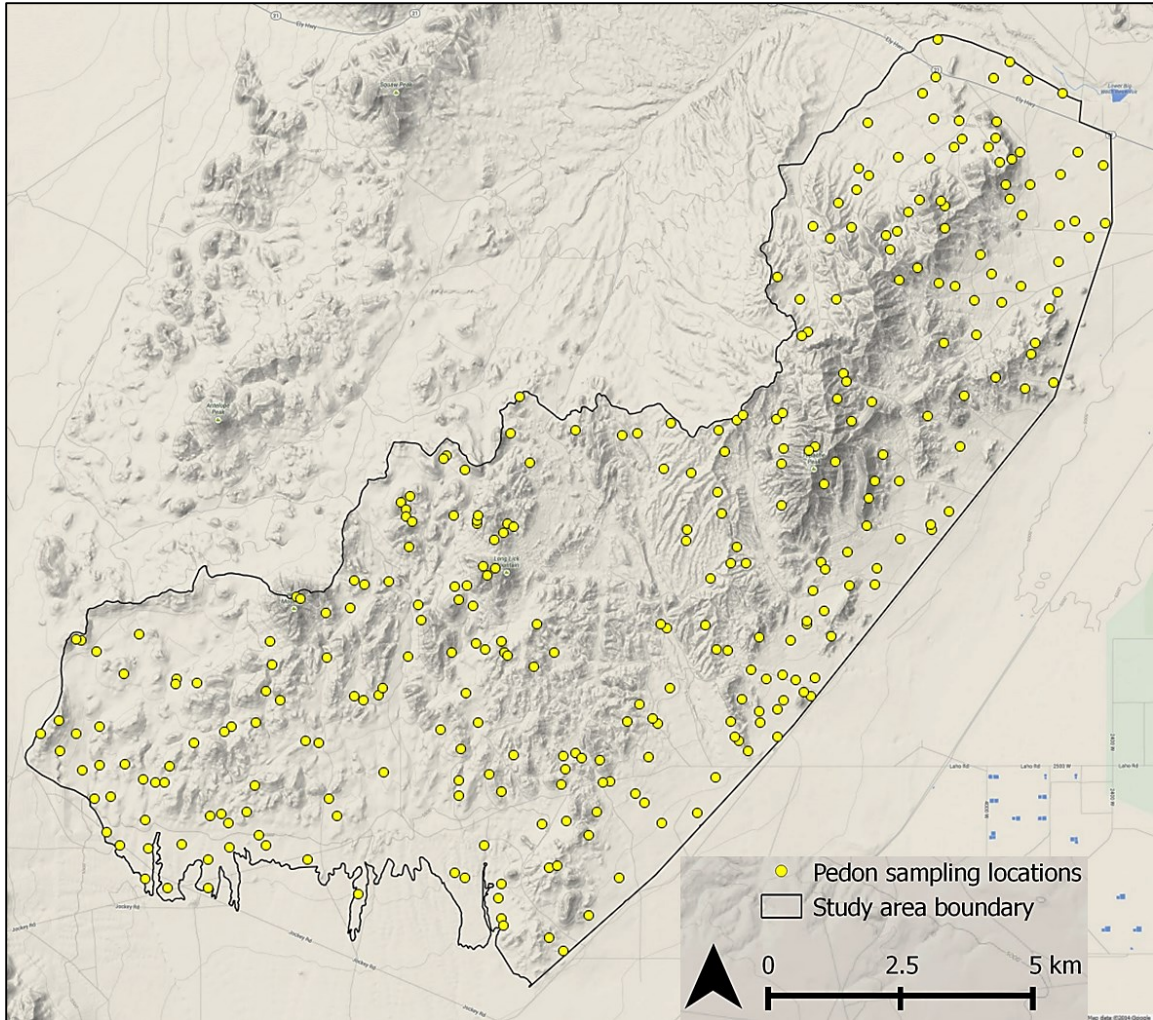


Fig. 2-3. Spatial distribution of pedon observation locations in the UT study area overlain on google physical map. Total number of pedon observations was 297.

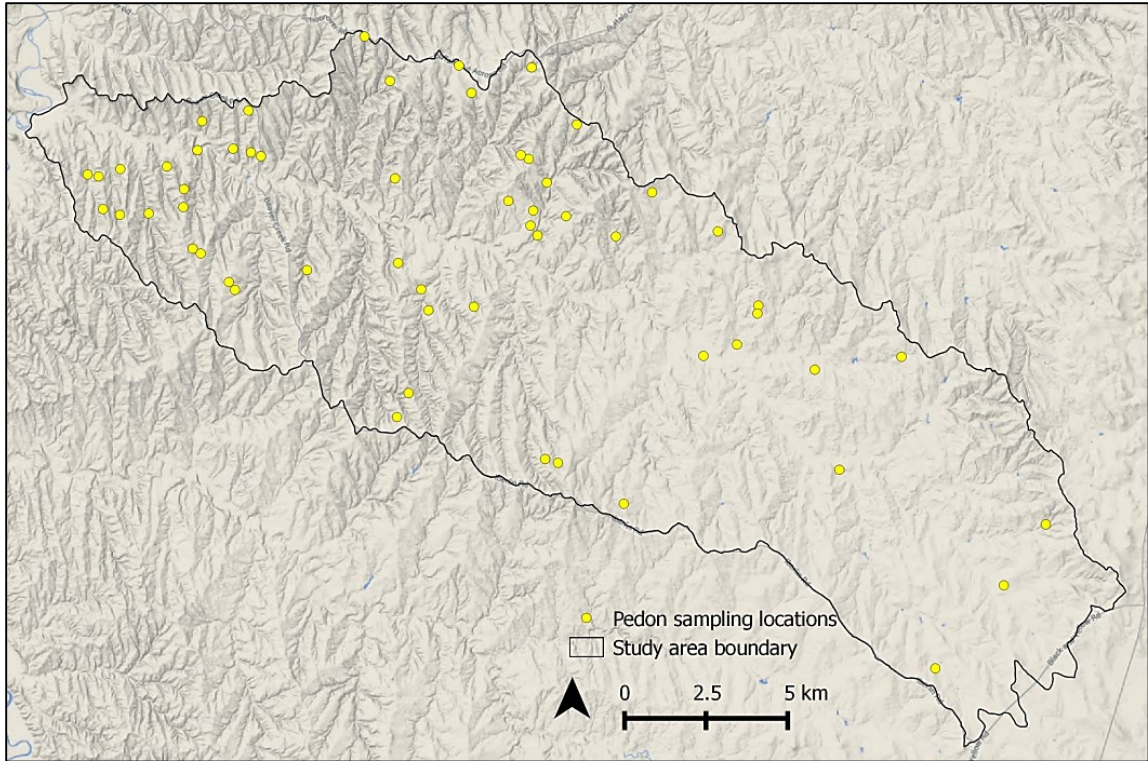


Fig. 2-4. Spatial distribution of pedon observation locations in the WY study area overlain on google physical map. Total number of pedon observations was 57.

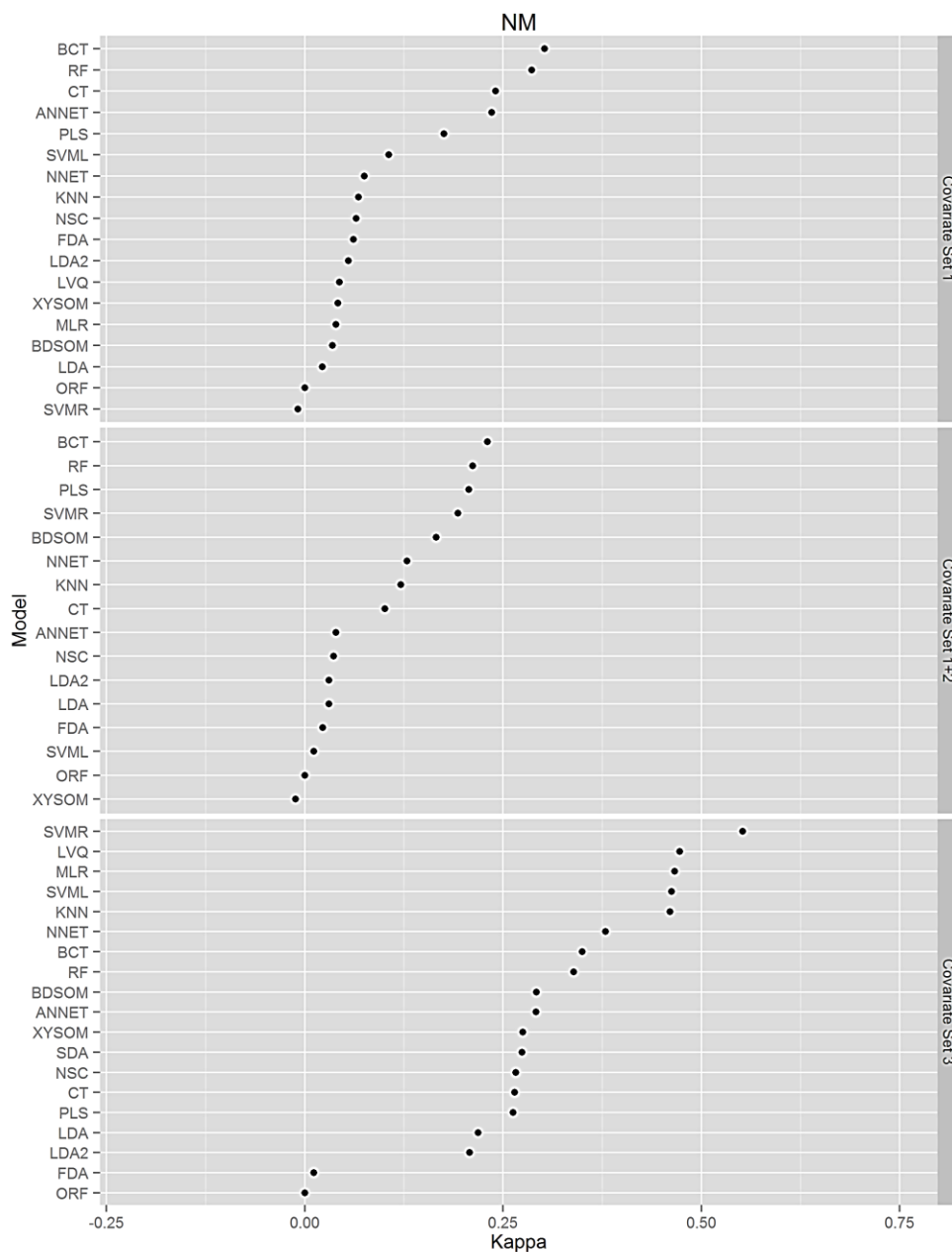


Fig. 2-5. Kappa for the NM study area. Model with highest kappa is the most accurate classifier. Abbreviations are as follows: Bagged Classification Tree (BCT), Bi-Directional Self-Organizing Map (BDSOM), Classification Tree (CT), Flexible Discriminant Analysis (FDA), Flexible discriminant analysis using MARS functions (BFDA), K Nearest Neighbors (KNN), Learned Vector Quantization (LVQ), Linear Discriminant Analysis (LDA), Linear Discriminant Analysis tuned by number of functions (LDA2), Linear Support Vector Machines (SVML), Multinomial Logistic Regression (MLR), Nearest Shrunken Centroids (NSC), Neural Networks using Model Averaging (ANNET), Oblique Random Forests based on Linear Support Vector Machines (ORF), Partial Least Squares (PLS), Radial Basis Support Vector Machines (SVMR), Random Forests (RF), Shrinkage Discriminant Analysis (SDA), Single-Hidden-Layer Neural Networks (NNET), X-Y Fused Self-Organizing Map (XYSOM).

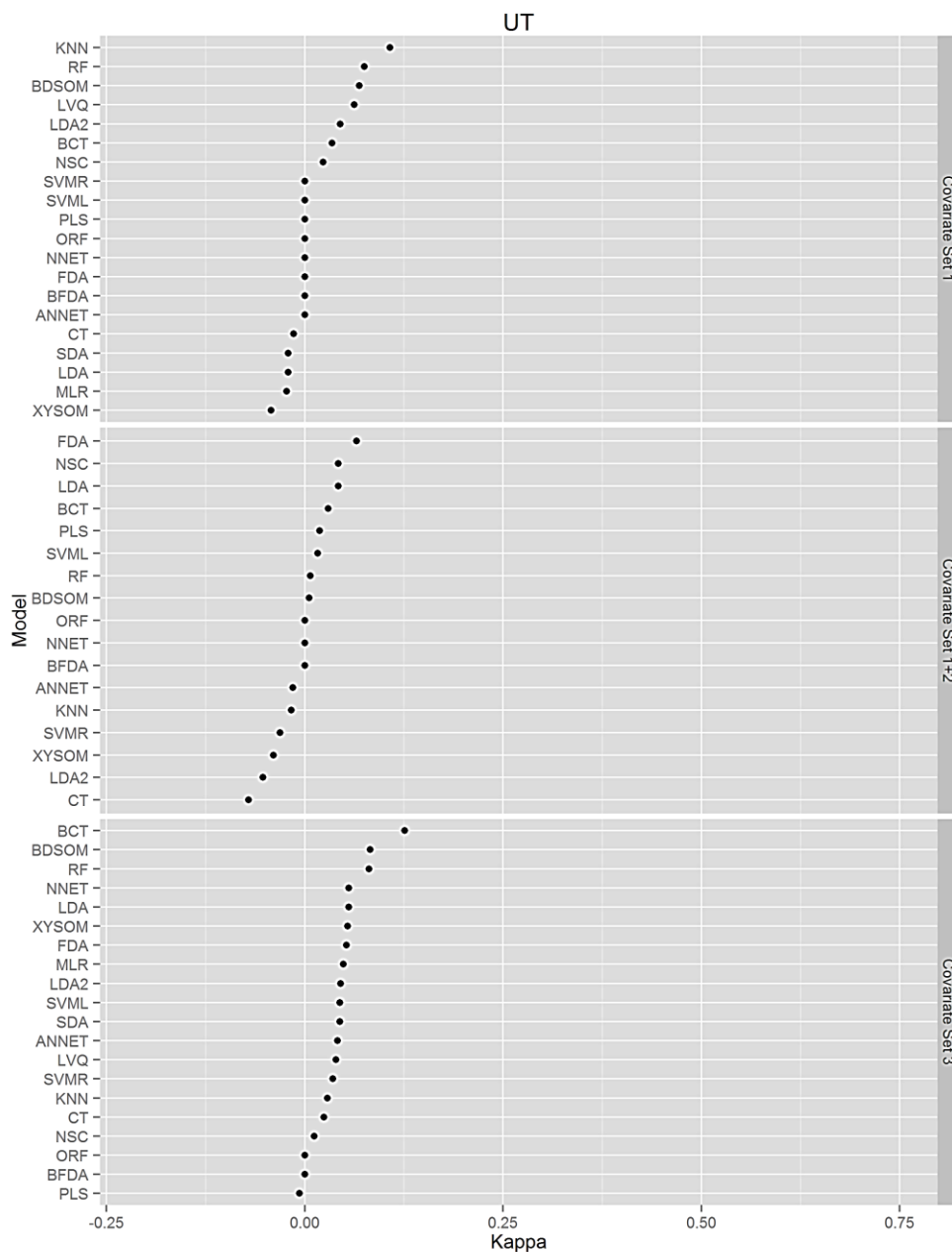


Fig. 2-6. Kappa for the UT study area. Model with highest kappa is the most accurate classifier. Abbreviations are as follows: Bagged Classification Tree (BCT), Bi-Directional Self-Organizing Map (BDSOM), Classification Tree (CT), Flexible Discriminant Analysis (FDA), Flexible discriminant analysis using MARS functions (BFDA), K Nearest Neighbors (KNN), Learned Vector Quantization (LVQ), Linear Discriminant Analysis (LDA), Linear Discriminant Analysis tuned by number of functions (LDA2), Linear Support Vector Machines (SVML), Multinomial Logistic Regression (MLR), Nearest Shrunken Centroids (NSC), Neural Networks using Model Averaging (ANNET), Oblique Random Forests based on Linear Support Vector Machines (ORF), Partial Least Squares (PLS), Radial Basis Support Vector Machines (SVMR), Random Forests (RF), Shrinkage Discriminant Analysis (SDA), Single-Hidden-Layer Neural Networks (NNET), X-Y Fused Self-Organizing Map (XY SOM).

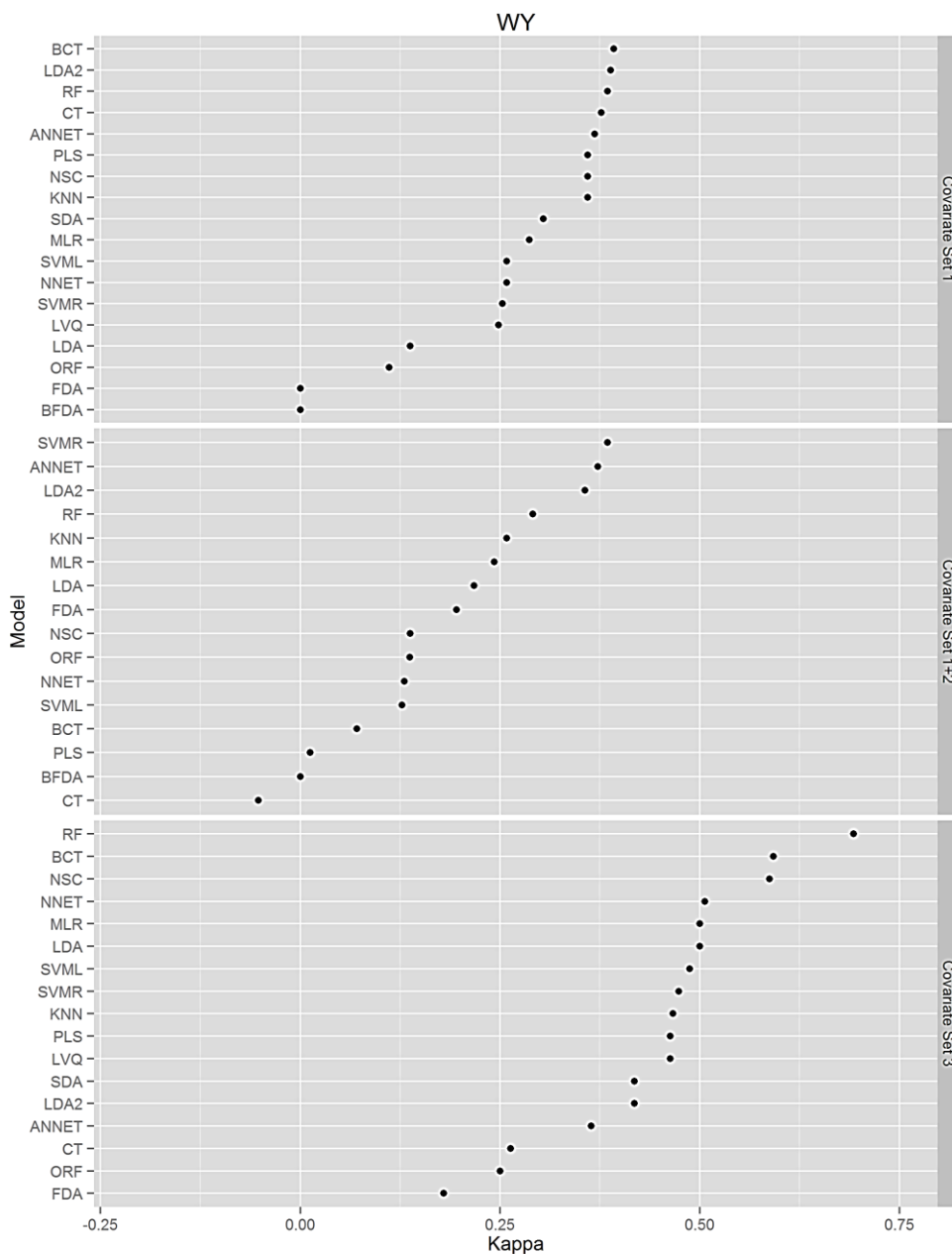


Fig. 2-7. Kappa for the WY study area. Model with highest kappa is the most accurate classifier. Abbreviations are as follows: Bagged Classification Tree (BCT), Bi-Directional Self-Organizing Map (BDSOM), Classification Tree (CT), Flexible Discriminant Analysis (FDA), Flexible discriminant analysis using MARS functions (BFDA), K Nearest Neighbors (KNN), Learned Vector Quantization (LVQ), Linear Discriminant Analysis (LDA), Linear Discriminant Analysis tuned by number of functions (LDA2), Linear Support Vector Machines (SVML), Multinomial Logistic Regression (MLR), Nearest Shrunken Centroids (NSC), Neural Networks using Model Averaging (ANNET), Oblique Random Forests based on Linear Support Vector Machines (ORF), Partial Least Squares (PLS), Radial Basis Support Vector Machines (SVMR), Random Forests (RF), Shrinkage Discriminant Analysis (SDA), Single-Hidden-Layer Neural Networks (NNET), X-Y Fused Self-Organizing Map (XYSOM).

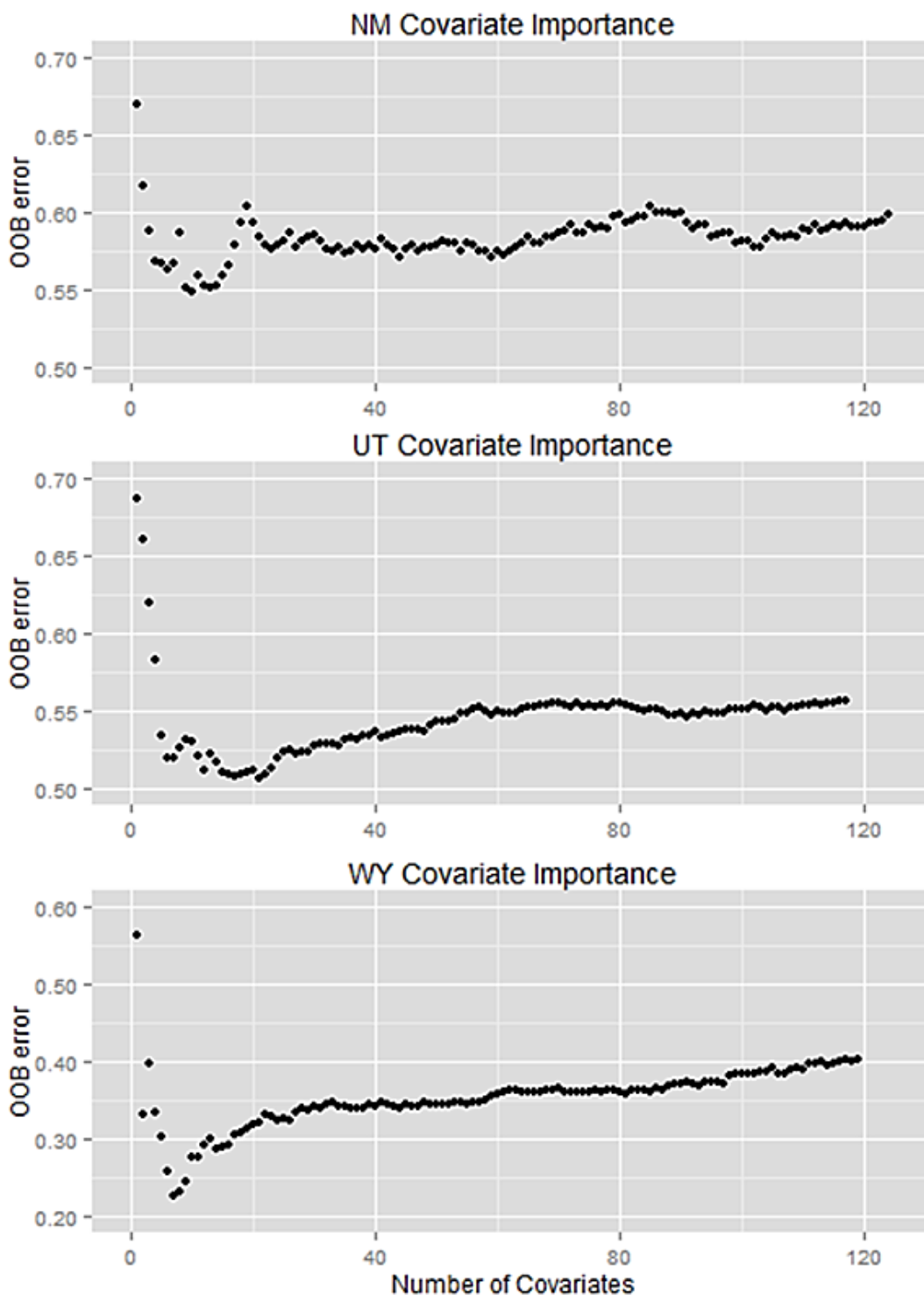


Fig. 2-8. Variable importance as represented by out of bag (OOB) error (misclassification error) using random forests. Random forests models were begun with the total available variables and the least important variable was iteratively removed. The set of “most important variables” were selected as those variables that returned the lowest OOB error and which had the fewest variables.

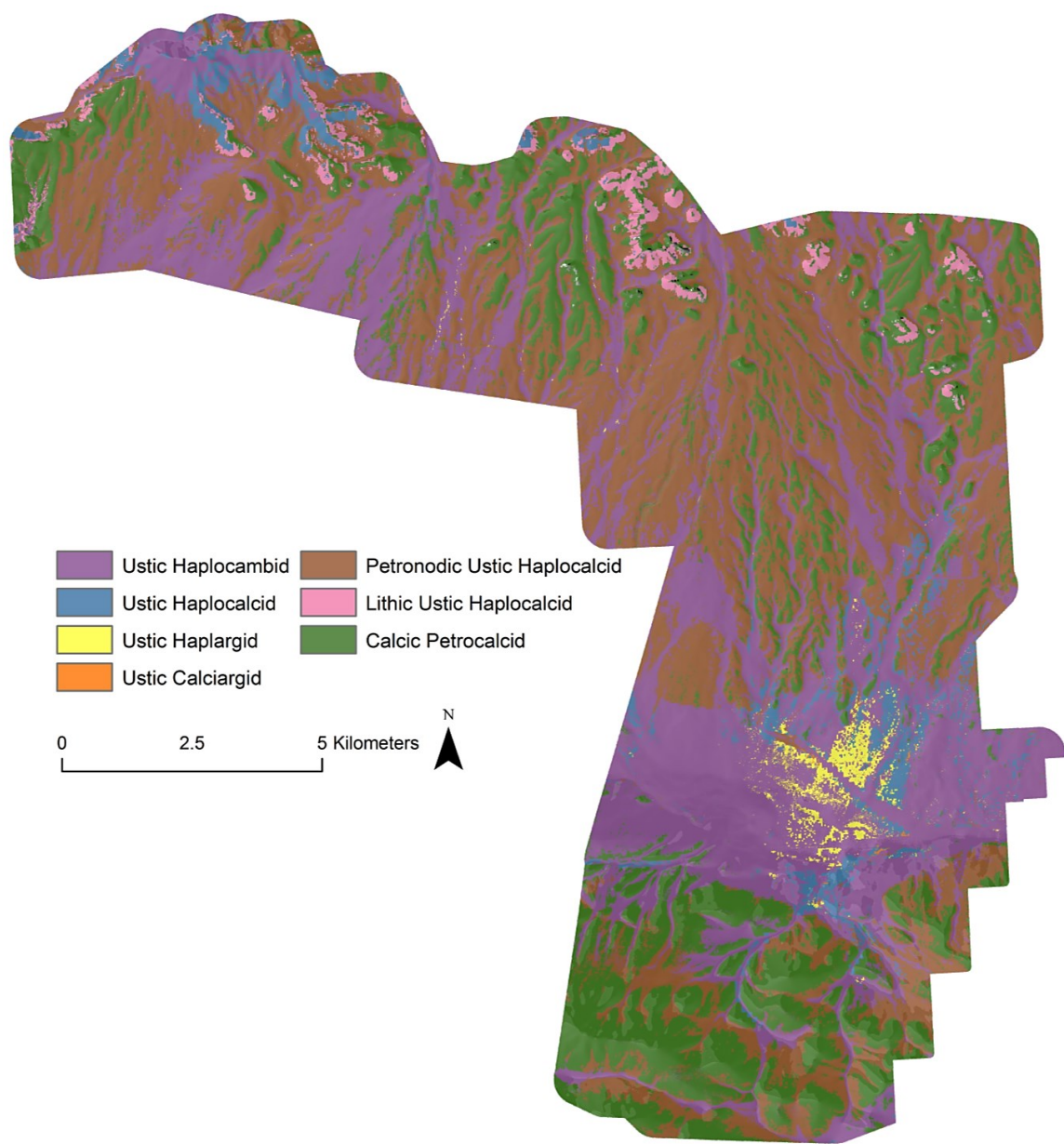


Fig. 2-9. Spatial predictions of subgroup classes for the NM study area using radial basis support vector machines (SVMR) overlain on an image of aspect. Only major subgroups visible at this scale are shown (7 of 10 subgroups).

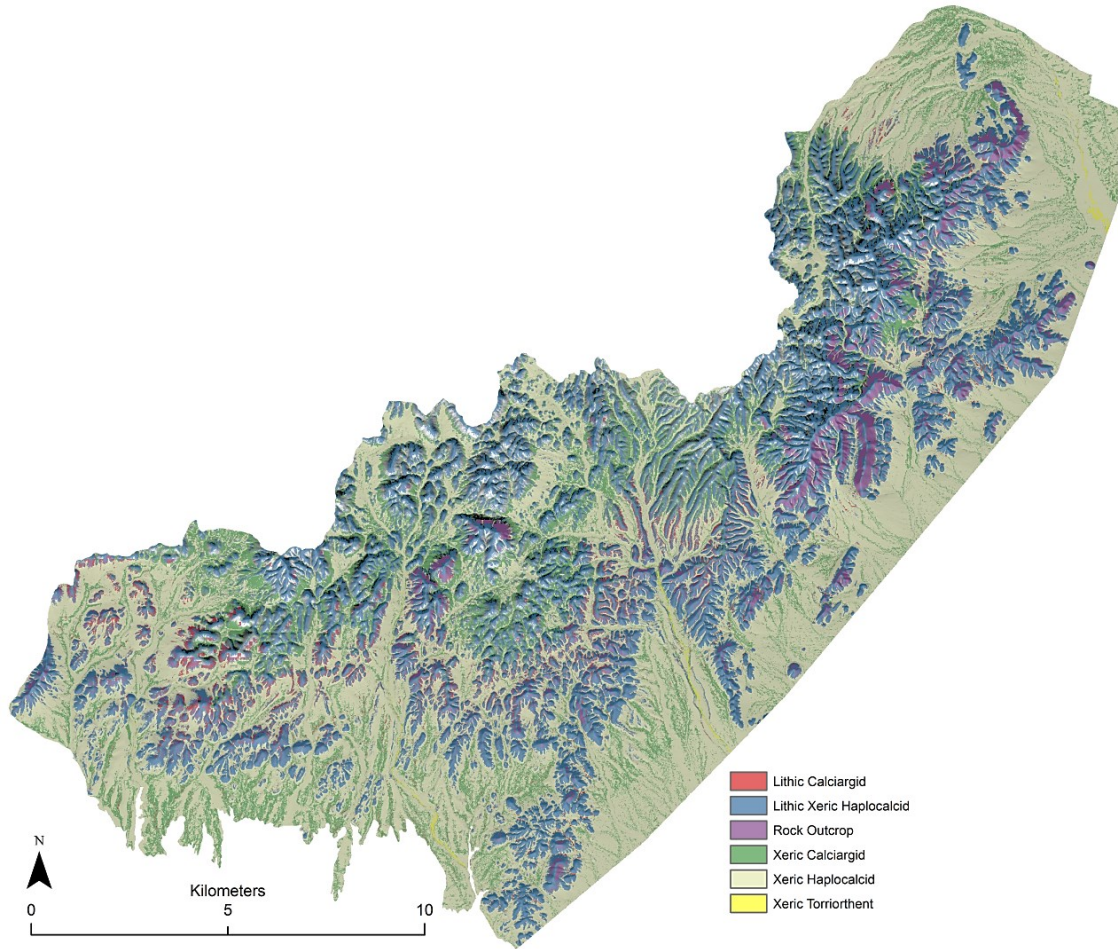


Fig. 2-10. Spatial predictions of subgroup classes for the UT study area made using a bagging classification tree (BCT) overlain on a hillshade. Only major subgroups visible at this scale are shown (6 of 15 subgroups).

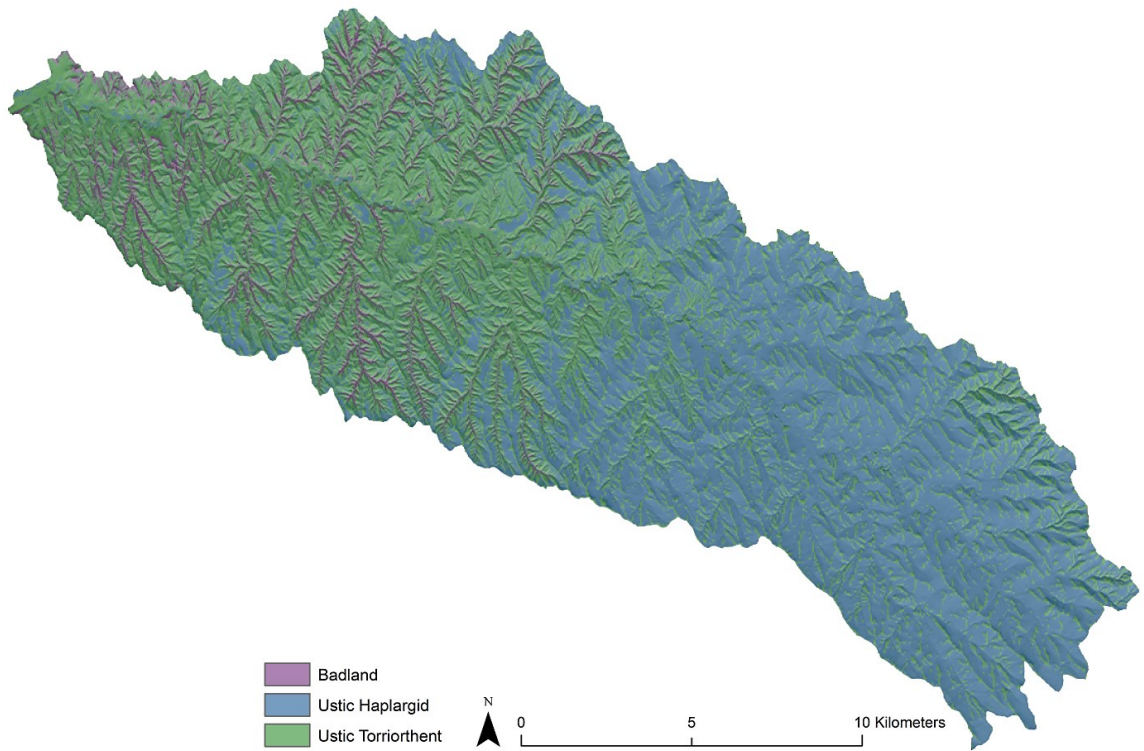


Fig. 2-11. Spatial predictions of subgroup classes for the WY study area made using random forests (RF) overlain on a hillshade. Only major subgroups visible at this scale are shown (3 of 5 subgroups).

CHAPTER 3

SPATIAL PREDICTIONS OF POTENTIAL BIOLOGICAL SOIL CRUST LEVEL OF DEVELOPMENT CLASSES
AROUND CANYONLANDS NATIONAL PARK**Abstract**

Biological soil crusts (BSC) are key components of arid and semi-arid ecosystems, but are susceptible to surface disturbance. Surface disturbance is often a direct result of land use practices, thus it would be useful to understand how past disturbance has affected potential BSC distribution. Potential BSC (BSC in the absence of major soil surface disturbance) could be inferred from undisturbed areas. Canyonlands National Park is one of the best available areas on the Colorado Plateau to assess potential BSC development. Biological soil crust distribution depends upon climate and soil properties which can be represented by spatially explicit biophysical environmental covariates derived from remote sensing and terrain analysis. The objectives of this study were to use BSC observations from Canyonlands National Park and environmental covariates to predict potential BSC distribution over approximately 8300 km² surrounding Canyonlands National Park.

Biological soil crust observations from Canyonlands National Park were obtained from a recent soil survey update. Observations consisted of seven level-of-development (LOD) classes representing a BSC development sequence. The seven LOD classes were combined into three broad LOD classes: low, moderate and high. Abiotic environmental covariates representative of soil properties and microclimate effects influencing BSC distribution were derived from Landsat 7 ETM+ imagery and a 30 m digital elevation model. Stochastic gradient boosting, random forests and logistic regression models were compared for LOD class prediction.

Moderate BSC LOD class distribution was predicted with reasonable accuracy. Although predicted spatial patterns of the low and high LOD classes appear plausible, poor accuracy metrics indicate that spatial predictions of these classes may not be reliable. Prediction accuracy

of all LOD classes could likely be improved through the use of additional covariates. Spatial predictions of LOD classes may be useful for assessing the impact of past land uses on biological soil crusts. Spatially explicit covariates related to soil/geological type and slope are the most important covariates for predicting potential BSC LOD classes.

1. Introduction

Biological soil crusts are communities of cyanobacteria, microfungi, lichens and mosses that form at the soil surface (Belnap et al., 2001). In arid and semi-arid areas they stabilize soil, reduce wind and water erosion, and are important sources of soil N and organic C (Belnap, 2002; Belnap and Gillette, 1998; Bowker and Belnap, 2008).

Because they occur at the soil surface, biological soil crusts (BSCs) are susceptible to disturbance from a number of sources including livestock grazing, off-road vehicle traffic, mining exploration, and other natural and anthropogenic dynamics (Belnap and Eldridge, 2003; Belnap et al., 2001; Kuske et al., 2012). Recovery of BSCs following disturbance depends upon the type, severity and timing of the disturbance as well as the physical environment, but recovery times on the Colorado Plateau for cyanobacteria are around 40 years; recovery of lichens and mosses can be significantly longer (Belnap, 1993; Belnap and Eldridge, 2003)

Because recovery from disturbance is a lengthy process and because surface disturbance is often a direct result of land use practices, it would be useful to understand the impact of different land use practices on the spatial distribution of BSCs. Understanding land use impacts on BSCs requires knowing both the actual and potential BSC cover in a given area (Bowker et al., 2006a). Actual (existing) BSC cover can be obtained by field observation. Potential BSC cover (biological soil crust in the absence of surface disturbance) must either be observed before surface disturbance occurs or inferred from undisturbed areas. Canyonlands National Park has been protected from livestock grazing and mineral exploration for about 50

years (1964 - 2014), potentially long enough for the influences of past disturbance on cyanobacteria dominated BSCs to be significantly reduced (Belnap, 1993), making it one of the best available areas on the Colorado Plateau to assess potential cyanobacteria dominated BSC development in the absence of major soil surface disturbance.

The spatial distribution of biological soil crusts (BSCs) depends upon climate and soil properties. The timing and magnitude of precipitation, temperature, and potential evapotranspiration are the main controls of regional scale differences in BSC structure and composition (Belnap et al., 2001; Rosentreter and Belnap, 2003). Soil physical and chemical properties as well as topography (slope and aspect) control differences in BSC development and composition at local and landscape scales (Belnap et al., 2001; Rosentreter and Belnap, 2003). On the Colorado Plateau, soil texture, mineralogy (in particular gypsum and CaCO_3 concentrations) and depth are the most important soil properties influencing BSC development and distribution (Bowker and Belnap, 2008; Bowker et al., 2006b). Soils on the arid to semi-arid Colorado Plateau are weakly developed, and soil properties generally reflect their geologic origins. Thus, geologic type may also be a factor influencing BSC development (Bowker and Belnap, 2008).

Spatially explicit quantitative environmental covariates derived from remote sensing and terrain analysis (McBratney et al., 2003; McKenzie and Ryan, 1999) can represent many of the factors which influence the spatial distribution of BSCs. For example regional climate can be estimated using gridded spatial climate datasets such as PRISM (PRISM Climate Group, Oregon State University, <http://www.prism.oregonstate.edu/mtd/>) or DAYMET (Daily Surface Weather and Climatological Summaries, <http://daymet.ornl.gov/>). Landscape scale microclimate can be approximated by potential solar radiation (Beaudette and O'Geen, 2009). Digital elevation models can be used to calculate slope and aspect. Soil maps can represent soil properties

(Bowker et al., 2006b; Brungard and Boettinger, 2012). In the absence of soil maps remote sensing can infer geologic types (Nield et al., 2007; Stum et al., 2010) and thus serve as proxies for soil properties.

The level of cyanobacteria development in BSCs strongly influences BSC structure and function (Belnap, 2002; Belnap et al., 2008; Housman et al., 2006) and surface hydrology (Belnap et al., 2013). The level of cyanobacteria development in BSCs can be identified using level-of-development classes (Belnap et al., 2008). Level-of-development (LOD) classes represent a development sequence and range from Class 1 to Class 6, with LOD Class 1 the least developed and LOD Class 6 the most developed. During a recent (2006-2009) soil survey update of Canyonlands National Park, U.S. Department of Agriculture - Natural Resources Conservation Service (USDA-NRCS) soil surveyors recorded LOD class observations at many locations.

Because surface disturbance has a significant influence on BSC distribution, but knowledge of the spatial distribution of BSC potential on the Colorado Plateau is limited, our objectives were to produce spatial estimates of BSC potential. Specifically we hypothesized that BSC LOD class observations from soil survey data collected within Canyonlands National Park and environmental covariates representing the factors controlling BSC distribution could be used to accurately predict potential BSC LOD classes to a larger area surrounding Canyonlands National Park. Our ultimate goal is to provide land managers with a tool to compare potential BSC LOD classes with observations of existing BSC LOD classes to assess the impacts of land use and surface disturbance on ecosystem health.

2. Methods

2.1 Study area

Canyonlands National Park (CNP) covers approximately 1370 km² and is dissected by the Green and Colorado Rivers, which converge at the center of the park (Fig. 3-1). Average annual

temperature is 11.6 °C and average annual precipitation is 228.6 mm (Western Regional Climate Center, <http://www.wrcc.dri.edu/cgi-bin/cliMAIN.pl?ut1163>). Elevation in CNP ranges between approximately 1130 m and 2190 m.

Soil development in CNP is often minimal because of the arid environment and the bedrock controlled landscape; thus, soil properties are often highly dependent upon the underlying geology. Geology in CNP consists mostly of highly eroded, interbedded sandstone and shale, but areas of limestone and mudstone also exist (Baars, 2003). Areas of windblown sand, rock fall debris, and alluvial deposits also occur (Billingsley et al., 2002).

Vegetation consists of grasses, shrubs, and trees common to the Colorado Plateau including galleta (*Hilaria jamesii*), indian ricegrass (*Stipa hymenoides*), basin big sagebrush (*Artemisia tridentata* var. *tridentata*), Bigelow's sagebrush (*Artemisia bigelovii*), blackbrush (*Coleogyne ramosissima*), four-wing saltbush (*Atriplex canescens* var. *canescens*), graystem rabbitbrush (*Chrysothamnus nauseosus* var. *gnaphalodes*), green ephedra (*Ephedra viridis* var. *viridis*), two-needle pinon (*Pinus edulis*), Utah juniper (*Juniperus osteosperma*), and Gambel's oak (*Quercus gambelii* var. *gambelii*) (Tendick et al., 2012). Adjacent to the rivers riparian vegetation such as Fremont cottonwood (*Populus fremontii*), coyote willow (*Salix exigua*) and tamarisk (*Tamarix spp.*) exist (Tendick et al., 2012).

A study area including and surrounding CNP was designated based on the similarity of geology and elevation. The area covered by all geologic units that occurred inside CNP was identified using a 1:500,000 geology map (Hintze et al., 2000). This area was then clipped to the same elevation range as inside CNP using the values from a 30-m digital elevation model (DEM, section 2.4). This resulted in a study area of approximately 8300 km².

2.2 Biological soil crust observations

Observations of BSC level-of-development (LOD) classes (Belnap et al., 2008) were obtained from a recent (2006-2009) soil survey update of Canyonlands National Park (CNP). Observations consisted of the six BSC LOD classes (Fig. 3-2) and observations of BSC absence (class 0), for a total of seven classes. At each location the dominant LOD crust class in an approximately 20 m² area was recorded (*personal communication* Cathy Scott, project leader for Canyonlands soil survey update). There were a total of 954 BSC LOD class observations inside CNP (Fig. 3-1).

Previous spatial modeling of individual LOD classes inside CNP showed significant confusion between similar LOD classes (Brungard and Boettinger, 2012). Consequently, the seven LOD classes were combined into three broad LOD classes (Table 3-1): low, moderate and high (Table 3-1). Class combination was based on the ecohydrological characteristics of individual LOD classes identified by Belnap et al. (2013), who found that LOD class 1 had the lowest infiltration and most runoff while LOD classes 5 and 6 had the greatest infiltration and lowest runoff. Level-of-development classes 2, 3, and 4 were similar to each other and had intermediate run off and infiltration rates. These combined LOD classes were likely similar to the BSC classes used by Belnap and Gillette (1997) for assessing potential wind erosion on the Colorado Plateau.

The low class in this study is a combination of LOD classes 0 and 1 and represents both the absence of biological soil crust (class 0) as well as very weakly developed cyanobacteria crusts (class 1). The moderate class is a combination of LOD classes 2, 3, and 4, and represents moderately developed cyanobacteria crusts. The high class is a combination of LOD classes 5 and 6. Although LOD class 6 indicates very well developed cyanobacteria-dominated crust or a well-developed lichen-moss crust often associated with calcareous and gypsiferous soils

(*personal communication* J. Belnap), the few observations of LOD class 6 required its combination with LOD class 5.

2.3 Environmental covariates

Environmental covariates representative of soil, landscape and microclimate factors related to BSC development at the landscape level (Bowker et al., 2006a; Bowker et al., 2006b) were derived from Landsat 7 ETM+ imagery and a 30 m digital elevation model (DEM) (Table 3-2). Only abiotic covariates were chosen in an effort to reduce the influence of potential vegetation disturbance in areas outside of CNP.

Normalized band ratios were generated from two atmospherically corrected (Chavez, 1996) and mosaicked Landsat 7 ETM+ images acquired in June 2000. A normalized band ratio (NBR) was defined as:

$$NBR = \frac{b_1 - b_2}{b_1 + b_2}$$

where b_1 and b_2 are individual bands from the Landsat 7 ETM+ sensor that represent different portions of the electromagnetic spectrum. Individual bands used in normalized band ratios were band 7 (short wave infrared [2.09-2.35 μm]), band 5 (short wave infra-red [1.55-1.75 μm]), band 2 (green) and band 1 (blue). Normalized band ratios 5/7, 5/2, and 5/1 were used to discriminate between different geologic types (Inzana et al., 2003; Nield et al., 2007; Stum et al., 2010).

Digital elevation model derivatives used to represent potential microclimate were generated from a 30 m DEM, which was derived by resampling a 5 m DEM to 30 m (Utah Automated Geographic Reference Center, 2013). Elevation was used as a proxy for potential precipitation and temperature (Bowker et al., 2006a); higher elevations are normally correlated with higher precipitation and lower temperature. Yearly diffuse potential solar radiation, potential direct solar radiation, and the duration of potential solar radiation were used as

measures of microclimate; greater solar radiation was expected to increase soil temperatures and decrease soil moisture. Soil maps were important covariates for predicting BSC LOD classes inside CNP (Brungard and Boettinger, 2012), but soil maps were not used as covariates in this study, because much of the area outside of CNP does not have publically available soil maps.

2.4 Model building and analysis

Stochastic gradient boosting (De'ath, 2007; Moisen et al., 2006), random forests (Cutler et al., 2007; Peters et al., 2007) and logistic regression were compared for predicting potential LOD classes. All modeling, analysis and prediction was performed using the caret (Kuhn, 2013) and raster (Hijmans, 2014) packages in R statistical software (R Core Team, 2013). Because stochastic gradient boosting in the R statistical software is implemented only for a two class problem (random forests and logistic regression can use dependent variables with more than two classes), BSC LOD observations were treated as presence-absence observations, and a one-versus-all approach was taken. Each class (coded as 1) was modeled against all other classes (each coded as zero). This was repeated for the remaining LOD classes, resulting in nine separate models (three for each LOD class).

2.4.1 Stochastic gradient boosting

Stochastic gradient boosting (SGB) is a sequence of bagged (sampling with replacement) classification trees, with successive trees built using re-weighted versions of the data (De'ath, 2007). For each tree, observations are classified based on the current sequence of trees and the classification error calculated. Classification error is then used to weight observations in the next tree in the sequence. Thus increasing the chance that incorrectly classified observations will be correctly classified in the next tree. The final classification of each observation is determined by the weighted majority of classification across the sequence of trees (De'ath, 2007). Accurate

classification depends upon three tuning parameters: the number of trees (*ntree*), the number of nodes in each tree (*depth*), and a learning rate that avoids sub-optimal models (*shrinkage*). The improvement in classification error attributed to each covariate is summed within each tree and averaged across the entire ensemble to yield an estimate of covariate importance (Kuhn and Johnson, 2013).

2.4.2 Random forests

Random forests (RF) is an ensemble (forest) of bagged classification trees (typically 500 to 1000). In contrast to SGB, RF classification trees are independent and the classification of samples does not depend upon previous trees in the ensemble. For each tree, decision nodes are split using a random subset of available covariates, resulting in low correlations between trees. RF has two required tuning parameters: the number of covariates tried at each node (*mtry*) and the number of trees in the forest (*ntree*). The *mtry* parameter must be optimized for accurate classification, whereas RF is not highly sensitive to *ntree* values greater than the default (500). Classification of a new sample is the majority vote of the ensemble. Classification probability of a new sample is the proportion of the forest that classifies each observation into the class of interest (Kuhn and Johnson, 2013). Covariate importance is estimated by randomly permuting the values of each covariate one at a time for each tree. The difference in predictive performance between the original sample and the permuted sample when aggregated across the entire forest is an indication of the importance of that covariate (Kuhn and Johnson, 2013).

2.4.3 Logistic regression

Logistic regression (LR) is a member of the family of generalized linear models and is used when the response variable is a categorical variable (Kempen et al., 2009). The probability that individual observations belong to the class of interest is modeled using the relationship

between the log of the odds ratio and a linear combination of covariates (Kempen et al., 2009; Kuhn and Johnson, 2013).

2.4.4 Model training and testing

Observations of the low ($n = 353$) and moderate ($n = 490$) crust LOD classes were split into training (about 80%) and testing (about 20%) datasets (Table 3-1, Fig. 2-1). The training dataset was used for model construction and the testing dataset was used to test model accuracy for low and moderate LOD classes. Splitting observations into training/testing sets is a common practice for predicting other soil-related attributes (e.g., soil depth, Tesfa et al., 2009). Because relatively fewer observations existed for the high LOD class ($n = 111$), it was anticipated that splitting observations into separate training and testing datasets would result in too few observations for accurate model training; thus, all high LOD class observations were used for model construction. Estimates of model accuracy for the high LOD class were derived using bootstrap sampling repeated 100 times. Bootstrap sampling is sampling with replacement and divides a given dataset into two parts referred to as in-bag and out-of-bag samples. The in-bag sample is the same size as the original dataset (some observations are sampled more than once while other observations are not sampled). Out-of-bag samples (those samples not used in model construction, about 30% of the data) are used to assess model accuracy (Kuhn and Johnson, 2013).

2.4.5 Model tuning and accuracy

Bootstrap sampling repeated 100 times was used to test multiple sets of required tuning parameters for SGB (*ntree*, *depth*) and RF (*mtry*). Default values for SGB *shrinkage* (0.01) and RF *ntree* (500) parameters were used. Logistic regression had no required tuning parameters. The tuning parameters that returned the highest area under the receiver operator characteristic

curve (AUC) for each model were selected as optimal (Table 3-3). Receiver operating characteristic curves (ROC) are useful for assessing model performance when two classes exist (Fielding and Bell, 1997; Moisen et al., 2006; Zweig and Campbell, 1993). Accurate models will have an AUC near 1 and poor models will have an AUC near 0.5 (Moisen et al., 2006).

Model accuracy was quantified with AUC, sensitivity, and specificity. Sensitivity (or true positive rate) is the proportion of observed presences that are predicted as presences, and as such, is the probability that the model will correctly classify a presence (Allouche et al., 2006; Kuhn and Johnson, 2013; Moisen et al., 2006). Conversely, specificity (or true negative rate) is the proportion of observed absences that are predicted as absences, and as such, is the probability that the model will correctly classify an absence (Allouche et al., 2006). Sensitivity quantifies errors of omission, specificity quantifies errors of commission (Allouche et al., 2006). Sensitivity and specificity range between 0 and 1, with values closer to one indicating better classification. Multiple models are equal in overall model performance if sensitivity and specificity are equal between models (Allouche et al., 2006).

For the low and moderate LOD classes, AUC, sensitivity, specificity, were calculated by classifying the test dataset. For the high LOD class, which lacked a separate test dataset, sensitivity, specificity, and AUC were taken as the mean value from bootstrap sampling used during model optimization.

Model accuracy for the moderate LOD class was also assessed using an independent validation set of 11 LOD class observations (Table 3-1, Fig. 3-1). These observations were from fenced exclosures, built between 1957 and 1978, which excluded livestock, and in some cases, deer and elk. These exclosures were the only known areas outside of CNP which have been excluded from major soil surface disturbance for approximately the same length of time as CNP.

Brier scores were used to assess model accuracy at these locations (Brier, 1950; Mason, 2004).

For a binary response variable, the Briar score (BS) is:

$$BS = \frac{1}{N} \sum_{t=1}^N (f_t - O_t)^2$$

where N is the number of locations being predicted as a particular class, f_t is the predicted probability of a particular class at the observation location, and O_t is the actual class observation (0 if not the predicted class of interest, 1 if the predicted class of interest). Models that predict a high probability of the actual observed class will have a low Brier score and be considered the most accurate model.

Visual assessment of BSC LOD spatial prediction was used to evaluate the ability of each model to predict meaningful spatial patterns. In the absence of clear differences in model accuracy metrics and predicted spatial patterns between models, the model with the highest sensitivity was chosen as the most accurate model for each LOD class.

2.4.6 Spatial prediction

Spatial prediction of potential LOD classes to the larger area surrounding Canyonlands National Park was accomplished by applying the most accurate of each LOD class to the environmental covariates covering the study area. This resulted in spatial predictions (maps) of potential LOD class probabilities. Pixel values in each map represented LOD class probability of occurrence. The final LOD class map was created by stacking predicted probability maps and identifying the LOD class with the highest probability of occurrence at each pixel. Prediction confidence was taken as the specific probability value associated with the identified class at each pixel. Pixels with higher probability values indicated greater confidence in the final LOD classification at each pixel.

2.4.7 Variable importance

For LOD classes where SGB or RF was deemed the most accurate model, covariate importance was taken directly from the variable importance scores of these models. For LOD classes where LR was the most accurate model, variable importance was estimated using the AUC as there are no internal variable importance measures for LR. In this case each covariate was used in place of predicted probabilities to calculate the AUC. If a covariate could perfectly separate the classes there would be a cutoff value for the covariate that would achieve an AUC of 1 and irrelevant covariates would have a AUC of 0.5 (Kuhn and Johnson, 2013). Because variable importance scores from different model types are reported on different scales, all variable importance scores were standardized to fall in the range 0 to 1 for between model comparisons.

3. Results and discussion

3.1 Modeling

The low LOD class was poorly predicted by all models, indicated by sensitivity < 0.5 and specificity around 0.9. No one model was a significantly better predictor of the low LOD class (Table 3-4). However, RF was chosen to produce spatial predictions for the low LOD class because sensitivity was slightly higher and spatial predictions did not reveal any significantly erroneous patterns.

No single model was a significantly better predictor of the moderate LOD class (Table 3-4). Sensitivity, specificity and AUC were similar between models, and were all about 0.7. However, given the high spatial variability of LOD classes and the large spatial extent over which LOD classes were observed, we considered models with sensitivity and specificity values of 0.7 to be highly accurate. This suggests that moderate LOD class spatial predictions are reliable. Although relatively high sensitivity values suggested that SGB was the most accurate model for

predicting the moderate LOD class (Table 3-4), Brier scores from the independent validation dataset (0.140, 0.124, 0.095, for SGB, RF, and LR, respectively) indicated that LR may be a more accurate classifier. Thus, LR was chosen to produce spatial predictions of the moderate LOD class.

The high LOD class was the least accurately modeled LOD class (Table 3-4). AUC for LR was 0.53, indicating that the LR model was only slightly better than a random classifier. Although AUC values for both SGB and RF were similar to those for the moderate LOD class (both were approximately 0.7, Table 3-4), AUC values for the high LOD class reflect the large imbalance between sensitivity and specificity. Sensitivity was close to or equal to zero, while specificity was close to or equal to one. Sensitivity values indicate that presence observations were almost never correctly classified, regardless of the model used. Sensitivity values indicate that all models were able to correctly classify absence observations most of the time. Low sensitivity and high specificity is likely because the high LOD class is only associated with specific soil properties which may not have been adequately captured by the chosen environmental covariates. Visual inspection of predicted probabilities revealed that only SGB predicted any pixels with probabilities > 0 . As SGB also had a slightly higher sensitivity than the other models, SGB was chosen to produce final predictions. Spatial predictions of the high LOD class are not anticipated to be highly accurate.

Model accuracy could potentially be improved through the use of additional environmental covariates such as the grain size index (Xiao et al., 2006), climatic parameters (e.g. PRISM climate surfaces, <http://www.prism.oregonstate.edu/>), or spatial predictions of specific soil properties (e.g surface texture) from digital soil mapping (McBratney et al., 2003; Sanchez et al., 2009). Detailed soil maps were the strongest predictor of actual BSCs inside CNP (Brungard and Boettinger, 2012), thus model accuracy would also likely improve if detailed soil

maps were available over the entire study area. Strongly developed BSCs in the high LOD class commonly only occur on specific geological substrates (e.g. Carmel formation), thus detailed geology maps would likely be useful for improving high LOD class model accuracy. Overall similarity in accuracy metrics between models in each LOD class suggests that use of different modeling techniques would likely not result in increased predictive accuracy.

3.2 Spatial prediction

Spatial predictions of potential LOD class probabilities are presented in Figs. 3-3, 3-4, & 3-5. In general, predicted probabilities are lowest in highly dissected landscapes around the rivers. Predicted probabilities are highest on flatter, more stable surfaces farther away from the rivers. Both the low and moderate LOD class probabilities have similar ranges in predicted probabilities (Figs. 3-3 & 3-4 legends), while the high class has a much lower range of predicted probabilities (Fig. 3-5 legend).

Existing biological soil crusts in CNP exhibit highly heterogeneous spatial patterns; many different LOD classes can often be found within the area covered by one pixel (30 m) (personal observation). Because of such spatial variability, predicted LOD class probabilities should be interpreted as the likelihood that a particular LOD class would be the dominant LOD class, not the only LOD class, in the absence of 50 years of soil surface disturbance. Predicted probabilities will likely be more useful for assessing the impact of disturbance on LOD classes over large areas, than for site specific assessment.

Based on accuracy metrics (Table 3-4 and Brier scores), moderate LOD class predicted probabilities are likely reliable, particularly when considering the spatial variability of biological soil crusts in this area. Given the low accuracy metrics for the low and high LOD classes, predicted probabilities for these classes must be treated with caution. Relatively low maximum predicted probabilities of the high LOD class (0.51, Fig. 3-5) and model specificity near 1, suggest

that the high LOD class probability map may indicate areas where the high LOD class likely would not occur.

The final LOD class map shows the study area is dominantly predicted to be the low and moderate LOD classes (Fig. 3-6). In general the low LOD crust class was predicted in alluvial drainages and areas of steep cliffs and canyons, where frequent, natural soil erosion is likely to result in little biological soil crust development. The moderate class was predicted on large nearly level surfaces (Fig. 3-6), which likely have more stable soils than steep cliffs and canyons. Some areas (e.g., in the southwest) were predicted to be the high LOD class. These areas may have specific geology types (e.g., limestone or gypsum) associated with highly developed BSC. Final LOD class prediction confidence is highest in broad, relatively flat areas and lowest in areas dominated by cliff and canyon landscapes (Fig. 3-7).

Spatial predictions of potential biological soil crust LOD classes, prediction confidence, and individual LOD class probabilities provide knowledge of what dominant BSC might be in the absence of 50 years of soil surface disturbance. Spatial predictions of the moderate LOD class are anticipated to provide a useful spatially explicit decision support tool for land managers when assessing land use impacts and resource allocation. For example, predicted probabilities of the moderate LOD class could be compared to observations of actual crust. If an area has a high predicted probability of the moderate LOD class and actual LOD class observation was the low LOD class, it may be that surface disturbance has changed the LOD class in that area. Assuming that disturbance history at that site is known, or can be inferred, this may provide estimates of how land use activities affect the moderate LOD BSC class. Conversely if visiting an area with high predicted probability the moderate LOD class and actual crust class is the high LOD class than the spatial predictions are likely wrong. Spatial predictions of the moderate LOD class may also prove useful to land managers, because high predicted class probabilities (Fig. 3-

4) and high model confidence (Fig. 3-7) occur on broad, nearly level, landforms where potential surface disturbance from grazing or other land use activities is likely to be concentrated. Given the low accuracy metrics, it is unknown if spatial predictions of the low and high LOD classes would prove useful as spatially explicit decision support tools for land managers. If used, spatial predictions of low and high classes must be treated with caution.

3.3 Variable importance

The most important covariates for predicting the low and moderate LOD classes were normalized band ratios 5/2 and 5/1 (Fig. 3-8). As soil characteristics in this area are driven primarily by the underlying geological substrate, the importance of NBR 5/2 and 5/1 for the low and moderate LOD classes are likely a result of the ability of these band ratios to discriminate between different geologic types (Stum et al., 2010) and thus capture differences in soil physical and geochemical properties important to these two classes.

Slope was the most important covariate for the high LOD class (Fig. 3-8), and is likely related to the comparatively narrower range of slope values for this class (standard deviation = 8.6 vs. 19.3 and 13.3, for the low and moderate LOD classes, respectively). Although less important than slope, normalized band ratio 5/7 was also an important covariate of the high LOD class. This band ratio has been found helpful for distinguishing areas of surficial gypsum (Nield et al., 2007). In CNP and nearby areas, Bowker et al. (2006a) and Bowker and Belnap (2008) found moss and lichen cover positively associated with calcareous and gypsic soils. High LOD classes are associated with increased moss/lichen content (Belnap et al., 2008), thus it may be that normalized band ratio 5/7 is distinguishing areas of calcareous and/or gypsic soils which favor high LOD classes. As gypsiferous soils are relatively rare in this study area the lack of optimal soil characteristics required for high BSC development may help explain the few observations and thus poor model performance of the high LOD class.

4. Conclusions

We spatially predicted moderate BSC LOD class distribution to a large area surrounding CNP with reasonable accuracy. Prediction validation using observations in areas protected from major surface disturbance outside of CNP suggests that spatial predictions of the moderate LOD class do indeed represent potential biological soil crust distribution in areas outside CNP. Although predicted spatial patterns of the low and high LOD classes appear plausible, poor accuracy metrics indicate that spatial predictions of these classes may not be reliable. Model specificity suggests that high LOD class predicted probabilities class may be most useful for determining areas where this class likely would not occur. Prediction accuracy for all LOD classes could likely be improved through the collection of additional observations or the use of additional covariates.

Spatial predictions of LOD class probabilities and the final class map may be useful for assessing the impact of past land use practices on BSCs. Spatially explicit covariates related to soil/geological type and slope are the most important covariates for predicting potential BSC LOD classes.

5. References

- Allouche, O., Tsoar, A., Kadmon, R., 2006. Assessing the accuracy of species distribution models: prevalence, kappa and the true skill statistic (TSS). *J. Appl. Ecol.* 43, 1223–1232. doi:10.1111/j.1365-2664.2006.01214.x
- Baars, D.L., 2003. Geology of Canyonlands National Park, Utah, in: Sprinkel, D.A., Chidsey, Jr, T.C., Anderson, P.B. (Eds.), *Geology of Utah's Parks and Monuments*. Utah Geological Association, Salt Lake City, pp. 61–83.
- Beaudette, D.E., O'Geen, A.T., 2009. Quantifying the aspect effect: an application of solar radiation modeling for soil survey. *Soil Sci. Soc. Am. J.* 73, 1345–1352. doi:10.2136/sssaj2008.0229
- Belnap, J., 1993. Recovery rates of cryptobiotic crusts: inoculant use and assessment methods. *Gt. Basin Nat.* 53, 89–95.

- Belnap, J., 2002. Nitrogen fixation in biological soil crusts from southeast Utah, USA. *Biol. Fertil. Soils* 35, 128–135. doi:10.1007/s00374-002-0452-x
- Belnap, J., Eldridge, D., 2003. Disturbance and recovery of biological soil crusts, in: Belnap, J., Lange, O.L. (Eds.), *Biological Soil Crusts: Structure, Function, and Management*, Ecological Studies. Springer, Berlin, pp. 363–383.
- Belnap, J., Gillette, D.A., 1997. Disturbance of biological soil crusts: impacts on potential wind erodibility of sandy desert soils in southeastern Utah. *Land Degrad. Dev.* 8, 355–362. doi:10.1002/(SICI)1099-145X(199712)8:4<355::AID-LDR266>3.0.CO;2-H
- Belnap, J., Gillette, D.A., 1998. Vulnerability of desert biological soil crusts to wind erosion: the influences of crust development, soil texture, and disturbance. *J. Arid Environ.* 39, 133–142. doi:10.1006/jare.1998.0388
- Belnap, J., Kaltenecker, J.H., Rosentreter, R., Williams, J., Leonard, S., Eldridge, D., 2001. *Biological soil crusts: ecology and management*, Technical Reference No. 1730-2. U.S. Geological Survey, Forest and Rangeland Ecosystem Science Center, Denver.
- Belnap, J., Phillips, S.L., Witwicki, D.L., Miller, M.E., 2008. Visually assessing the level of development and soil surface stability of cyanobacterially dominated biological soil crusts. *J. Arid Environ.* 72, 1257–1264. doi:10.1016/j.jaridenv.2008.02.019
- Belnap, J., Wilcox, B.P., Van Scoyoc, M.W., Phillips, S.L., 2013. Successional stage of biological soil crusts: an accurate indicator of ecohydrological condition. *Ecohydrology* 6, 474–482. doi:10.1002/eco.1281
- Billingsley, G.H., Block, D.L., Felger, T.J., 2002. *Surficial Geologic Map of The Loop and Druid Arch Quadrangles, Canyonlands National Park, Utah*. U.S. Geological Survey Miscellaneous Field Studies Map MF-2411. U.S. Geological Survey, Flagstaff.
- Bowker, M.A., Belnap, J., 2008. A simple classification of soil types as habitats of biological soil crusts on the Colorado Plateau, USA. *J. Veg. Sci.* 19, 831–840. doi:10.3170/2008-8-18454
- Bowker, M.A., Belnap, J., Davidson, D.W., Goldstein, H., 2006a. Correlates of biological soil crust abundance across a continuum of spatial scales: support for a hierarchical conceptual model. *J. Appl. Ecol.* 43, 152–163. doi:10.1111/j.1365-2664.2006.01122.x
- Bowker, M.A., Belnap, J., Miller, M.E., 2006b. Spatial modeling of biological soil crusts to support rangeland assessment and monitoring. *Rangel. Ecol. Manag.* 59, 519–529. doi:10.2111/05-179R1.1
- Brier, G.W., 1950. Verification of forecast expressed in terms of probability. *Mon. Weather Rev.* 78, 1–3. doi:http://dx.doi.org/10.1175/1520-0493(1950)078<0001:VOFEIT>2.0.CO;2
- Brungard, C.B., Boettinger, J.L., 2012. Spatial prediction of biological soil crust classes; value added DSM from soil survey, in: Minasny, B., Malone, B.P., McBratney, A. (Eds.), *Digital*

Soil Assessments and Beyond: Proceedings of the 5th Global Workshop on Digital Soil Mapping. CRC Press, Sydney, pp. 57–60.

- Chavez Jr, P.S., 1996. Image-based atmospheric corrections - revisited and improved. *Photogramm. Eng. Remote Sens.* 62, 1025–1036.
- Cutler, D.R., Edwards, T.C., Beard, K.H., Cutler, A., Hess, K.T., Gibson, J., Lawler, J.J., 2007. Random forests for classification in ecology. *Ecology* 88, 2783–2792. doi:10.1890/07-0539.1
- De'ath, G., 2007. Boosted trees for ecological modeling and prediction. *Ecology* 88, 243–251. doi:10.1890/0012-9658(2007)88[243:BTFEMA]2.0.CO;2
- Fielding, A.H., Bell, J.F., 1997. A review of methods for the assessment of prediction errors in conservation presence/absence models. *Environ. Conserv.* 24, 38–49. doi:10.1017/S0376892997000088
- Hijmans, R.J., 2014. raster: raster: geographic data analysis and modeling. R package version 2.2-31. <http://CRAN.R-project.org/package=raster>.
- Hintze, L.F., Willis, G.C., Laes, D.Y.M., Sprinkel, D.A., Brown, K.D., 2000. 1:500000 Digital Geologic Map of Utah. Utah Geological Survey, Salt Lake City.
- Housman, D.C., Powers, H.H., Collins, A.D., Belnap, J., 2006. Carbon and nitrogen fixation differ between successional stages of biological soil crusts in the Colorado Plateau and Chihuahuan Desert. *J. Arid Environ.* 66, 620–634. doi:10.1016/j.jaridenv.2005.11.014
- Inzana, J., Kusky, T., Higgs, G., Tucker, R., 2003. Supervised classifications of Landsat TM band ratio images and Landsat. *J. Afr. Earth Sci.* 37, 59–72. doi:10.1016/S0899-5362(03)00071-X
- Kempen, B., Brus, D.J., Heuvelink, G.B.M., Stoorvogel, J.J., 2009. Updating the 1:50,000 Dutch soil map using legacy soil data: A multinomial logistic regression approach. *Geoderma* 151, 311–326. doi:10.1016/j.geoderma.2009.04.023
- Kuhn, M., 2013. caret: Classification and Regression Training. R package version 5.17-7. <http://CRAN.R-project.org/package=caret>.
- Kuhn, M., Johnson, K., 2013. *Applied Predictive Modeling*. Springer, New York.
- Kuske, C.R., Yeager, C.M., Johnson, S., Ticknor, L.O., Belnap, J., 2012. Response and resilience of soil biocrust bacterial communities to chronic physical disturbance in arid shrublands. *ISME J.* 6, 886–897. doi:10.1038/ismej.2011.153
- Mason, S.J., 2004. On using “climatology” as a reference strategy in the brier and ranked probability skill scores. *Mon. Weather Rev.* 132, 1891–1895.

- McBratney, A.B., Mendonça Santos, M.D.L., Minasny, B., 2003. On digital soil mapping. *Geoderma* 117, 3–52. doi:10.1016/S0016-7061(03)00223-4
- McKenzie, N.J., Ryan, P.J., 1999. Spatial prediction of soil properties using environmental correlation. *Geoderma* 89, 67–94. doi:10.1016/S0016-7061(98)00137-2
- Moisen, G.G., Freeman, E.A., Blackard, J.A., Frescino, T.S., Zimmermann, N.E., Edwards Jr., T.C., 2006. Predicting tree species presence and basal area in Utah: a comparison of stochastic gradient boosting, generalized additive models, and tree-based methods. *Ecol. Model.* 199, 176–187. doi:10.1016/j.ecolmodel.2006.05.021
- Nield, S.J., Boettinger, J.L., Ramsey, R.D., 2007. Digitally mapping gypsic and natric soil areas using Landsat ETM data. *Soil Sci. Soc. Am. J.* 71, 245. doi:10.2136/sssaj2006-0049
- Peters, J., Baets, B.D., Verhoest, N.E.C., Samson, R., Degroeve, S., Becker, P.D., Huybrechts, W., 2007. Random forests as a tool for ecohydrological distribution modelling. *Ecol. Model.* 207, 304–318. doi:10.1016/j.ecolmodel.2007.05.011
- R Core Team, 2013. R: A language and environment for statistical computing. R Foundation for Statistical Computing, Vienna, Austria. <http://www.R-project.org/>.
- Rosentreter, R., Belnap, J., 2003. Biological soil crusts of North America, in: Belnap, J., Lange, O.L. (Eds.), *Biological Soil Crusts: Structure, Function, and Management*, Ecological Studies. Springer, Berlin, pp. 31–50.
- Sanchez, P.A., Ahamed, S., Carre, F., Hartemink, A.E., Hempel, J., Huising, J., Lagacherie, P., McBratney, A.B., McKenzie, N.J., Mendonca-Santos, M. de L., Minasny, B., Montanarella, L., Okoth, P., Palm, C.A., Sachs, J.D., Shepherd, K.D., Vagen, T.G., Vanlauwe, B., Walsh, M.G., Winowiecki, L.A., Zhang, G.L., 2009. Digital soil map of the world. *Science* 325, 680–681. doi:10.1126/science.1175084
- Stum, A.K., Boettinger, J.L., White, M.A., Ramsey, R.D., 2010. Random forests applied as a soil spatial predictive model in arid Utah, in: Boettinger, J.L., Howell, D.W., Moore, A.C., Hartemink, A.E., Kienast-Brown, S. (Eds.), *Digital Soil Mapping: Bridging Research, Environmental Application, and Operation*, Springer, Dordrecht, pp. 179–190.
- Tendick, A., Coles, J., Decker, K., Hall, M., Von Loh, J., Belote, T., Wight, A., Wakefield, G., Evenden, A., 2012. Vegetation classification and mapping project report, Canyonlands National Park. Natural Resource Technical Report NPS/NCPN/NRTR—2012/577. National Park Service, Fort Collins.
- Tesfa, T.K., Tarboton, D.G., Chandler, D.G., McNamara, J.P., 2009. Modeling soil depth from topographic and land cover attributes. *Water Resour. Res.* 45, W10438. doi:10.1029/2008WR007474
- Utah Automated Geographic Reference Center, 2013. 5 Meter Auto-Correlated Elevation Models. <http://gis.utah.gov/data/elevation-terrain-data/5-meter-auto-correlated-elevation-models/> (last accessed: 7/5/2014).

Xiao, J., Shen, Y., Tateishi, R., Bayaer, W., 2006. Development of topsoil grain size index for monitoring desertification in arid land using remote sensing. *Int. J. Remote Sens.* 27, 2411–2422. doi:10.1080/01431160600554363

Zweig, M.H., Campbell, G., 1993. Receiver-operating characteristic (ROC) plots: a fundamental evaluation tool in clinical medicine. *Clin. Chem.* 39, 561–577.

Table 3-1. The number of observations per combined LOD class in the training, testing and validation datasets. Numbers in parentheses indicate the original LOD classes assigned to each combined LOD class. Training data was used for model construction. Testing observations was used to validate model parameters. No separate testing data was used for the high LOD class because of few observations. Validation observations consisted of an independent dataset of LOD classes observations inside livestock and deer exclosures approximately the same age as CNP. No observations of Low and High LOD classes were available in the validation dataset.

| Combined LOD Class | Training | Testing | Validation |
|--------------------|----------|---------|------------|
| Low (0, 1) | 283 | 70 | 0 |
| Moderate (2, 3, 4) | 392 | 98 | 11 |
| High (5, 6) | 111 | 0 | 0 |

Table 3-2. Covariates, the source of the covariate, and the rationale for inclusion. All covariates had a resolution of 30 m.

| Environmental variable | Source | Reason for inclusion |
|---|----------------|---|
| Elevation | DEM | Proxy for temperature and precipitation |
| Slope | DEM | Representative of topography |
| Diffuse Potential Solar Radiation (DiPSR) | DEM | Proxy for microclimate |
| Duration of Potential Solar Radiation (DuPSR) | DEM | Proxy for microclimate |
| Total Potential Solar Radiation (TPSR) | DEM | Proxy for microclimate |
| Normalized Landsat Band Ratio 5/7 (NBR 5/2) | Landsat 7 ETM+ | Proxy for soil/geologic properties |
| Normalized Landsat Band Ratio 5/2 (NBR 5/7) | Landsat 7 ETM+ | Proxy for soil/geologic properties |
| Normalized Landsat Band Ratio 5/1 (NBR 5/1) | Landsat 7 ETM+ | Proxy for soil/geologic properties |

Table 3-3. Optimal model parameters for SGB and RF, and area under the receiver operator characteristic curve (AUC) for each LOD class. Optimal model parameters were selected as those parameters that returned the highest AUC estimated by bootstrap sampling repeated 100 times.

| LOD class | Model Parameters | Model | | |
|-----------|------------------|------------------|-----------------|-----------------|
| | | SGB ^a | RF ^b | LR ^c |
| Low | <i>ntree</i> | 300 | 500 | - |
| | <i>depth</i> | 3 | - | - |
| | <i>mtry</i> | - | 1 | - |
| AUC | | 0.74 | 0.76 | 0.67 |
| Moderate | <i>ntree</i> | 350 | 500 | - |
| | <i>depth</i> | 2 | - | - |
| | <i>mtry</i> | - | 1 | - |
| AUC | | 0.69 | 0.70 | 0.66 |
| High | <i>ntree</i> | 1000 | 500 | - |
| | <i>depth</i> | 3 | - | - |
| | <i>mtry</i> | - | 1 | - |
| AUC | | 0.69 | 0.69 | 0.53 |

^a *depth* only required for SGB

^b *mtry* only required for RF

^c tuning parameters not required for LR

Table 3-4. Accuracy metrics for each model by LOD class.

| LOD Class | Metric | Model | | |
|-------------------|-------------|-------|------|------|
| | | SGB | RF | LR |
| Low | AUC | 0.73 | 0.74 | 0.71 |
| | Sensitivity | 0.41 | 0.47 | 0.46 |
| | Specificity | 0.91 | 0.90 | 0.93 |
| Moderate | AUC | 0.74 | 0.76 | 0.71 |
| | Sensitivity | 0.76 | 0.71 | 0.72 |
| | Specificity | 0.59 | 0.71 | 0.64 |
| High ^a | AUC | 0.69 | 0.69 | 0.53 |
| | Sensitivity | 0.07 | 0.02 | 0.00 |
| | Specificity | 0.97 | 0.99 | 1.00 |

^a mean values from resampling not separate test set

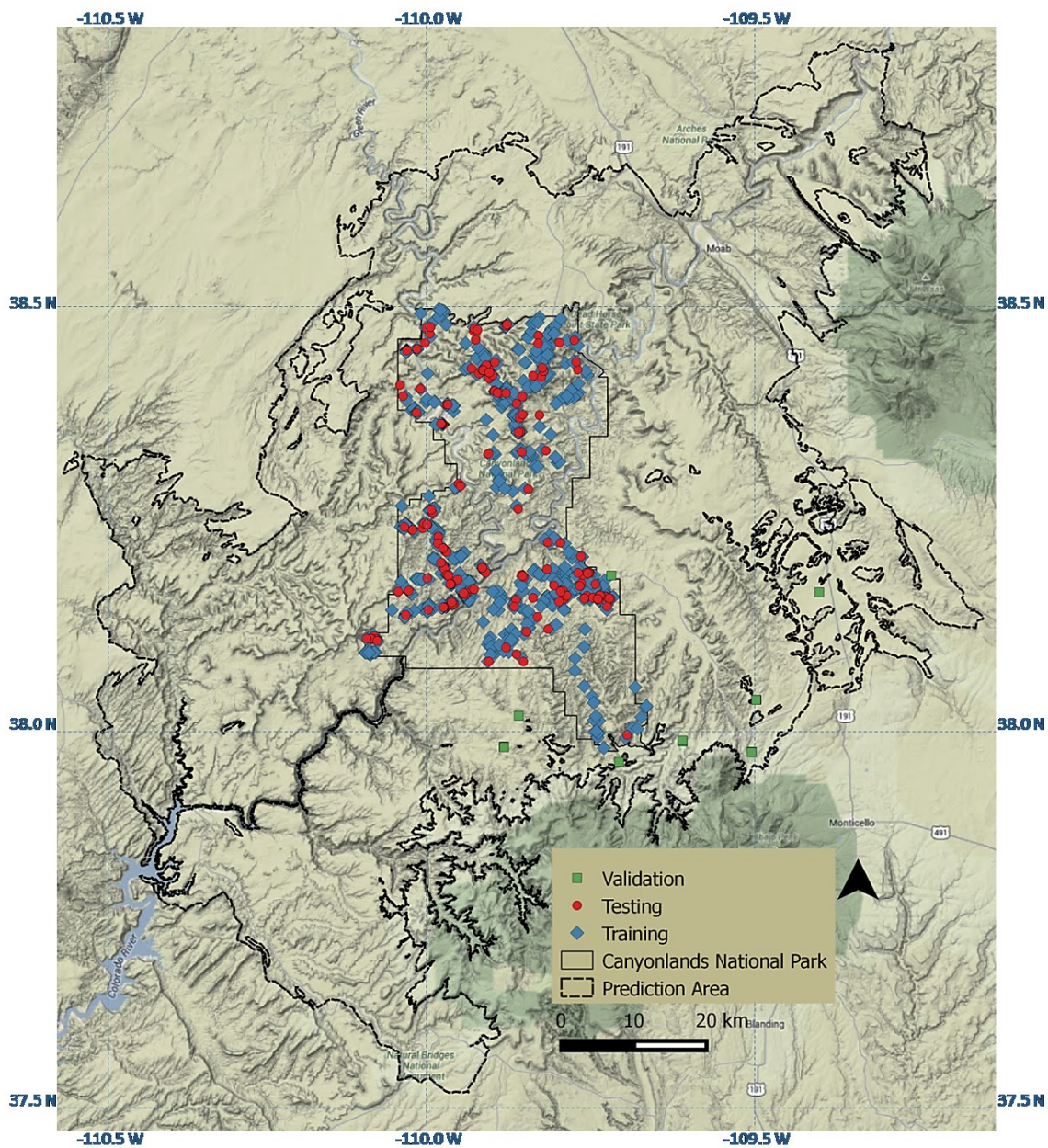


Fig. 3-1. The project area location in southeastern Utah, overlain on Google Earth Terrain imagery. The dashed line is the area to which spatial predictions were extrapolated. The solid line is Canyonlands National Park. Blue diamonds and red circles are training and testing observations of LOD classes from Soil Survey data, respectively. Green squares are validation observations inside fenced enclosures.

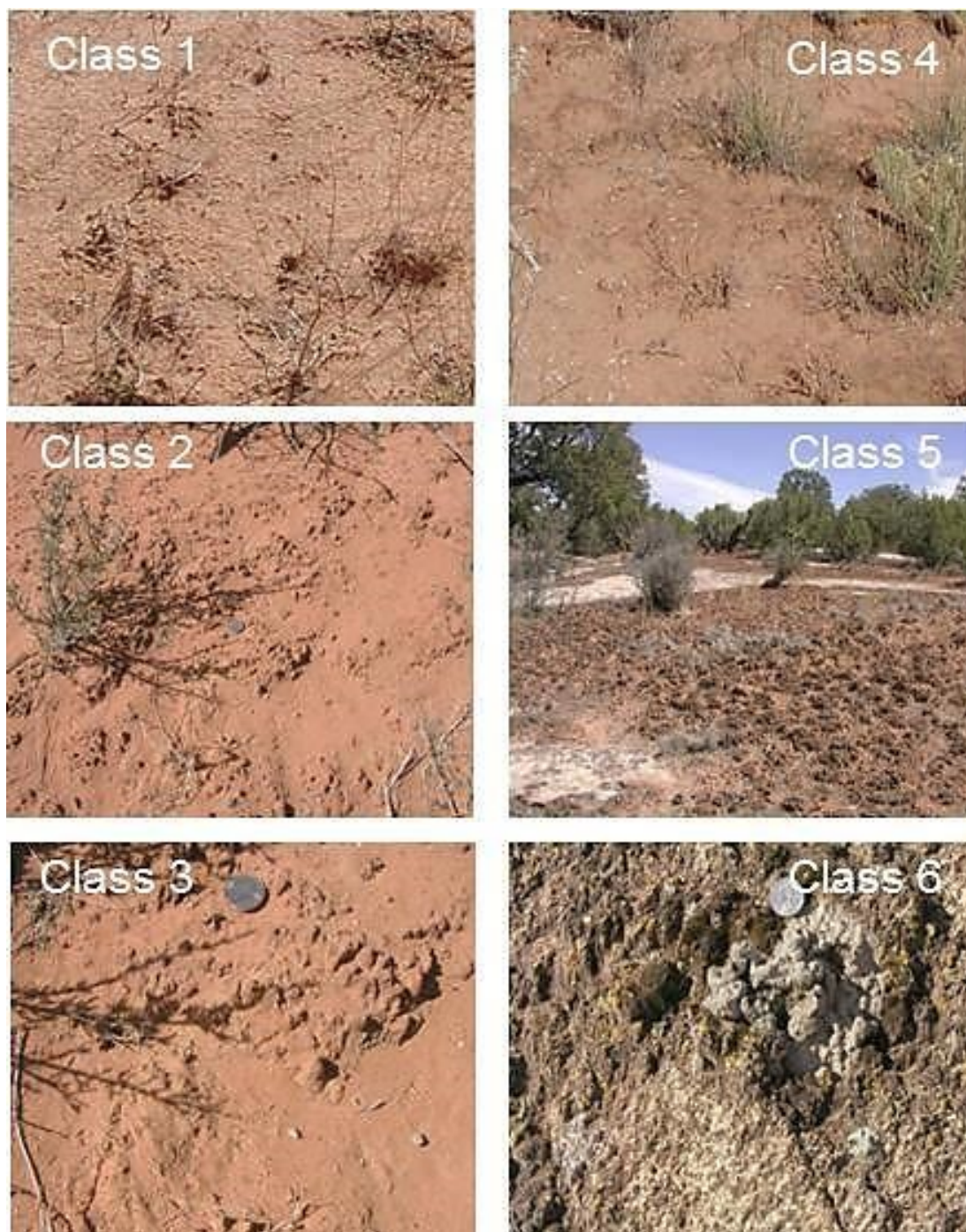


Fig. 3-2. Biological soil crust LOD classes used by soil surveyors in Canyonlands National Park.

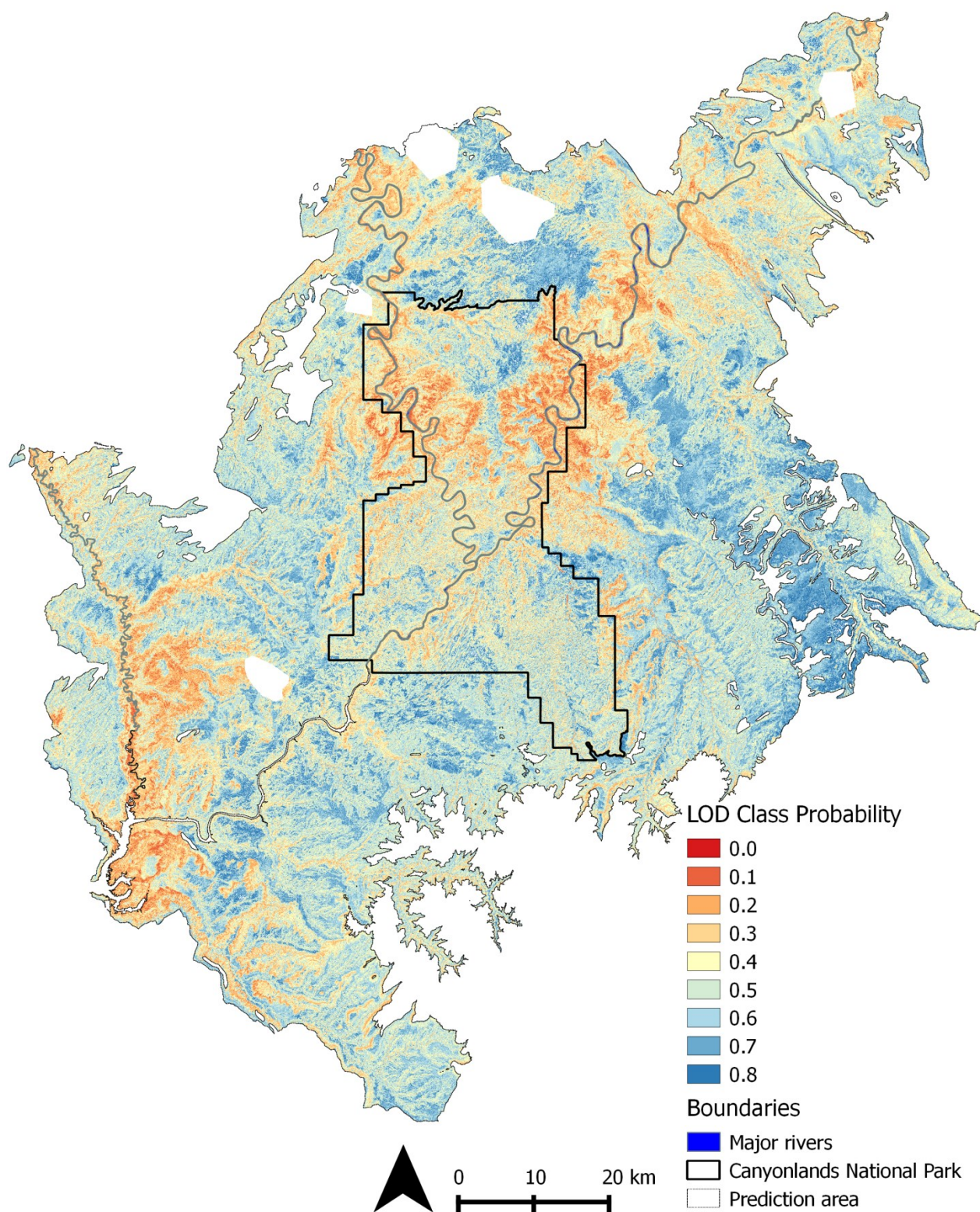


Fig. 3-3. Low LOD class predicted probability using RF. Irregular white areas inside the prediction area are areas masked because of clouds in the Landsat 7 ETM+ imagery used to derive covariates.

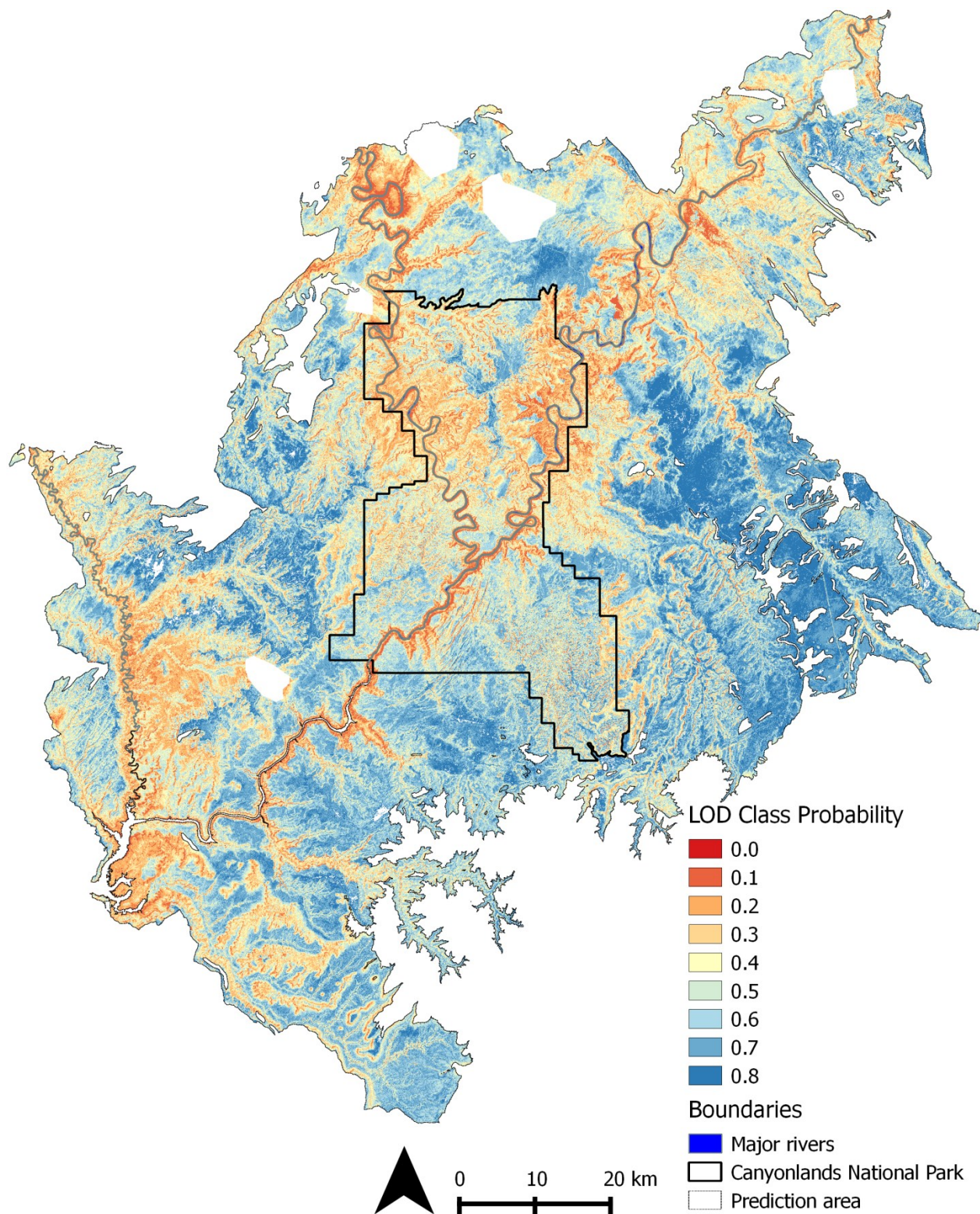


Fig. 3-4. Moderate LOD class predicted probability using logistic regression. Irregular white areas inside the prediction area are areas masked because of clouds in the Landsat 7 ETM+ imagery used to derive covariates.

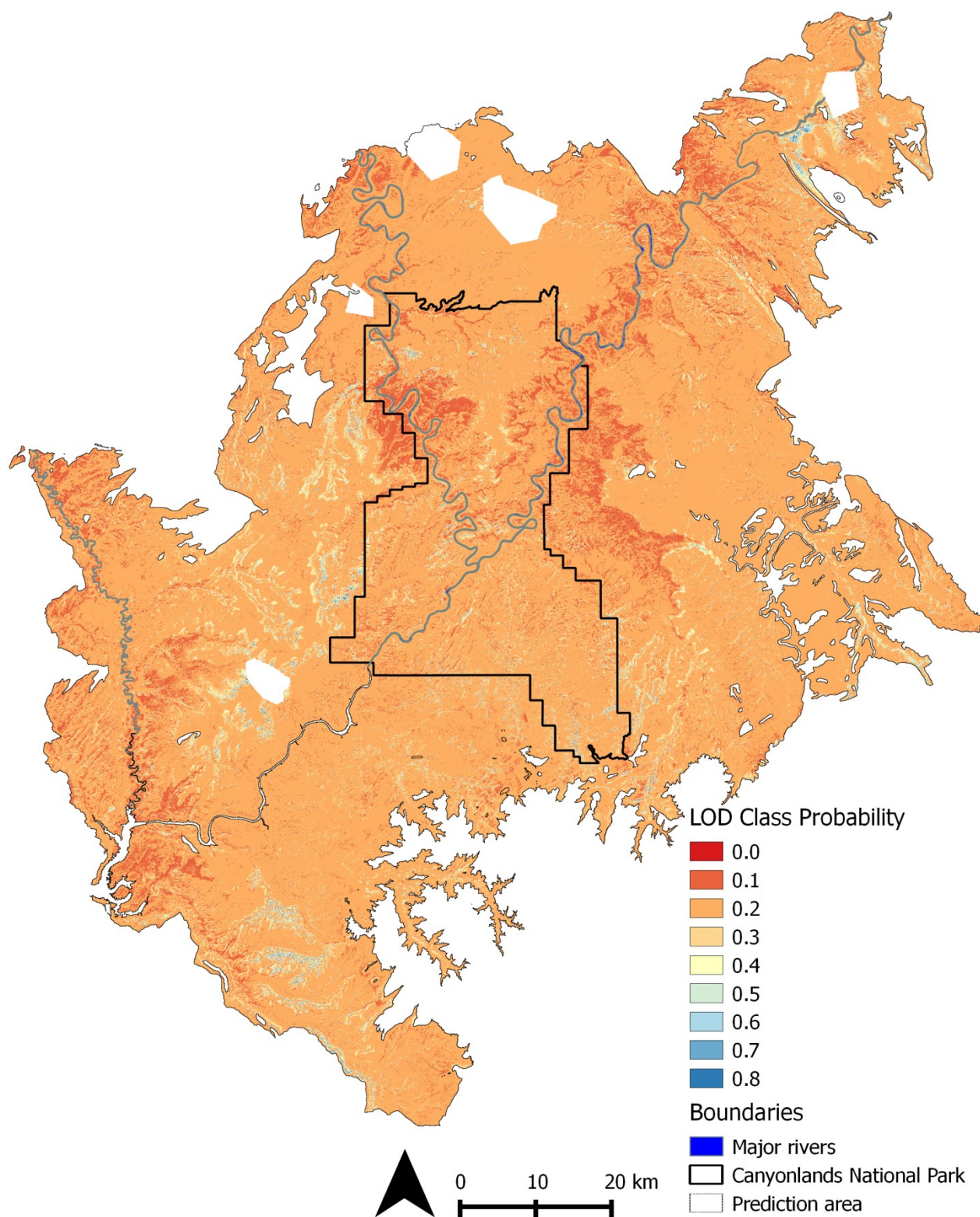


Fig. 3-5. High LOD class predicted probability using stochastic gradient boosting. Irregular white areas inside the prediction area are areas masked because of clouds in the Landsat 7 ETM+ imagery used to derive covariates.

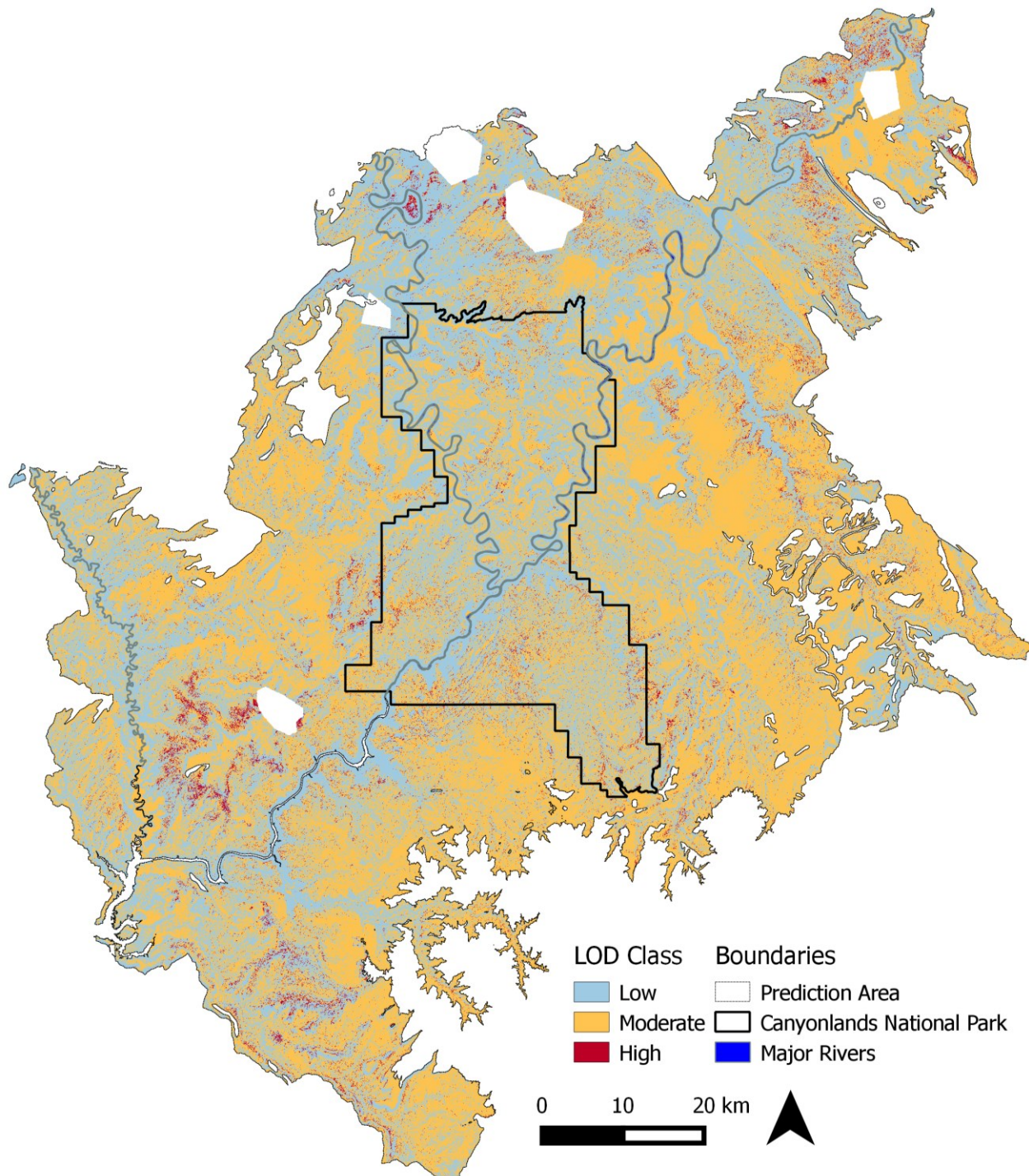


Fig. 3-6. Final LOD classification from combining all predicted probabilities and extracting the class with the highest value. White areas inside prediction area were masked out because of clouds in the Landsat 7 ETM+ imagery used to produce environmental covariates.

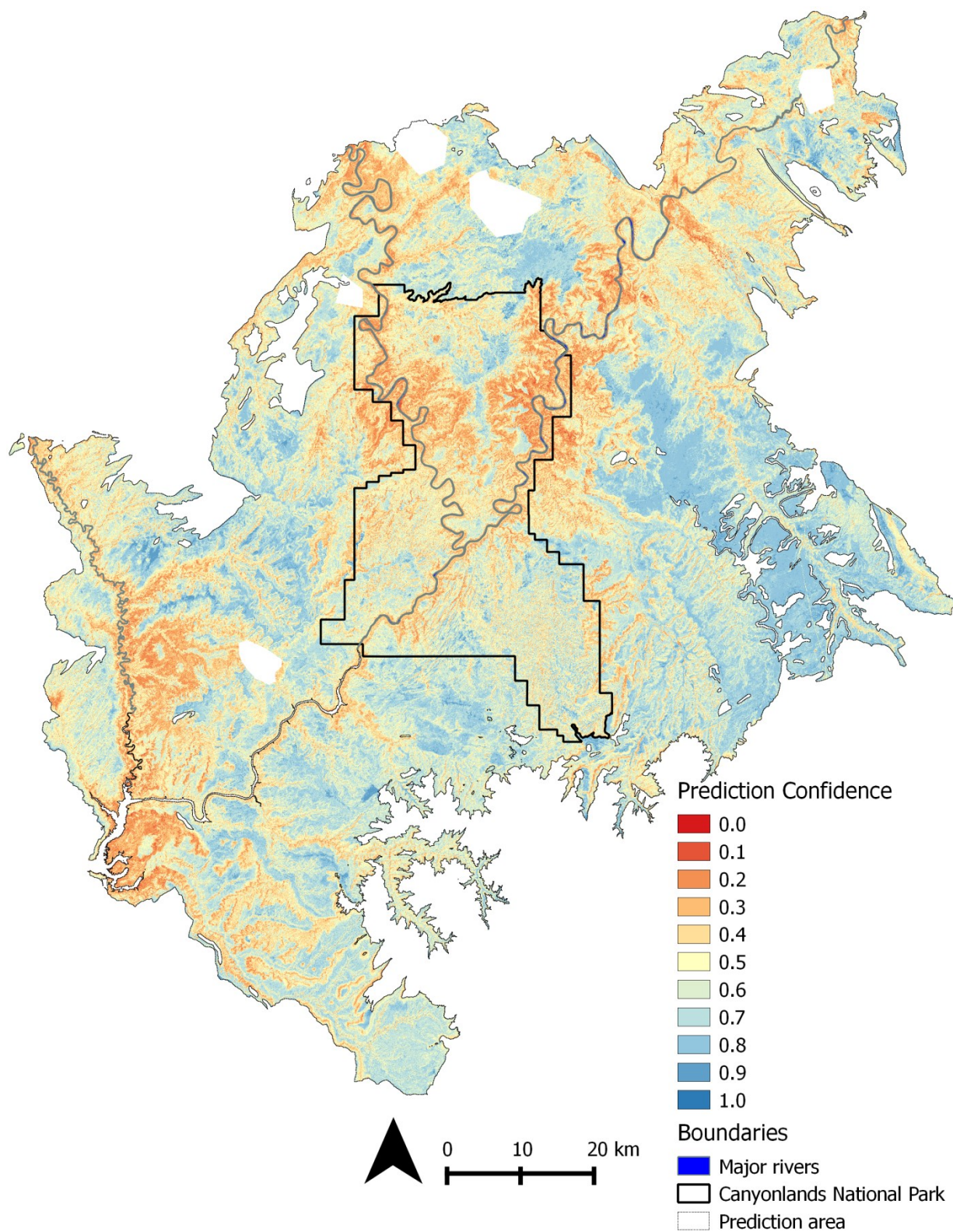


Fig. 3-7. Final LOD classification confidence from combining all predicted probabilities and extracting the highest value. Values closer to 1 indicate higher confidence in final LOD classification. White areas inside prediction area were masked out because of clouds in the Landsat 7 ETM+ imagery used to produce environmental covariates

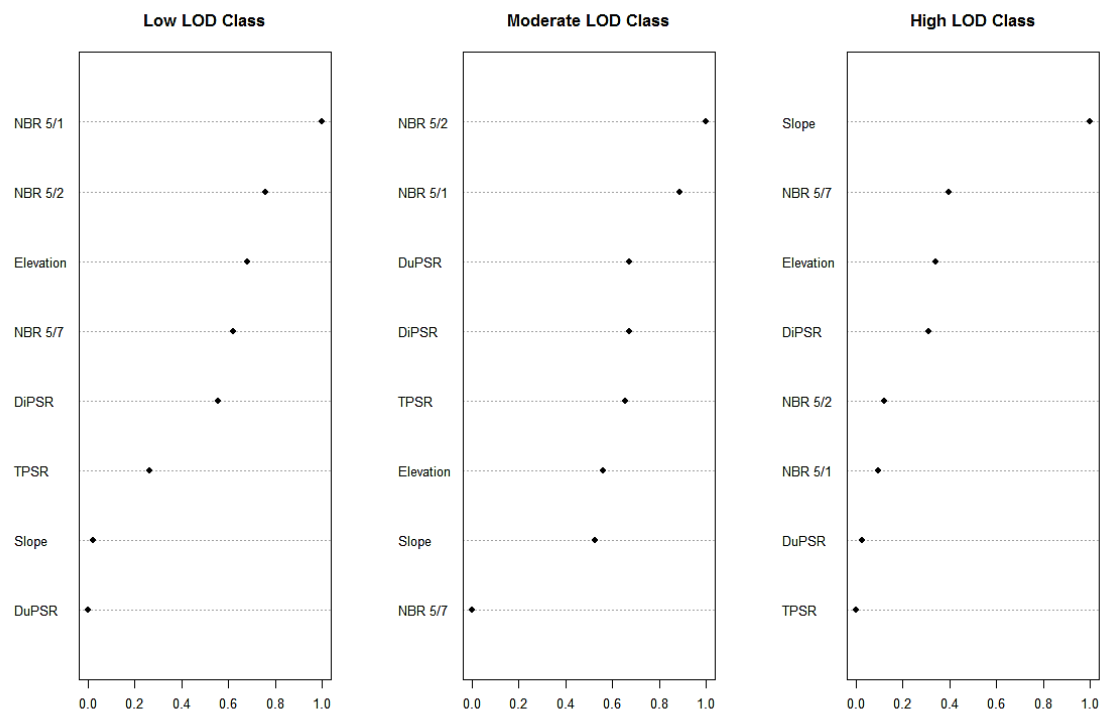


Fig. 3-8. Covariate importance for each LOD class. Importance scores for the low, moderate, and high LOD classes were taken from random forests, AUC estimates, and stochastic gradient boosting, respectively.

CHAPTER 4

THRESHOLD FRICTION VELOCITY OF LACUSTRINE AND ALLUVIAL SOILS BEFORE AND AFTER
DISTURBANCE IN THE EASTERN GREAT BASIN, USA**Abstract**

A spatially explicit wind erosion model could be used to assess the potential impacts of anthropogenic soil surface disturbance and proposed ground water withdrawal on wind erosion in the eastern Great Basin, USA. Such a model requires input of threshold friction velocity (TFV), the minimum turbulence required for wind erosion to occur. Little is known about TFV of soils in the eastern Great Basin. Additionally TFV is time consuming and difficult to accurately measure. A method to estimate TFV from alternate measurements would be useful. The objectives of this research were threefold: 1) to measure TFV in eastern Great Basin lacustrine and alluvial soils, 2) to assess the impact of soil disturbance on TFV, and 3) to develop relationships between TFV and alternate measures of soil properties as a first step towards spatial modeling of wind erosion in the eastern Great Basin.

Threshold friction velocity was measured with a portable open-bottomed wind tunnel at 33 sites in alluvial and lacustrine soils in Snake Valley, a broad valley on the Utah/Nevada border. The amount of sediment mobilized at TFV and alternate easy-to-measure soil surface properties thought likely correlated with TFV were also measured. Soil surfaces were assigned to one of five crust classes: biological crust, hard salt crust, surficial rock fragments, hard physical crust, and weak physical crust. Threshold friction velocity and sediment production were compared between undisturbed and disturbed soil surface conditions for each crust class. Multiple linear regression was conducted to find relationships between TFV and alternate soil surface properties.

Only soils with surficial rock fragments or weak physical crusts reached TFV in undisturbed conditions. Average TFV was lowest and average sediment production highest for

soils with undisturbed weak physical crusts. All crust classes reached TFV after disturbance. After disturbance, average TFV was lowest and average sediment production highest for disturbed weak physical crusts. Disturbance reduced TFV and sediment production on soils with surficial rock fragments and weak physical crusts.

All disturbed soils and undisturbed soils with surficial rock fragments or weak physical crusts would likely be susceptible to wind erosion in the eastern Great Basin. Soils with weak physical crusts are expected to be the most susceptible to wind erosion. Soils with biological crusts, hard salt crusts, and hard physical crusts, while likely to reach TFV when disturbed, may not be highly susceptible to erosion. Future work on wind erosion in the eastern Great Basin should focus on non-crusted/weakly crusted soils and soils formed in alluvium overlying lacustrine materials. Soils with other crust types are likely not susceptible to wind erosion. Threshold friction velocity in undisturbed soils with weak physical crusts and surficial rock fragments could be predicted using a combination of penetrometer resistance, rock fragment cover, and silt concentration (%). It is unlikely that TFV in disturbed soils could be predicted using any of the measured soil surface properties.

1. Introduction

Aeolian dust from arid lands is an important biogeochemical flux in many ecosystems (Lawrence and Neff, 2009; Painter et al., 2010; Reynolds et al., 2006) and can impact human health (Goudie and Middleton, 2006). The eastern Great Basin is a major source of aeolian dust in the western USA (Prospero et al., 2002) and dust from lacustrine surfaces in the eastern Great Basin often impacts air quality in Salt Lake City and other areas along Utah's Wasatch front (Hahnenberger and Nicoll, 2012).

Aeolian dust is the result of wind erosion of soil. Soil wind erosion occurs when wind-induced shear stress exceeds the cohesive forces of the soil surface to resist particle

detachment (Goudie and Middleton, 2006). Wind erosion does not occur uniformly across a landscape. Instead, wind erosion is often a “hot spot” phenomenon (Gillette, 1999), exhibiting high spatial variation (Gillette et al., 1997; Hahnenberger and Nicoll, 2014; Sweeney et al., 2011). Identifying areas susceptible to wind erosion is important for land managers responsible for understanding and managing the impacts of various land use practices (e.g., off-highway vehicle use and livestock grazing), as anthropogenic soil surface disturbance often increases wind erosion (Belnap and Gillette, 1998; Belnap et al., 2007; Miller et al., 2012; Okin et al., 2001). Proposed groundwater extraction from eastern Great Basin valleys to meet southern Nevada population growth requirements (Southern Nevada Water Authority Water Resource Plan 2009, http://www.snwa.com/assets/pdf/wr_plan.pdf) could also influence wind erosion, as groundwater withdrawal has resulted in increased wind erosion from similar areas, such as Owens Valley, California (Gill, 1996).

To understand the spatial variability of soil wind erosion and to assess both the impacts of anthropogenic soil surface disturbance, and the potential influences of ground water withdrawal on wind erosion, a spatially explicit wind erosion model could be used (Okin, 2008; Okin and Gillette, 2004). This model requires threshold friction velocity as an input.

Threshold friction velocity (TFV) is the minimum friction velocity required for wind erosion to occur, and represents the ability of a soil surface to resist wind erosion (Shao and Lu, 2000). Friction velocity is one measure of turbulence intensity and is expressed in units of velocity. Threshold friction velocity is reached when near-surface wind shear transfers enough kinetic energy to the soil surface to overcome the gravitational and cohesive forces retarding soil particle movement (Shao and Lu, 2000).

Threshold friction velocity depends upon soil particle size distribution, but surface roughness (Marticorena and Bergametti, 1995), aggregate stability (Eldridge and Leys, 2003),

rock fragments (Batt and Peabody, 1999), soil moisture (Fécan et al., 1998), physical and biological soil crusts (Belnap and Gillette, 1998; Zhang et al., 2008), and surface salt (King et al., 2011) also influence TFV.

Multiple measurements of TFV in different soil-landscape units are required for accurate spatial modeling of wind erosion, particularly for large areas with high spatial heterogeneity; however, it is time-consuming and difficult to accurately measure. A method to estimate TFV from alternate measurements would be useful. Okin and Gillette (2004) used soil surface texture to estimate TFV, but they found information from soil survey maps of the Jornada Basin, NM, too general for accurate spatial estimates of TFV. In the Colorado Plateau and Mojave Desert, Li et al. (2010) found TFV to be correlated with soil surface penetrometer measurements, soil surface disturbance created by impact from an air gun, and percent rock cover.

Although wind erosion is common in the eastern Great Basin, particularly on soils developed in lacustrine parent material and/or recently disturbed soils (Hahnenberger and Nicoll, 2014), little is known about the TFV of soils in this region. Furthermore, soils formed in lacustrine sediments in the eastern Great Basin are dominantly derived from carbonate-rich parent material and likely have different properties than soils in the Mojave Desert and Colorado Plateau, where TFV has most often been studied (Belnap and Gillette 1997; Belnap et al., 2007; Gillette et al., 1982; Marticorena et al., 1997).

The objectives of this research were threefold: 1) to measure TFV in eastern Great Basin lacustrine and alluvial soils, 2) to assess the impact of soil disturbance on TFV, and 3) to develop relationships between TFV and easier-to-measure soil properties as a first step towards spatial modeling of wind erosion in the eastern Great Basin.

2. Methods

2.1 Study area

Snake Valley is a broad, hydrologically closed, north-south trending valley in the eastern Great Basin on the Utah/Nevada border (Fig. 4-1). Major landforms include alluvial fans and fan piedmonts with relatively coarse-textured soils surrounding lake plains with fine-grained lacustrine materials on the valley floor. Both wet and dry playas occur in the lowest elevations. Relict beaches and sand bars from Pleistocene Lake Bonneville also exist (Hintze and Davis, 2003).

In areas heavily influenced by Lake Bonneville, vegetation is dominantly greasewood [*Sarcobatus vermiculatus*], shadscale [*Atriplex confertifolia*], and Nevada tea [*Ephedra nevadensis*] (personal observation). In near-playa environments, vegetation is mostly salt grass [*Distichlis spicata*], alkali sacaton [*Sporobolus airoides*], and pickleweed [*Salicornia* spp.]. Halogeton [*Halogeton*] and cheat grass [*Bromus tectorum*] grow between shrubs in some areas. A few ranches exist where ephemeral streams enter the valley. Average annual precipitation is 161 mm; average annual temperature is 10.4 °C (Western Regional Climate Center, historical climate summary for Eskdale, UT, <http://www.wrcc.dri.edu/cgi-bin/cliMAIN.pl?ut2607>).

All sampling was performed in the Millard County, UT, portion of Snake Valley (approximate center 39° 16' 05" N, 113° 53' 17" W), below the Bonneville shoreline of Lake Bonneville (Currey et al., 1984). Sampling sites were selected to capture anticipated soil variability in the following sediments: alluvium, mixed alluvial/lacustrine materials, lacustrine gravel and lacustrine sand (Hintze and Davis, 2003).

2.2 Threshold friction velocity and mobilized sediment measurement

Threshold friction velocity (TFV) was estimated using the 15 cm x 240 cm portable, open-bottomed wind tunnel (Fig. 4-2) described by Belnap et al. (2007) and Li et al. (2010). A pre-weighed fiberglass filter (pore-size approximately 1 μm) was inserted into the sampling frame at the end of the expansion chamber to capture mobilized sediment.

All measurements of wind speed were recorded in units of pressure (inches of water column [in.wc.]) using a Fluke 922 Airflow Meter/Micromanometer (range ± 16 in.wc., resolution 0.001 in.wc., accuracy $\pm 1\% + 0.01$ in.wc., www.fluke.com/922) attached to a pitot tube inside the wind tunnel. Measurements of pressure at a constant wind speed at seven heights above the soil surface (0, 0.318, 0.635, 1.27, 2.54, 5.08, 7.62 and 10.16 cm) were referred to as a velocity profile. Wind tunnel design required that all sites be within about 20 m of a road, but care was taken to avoid areas disturbed during road construction and maintenance. All field sampling was conducted during July 2012, and 33 separate sites were visited.

Wind tunnel measurements were performed on both the existing “undisturbed” soil surface and a disturbed surface at each sampling location. Care was taken to avoid any disturbance before wind tunnel placement on the undisturbed soil surface. The disturbed soil surface was created by driving a 1/2-ton truck once forward and then once in reverse so that that only the front wheels passed twice over the surface.

Threshold friction velocity was defined as the velocity at which particles of the soil surface, or small rock fragments on the soil surface, began overall continuous forward movement (Li et al., 2010). For soil surfaces that lacked loose particles on the soil surface, TFV was defined as the velocity at which the integrity of the soil surface crust was compromised and fragments of the soil surface were detached and blown away (Belnap and Gillette, 1997; Belnap et al., 2007; Marticorena et al., 1997).

Threshold friction velocity measurement protocol for both undisturbed and disturbed soil surfaces is shown in Fig. 4-3. At each site the wind tunnel was placed on the soil surface and the pitot tube set at exactly 7.62 cm above the soil surface. Wind speeds were then gradually increased until either overall forward movement of the soil surface, or small rock fragments on the soil surface, was observed (i.e., TFV was reached) or a predetermined pressure of about 0.3 in.wc. was reached. This pressure approximated a wind speed of 13 ms^{-1} (1300 cm/s, this paper will use units of cm/s to conform to units used in related TFV literature) and was chosen so that collected sediment amounts would be comparable to Belnap et al. (2007). This predetermined pressure also allowed the calculation of TFV in the event that the wind velocity changed before a velocity profile could be recorded (see Equations 4-4 and 4-5 below).

Pressure measurements were converted to velocity (cm/s) using:

$$V = \sqrt{\frac{2 * \rho_w * g * h_w}{\rho_a}} * 100 \quad (4-1)$$

where V = velocity (cm/s), ρ_w is the density of water (1000 kg/m^3), g is the acceleration of gravity (9.8 m/s^2), h_w is measured pressure (inches of water column, converted to meters) from the airflow meter and ρ_a is the density of moist air (kg/m^3). Temperature, barometric pressure and dew point necessary for the calculation of ρ_a were averaged over the 30 minutes nearest the time each velocity profile was recorded from a nearby weather station (Salt Desert Shrub East, Nevada EPSCOR Snake Range Transect Stations, <http://www.wrcc.dri.edu/GBtransect/>).

Wind velocity profiles were then fit to the log wind profile law, also known as the law of the wall (Li et al., 2010):

$$U = \frac{u^*}{k} \ln\left(\frac{z}{z_0}\right) \quad (4-2)$$

which can be re-written in linear form as:

$$\ln(z) = \frac{k}{u^*} U + \ln(z_0) \quad (4-3)$$

where z is the height of the pitot tube above the soil surface (cm), u^* is actual friction velocity (cm/s), k is von Kármán's constant (set to 0.4), U is mean wind velocity at height z (cm/s), and z_0 is aerodynamic roughness height (cm). Assuming neutral conditions (no heating induced buoyancy) inside the wind tunnel when overall forward movement of the soil surface was observed (i.e., when TFV was reached), regression of the natural log of z (height above soil surface; cm) against U (mean wind speed; cm/s), allows the estimation of TFV from regression parameters (Wiggs, 1997; Zhang et al., 2008).

If wind velocity did not change between the time when overall forward movement of the soil surface was observed and measurement of the velocity profile, TFV was calculated from velocity profiles recorded when overall forward movement of the soil surface was observed as:

$$u^* = \frac{k}{a} \quad (4-4)$$

where u^* = TFV (cm/s), k = von Kármán's constant (0.4) and a = regression slope.

When wind velocity likely changed between the time when overall forward movement of the soil surface was observed and measurement of the velocity profile (this happened if mobilized sediment saturated the fiberglass filter and wind velocities slowed before the velocity profile was measured), TFV was calculated from predefined pressure velocity profiles as:

$$u^* = \frac{Uk}{\ln\left(\frac{z}{z_0}\right)} \quad (4-5)$$

where u^* = TFV (cm/s), U = wind speed (cm/s) at TFV measured at 7.62 cm above the soil surface, k = von Kármán's constant (0.4), z = 7.62 cm, and z_0 = aerodynamic roughness height (regression intercept).

Incorrect measurements were removed before performing regressions. Measurements were assumed to be incorrect if wind speeds at higher pitot tube heights were less than wind

speeds at lower pitot tube heights. Incorrect measurements likely occurred because the pitot tube was not perfectly aligned with wind flow along the wind tunnel.

Estimates of TFV measurement uncertainty (Table 4-1) were calculated by correcting measurements for instrument error and substituting upper and lower 95% regression coefficient confidence intervals for a in Equation 4-4. Plots of measured wind speed profiles at TFV for each sampling site (Figs. A-1 to A-20), and technical details of TFV measurement accuracy are reported in the Appendix A.

Following methods in Belnap et al. (2007), the amount of mobilized sediment from each soil surface was recorded as the weight of the filter plus the weight of sediment trapped in the expansion chamber minus pre-measurement filter weight. Measurements were converted to g/m^2 by dividing sediment weight by wind tunnel footprint area. If TFV was greater than 1300 cm/s , sediment weights collected at 1300 cm/s and TFV were combined to obtain final sediment weight.

2.3 Soil surface properties

2.3.1 Field methods

Following Li et al. (2010), soil surface resistance to wind erosion was estimated using the average area of soil (cm^2) displaced by a 760 Pumpmaster air gun shot at 45° to the soil surface and the average force required for a penetrometer (QA Supplies FT101) to be pushed 0.6 cm into the soil surface at 45° . Fifteen replicates of the air gun and penetrometer measurements were recorded at each wind site.

Soil aggregate stability was measured according to Herrick et al., (2001). Briefly, four 6-8 mm soil aggregates were soaked and repeatedly dipped in tap water then assigned to 1 of 6 classes based on how quickly aggregates slaked. The average class number was reported.

Physical crust thickness (measured to the nearest 0.5 cm) and biological soil crust class (Belnap

et al., 2008) were recorded at each site. Each measurement was made within 5 m of the wind tunnel location.

At each site, a 15-cm² aluminum frame was used to sample the soil surface to a depth equal to the thickness of the physical crust or 1 cm if no physical crust was present. These samples were sieved to <0.85-mm (U.S. Department of Agriculture, 2014) and both < 0.85-mm and ≥ 0.85-mm size fractions were bagged and transported back to the laboratory.

2.3.2 Laboratory methods

Both < 0.85-mm and ≥ 0.85-mm size fractions were air-dried and weighed. Average field-moist water content was 0.4% except for site #33 which had a field-moist water content of 14.3%. After weighing, both < 0.85-mm and > 0.85-mm size fractions were combined and gently crushed to break up aggregates. This composite sample was then sieved to <2-mm. All subsequent laboratory analysis was performed on the < 2-mm fraction. Sand, silt, and clay concentrations were determined by three experienced soil scientists using the texture by feel method

(http://www.nrcs.usda.gov/wps/portal/nrcs/detail/soils/edu/kthru6/?cid=nrcs142p2_054311).

Soils were classified into USDA texture classes (Schoeneberger et al., 2003b). Soil texture classes were mostly silt loam and silty clay loam, however clay, clay loam, loam, sandy clay loam, and sandy loam also occurred.

Electrical conductivity (EC) was measured using an Accumet XL30 conductivity meter on the supernatant following settling of most particles from a 1:4 soil:water mix, which was used instead of the standard 1:1 suspension because of the expansive nature of the clays in these soils. Soil pH was measured using colorimetric field indicators. Inorganic carbon was measured using an improved pressure calcimeter method (Fonnesbeck et al., 2013) and reported as % calcium carbonate equivalent (CCE). The soil properties of ten percent of the samples were

measured in duplicate to estimate measurement error. Standard deviation for pH, EC, and CCE was 0.1, 0.9 dS/m, and 1.0 %, respectively.

Percent rock fragment cover (defined as > 1-mm) was estimated using image analysis (Booth et al., 2005; Cagney et al., 2011; Duniway et al., 2012; Nguyen et al., 2007). Prior to installation of the wind tunnel, a steel frame equal in size to the footprint of the wind tunnel was carefully placed on the soil surface and two 12.1-megapixel photos were taken approximately 1.5 m directly above the frame. Rock fragments > 1-mm were clearly distinguishable in each image (0.3 mm/pixel ground sample distance). Photos were merged and eight line-point transects spaced evenly along the length of the steel frame. Line transects consisted a semi-transparent image of a 15-cm ruler scaled to the inside of the steel frame. The distance of each transect intersected by rock fragments > 1-mm was measured and percent rock fragment cover estimated as the total distance along all line-point transects (120 cm) minus the total distance not intersected by rock fragments.

2.4 Soil surface classes

Based on dominant soil surface characteristics, each sampling site was classified to one of five soil surface classes: biological crust, hard salt crust, surficial rock fragments, hard physical crust, and weak physical crust (Fig. 4-4). Soil surfaces in the biological crust class consisted of well-developed, dark cyanobacteria biological soil crusts (Belnap et al., 2008). Soil surfaces in the hard salt crust class had obvious salt accumulation at the surface and vegetation at these sites was dominantly salt-tolerant grasses. The surficial rock fragments class consisted of both well-developed desert pavement and hard physical crusts with significant amounts of surface rock fragments. Soil surfaces in the hard physical crust class had obvious, strong polygonal cracking. Soil surfaces in the weak physical crust class were either very weak (average resistance to penetrometer = 2.1 kg) or lacked a coherent soil crust.

We observed hard physical crusts to occur in fine-grained sediment in lake plains and dry playas (Peterson, 1981) and, based on nearby soil pedon descriptions, we interpreted many of these surfaces as exposed sub-surface soil horizons of clay accumulation (argillic or natric horizons). Hard salt crusts were dominantly located in soils formed in fine-grained lacustrine material (Hintze and Davis, 2003) where near-surface saline groundwater caused salt efflorescence. Surficial rock fragments were found in lacustrine sand and gravel, as well as mixed alluvial and lacustrine sediment (Hintze and Davis, 2003). Weak physical crusts mostly occurred in fine-grained lacustrine sediment, but also occurred in mixed alluvial and lacustrine sediment (Hintze and Davis, 2003).

2.5 Statistical analysis

Multiple linear regression was used to test relationships between TFV and the following variables: percent rock cover, average aggregate stability class, air gun disturbance area, penetrometer resistance, crust thickness, ratio of > 0.85 mm size fraction weight/total soil weight, electrical conductivity, pH, calcium-carbonate-equivalent, sand, silt, and clay. Relationships were tested for both undisturbed and disturbed soil surfaces, but only undisturbed soil surface observations that reached TFV were included in the analysis. All analysis was performed using R statistical software (R Core Team, 2012).

3. Results and discussion

3.1 Threshold friction velocity and sediment production

3.1.1 Undisturbed soil surfaces

Threshold friction velocity was not reached at undisturbed sites with biological and hard salt crusts (Table 4-1). Threshold friction velocity was reached at only two of the eight undisturbed sites with a hard physical crust (sites 9 and 23, Table 4-1). Site 9 had a very thin,

curled clay veneer. Site 23 was located in the former Baker Creek marsh which dried when water from Baker Creek was allocated for irrigation (*pers. comm.* Eskdale farm manager, Eskdale UT). It is likely that undisturbed soils with hard salt crusts, biological crusts, and the majority of undisturbed soils with hard physical crusts did not reach TFV because cohesive forces in these soil crusts were strong enough to resist the turbulence generated by the wind tunnel.

Threshold friction velocity was reached in 8 of the 12 undisturbed sites with surficial rock fragments. The four sites with surficial rock fragments that did not reach TFV (Sites 10, 25, 29, and 30, Table 4-1) were located on alluvial fans above the Provo shoreline, but below the Bonneville shoreline of Lake Bonneville (Currey et al., 1984) and contained little lacustrine material. Sites with surficial rock fragments that reached TFV appeared to be in relatively recent (late Holocene, Hintze and Davis, 2003) alluvium deposited over lacustrine material (personal observation). All sites with a weak physical crust reached TFV (Table 4-1). Average TFV for soils with surficial rock fragments and weak physical crusts was 119.0 cm/s and 106.1 cm/s, respectively (Fig. 4-5A). Average sediment production for undisturbed weak physical crusts was 193.8 g/m². This was greater than average sediment production from undisturbed soils with surficial rock fragments (159.8 g/m²), but both surface types had high variability in sediment production (Fig. 4-5B).

Similar to Snake Valley, soils with hard salt crusts and well-developed physical and biological crusts from the Mojave Desert and Colorado Plateau did not reach TFV (Belnap and Gillette, 1997; Gillette et al., 1982; Li et al., 2010; Marticorena et al., 1997). Threshold friction velocities for “loose-silty” soils (Marticorena et al., 1997) in the Mojave Desert were similar to TFVs of soils with weak physical crusts in Snake Valley, suggesting that for non-sandy lacustrine soils, non-crusted/weakly crusted soils are the most susceptible to wind erosion.

3.1.2 Disturbed soil surfaces

All sites reached TFV after disturbance (Table 4-1). Average TFV was lowest for disturbed weak physical crusts (43.2 cm/s), followed by disturbed biological soil crusts (56.9 cm/s), disturbed hard physical crusts (66.9 cm/s), disturbed hard salt crusts (80.6 cm/s), and disturbed soils with surficial rock fragments (84.4 cm/s, Fig. 4-5C). Disturbance reduced average TFV for soils with surficial rock fragments and weak physical crusts by 34.6 cm/s and 62.9 cm/s, respectively.

Average sediment production after disturbance was lowest for biological crusts (14.4 g/m²), followed by hard physical crusts (18.2 g/m²), hard salt crusts (35.7 g/m²), surficial rock fragments (79.7 g/m²) and weak physical crusts (163.7 g/m²). Soils with biological crusts, hard physical crusts, and hard salt crusts produced relatively little sediment after disturbance (Fig. 4-5D). This is because disturbance resulted in few wind erodible aggregates. Soils with biological crusts likely had particles “glued” together with polysaccharides and filaments resulting in larger aggregates that were more resistant to wind erosion (Mazor et al., 1996; Tisdall and Oades, 1982). Disturbance loosened few particles from the soil surface of hard physical and hard salt crusts, where at some sites there was little evidence that the truck tire had passed over the soil surface. Sediment collected from soils with hard salt crusts (Sites 13, 18, & 33, Table 4-1) appeared to be a mixture of both salt crust and soil particles. The exception was Site 33, where sediment appeared to consist entirely of surface salt. Site 33 was nearest the playa and had the thickest salt crust. Therefore, disturbance may not result in erosion of soil particles such as sand, silt, and clay.

Disturbance reduced average sediment production for soil surfaces with surficial rock fragments and weak physical crusts compared to undisturbed soil surfaces. The reduction in average sediment production following disturbance was greater for soils with surficial rock

fragments (80.1 g/m^2) than for soils with weak physical crusts (30.1 g/m^2). This reduction in sediment production after disturbance is surprising, but is likely because disturbance compacted loose particles on weak physical crusts (personal observation), while possibly burying or compacting loose gravel on soils with surficial rock fragments.

Similar to Belnap and Gillette (1997), Belnap et al. (2007), Gillette et al. (1982) and Marticorena et al. (1997), disturbance of the soil surface reduced TFV. Contrary to Belnap et al., (2007), disturbance generally reduced sediment production (compare Fig. 4-5B and 4-5D). This may be the result of differences in the methods of applied disturbance (trampling vs. passage with a truck) or differences in soil texture, as the soils tested by Belnap et al. (2007) were much sandier.

3.2 Predicting TFV from soil properties

Percent silt was the best predictor of undisturbed TFV for weak physical crusts (Table 4-2, Fig. 4-7). Penetrometer force and percent rock cover were the best predictors of undisturbed TFV for soils with surficial rock fragments (Table 4-2, Fig. 4-6). In a similar study on Colorado Plateau and Mojave Desert soils, Li et al. (2010) found mean air gun displacement area as well as penetrometer force and percent rock cover significant predictors of TFV. The lack of statistically significant relationships between TFV and mean air gun displacement in these soils is likely a result of surface crust strength. Soils tested by Li et al. (2010), which reached TFV, were sandy or had only weak biological or physical crusts, and had maximum penetrometer and mean air gun displacement area measurements of approximately 1.1 kg and 50 cm^2 , respectively. All soils in this study had penetrometer measurements $> 1.3 \text{ kg}$ and a maximum air gun displacement area of 12 cm^2 (data not shown).

No significant predictors of disturbed TFV for soils with surficial rock fragments, weak physical and hard physical crust classes were found. Insufficient observation numbers prohibited meaningful regressions for disturbed biological or hard salt crusts.

For developing spatially explicit estimates of TFV for input into a spatial wind erosion model, undisturbed soils with biological, hard salt, and hard physical crusts might be assumed not to reach TFV based on these wind tunnel measurements. TFV in undisturbed soils with weak physical crusts and surficial rock fragments could be predicted using a combination of silt concentration (%), penetrometer force, and percent rock cover measurements. Spatially explicit estimates of TFV in disturbed soils could not be developed using any of the measured soil surface properties.

4. Conclusions

This study reports wind tunnel measured threshold friction velocities and sediment production for undisturbed and disturbed lacustrine and alluvial soils in the eastern Great Basin. We found that the nature of the soil surface (biological crust, hard salt crust, surficial rock fragments, hard physical crust, and weak physical crust) can be used to help explain differences in wind tunnel measured TFV and sediment production. Undisturbed soils with surficial rock fragments and weak physical crusts had lower TFVs, and thus are more susceptible to wind erosion, than soils with biological crusts, hard salt crusts, and hard physical crusts. However, it is important to note that in this study TFV was measured with a 15-cm high wind tunnel, which physically restricted large scale (e.g., 2-km) turbulent eddies. Therefore, we cannot rule out that TFV of undisturbed soils with biological crusts, hard salt crusts, and hard physical crusts would not be reached in natural conditions. We expect that in undisturbed conditions, soils with weak physical crusts would produce more sediment than soils with surficial rock fragments, but there may be high variability in sediment production.

When disturbed, soils with weak physical crusts are expected to be the most susceptible to wind erosion, as they had the lowest average TFV and produced relatively large amounts of sediment compared with other soil surface types. Although soil surfaces with surficial rock fragments had relatively high TFVs in our study, such surfaces can also produce relatively large amounts of sediment if TFV is exceeded. Soils with biological crusts, hard salt crusts, and hard physical crusts, while likely to reach TFV when disturbed, may not be highly susceptible to erosion, because relatively little sediment was produced from these surface types. Future work on wind erosion in the eastern Great Basin should focus on non-crusted/weakly crusted soils and soils formed in alluvium overlying lacustrine materials. Soils with other surface types are likely less susceptible to wind erosion.

Our study results indicate that in the eastern Great Basin, which is dominated by carbonate-rich lacustrine and alluvial soils, spatially explicit estimates of TFV in undisturbed soils with weak physical crusts and surficial rock fragments could be produced using a combination of penetrometer force, percent rock fragment cover, and silt concentration (%). It is unlikely that spatially explicit estimates of TFV of disturbed soils could be produced using any of the measured soil surface properties.

5. References

- Batt, R.G., Peabody, S.A., 1999. Threshold friction velocities for large pebble gravel beds. *J. Geophys. Res. Atmospheres* 104, 24273–24279. doi:10.1029/1999JD900484
- Belnap, J., Gillette, D.A., 1997. Disturbance of biological soil crusts: impacts on potential wind erodibility of sandy desert soils in southeastern Utah. *Land Degrad. Dev.* 8, 355–362. doi:10.1002/(SICI)1099-145X(199712)8:4<355::AID-LDR266>3.0.CO;2-H
- Belnap, J., Gillette, D.A., 1998. Vulnerability of desert biological soil crusts to wind erosion: the influences of crust development, soil texture, and disturbance. *J. Arid Environ.* 39, 133–142. doi:10.1006/jare.1998.0388

- Belnap, J., Phillips, S.L., Herrick, J.E., Johansen, J.R., 2007. Wind erodibility of soils at Fort Irwin, California (Mojave Desert), USA, before and after trampling disturbance: implications for land management. *Earth Surf. Process. Landf.* 32, 75–84. doi:10.1002/esp.1372
- Belnap, J., Phillips, S.L., Witwicki, D.L., Miller, M.E., 2008. Visually assessing the level of development and soil surface stability of cyanobacterially dominated biological soil crusts. *J. Arid Environ.* 72, 1257–1264. doi:10.1016/j.jaridenv.2008.02.019
- Booth, D.T., Cox, S.E., Fifield, C., Phillips, M., Williamson, N., 2005. Image analysis compared with other methods for measuring ground cover. *Arid Land Res. Manag.* 91–100. doi:10.1080/15324980590916486
- Cagney, J., Cox, S.E., Booth, D.T., 2011. Comparison of point intercept and image analysis for monitoring rangeland transects. *Rangel. Ecol. Manag.* 309–315. doi:10.2111/REM-D-10-00090.1
- Currey, D.R., Atwood, G., Maybe, D.R., 1984. Map 73. Major Levels of Great Salt Lake and Lake Bonneville. Utah Geological and Mineral Survey, Salt Lake City.
- Duniway, M.C., Karl, J.W., Schrader, S., Baquera, N., Herrick, J.E., 2012. Rangeland and pasture monitoring: an approach to interpretation of high-resolution imagery focused on observer calibration for repeatability. *Environ. Monit. Assess.* 184, 3789–3804. doi:10.1007/s10661-011-2224-2
- Eldridge, D.J., Leys, J.F., 2003. Exploring some relationships between biological soil crusts, soil aggregation and wind erosion. *J. Arid Environ.* 53, 457–466. doi:10.1006/jare.2002.1068
- Fécan, F., Marticorena, B., Bergametti, G., 1998. Parametrization of the increase of the aeolian erosion threshold wind friction velocity due to soil moisture for arid and semi-arid areas. *Ann. Geophys.* 17, 149–157. doi:10.1007/s00585-999-0149-7
- Fonnesbeck, B.B., Boettinger, J.L., Lawley, J.R., 2013. Improving a simple pressure-calimeter method for inorganic carbon analysis. *Soil Sci. Soc. Am. J.* 77, 1553. doi:10.2136/sssaj2012.0381
- Gill, T.E., 1996. Eolian sediments generated by anthropogenic disturbance of playas: human impacts on the geomorphic system and geomorphic impacts on the human system. *Geomorphology* 17, 207–228. doi:10.1016/0169-555X(95)00104-D
- Gillette, D.A., 1999. A qualitative geophysical explanation for “hot spot” dust emitting source regions. *Contrib. Atmospheric Phys.* 72, 67–77.
- Gillette, D.A., Adams, J., Muhs, D., Kihl, R., 1982. Threshold friction velocities and rupture moduli for crusted desert soils for the input of soil particles into the air. *J. Geophys. Res. Oceans* 87, 9003–9015. doi:10.1029/JC087iC11p09003
- Gillette, D.A., Hardebeck, E., Parker, J., 1997. Large-scale variability of wind erosion mass flux rates at Owens Lake: 2. Role of roughness change, particle limitation, change of

threshold friction velocity, and the Owen effect. *J. Geophys. Res. Atmospheres* 102, 25989–25998. doi:10.1029/97JD00960

Goudie, A.S., Middleton, N.J., 2006. *Desert Dust in the Global System*. Springer, Berlin.

Hahnenberger, M., Nicoll, K., 2012. Meteorological characteristics of dust storm events in the eastern Great Basin of Utah, USA. *Atmos. Environ.* 60, 601–612. doi:10.1016/j.atmosenv.2012.06.029

Hahnenberger, M., Nicoll, K., 2014. Geomorphic and land cover identification of dust sources in the eastern Great Basin of Utah, U.S.A. *Geomorphology* 204, 657–672. doi:10.1016/j.geomorph.2013.09.013

Herrick, J.E., Whitford, W.G., de Soyza, A.G., Van Zee, J.W., Havstad, K.M., Seybold, C.A., Walton, M., 2001. Field soil aggregate stability kit for soil quality and rangeland health evaluations. *CATENA* 44, 27–35. doi:10.1016/S0341-8162(00)00173-9

Hintze, L.F., Davis, F.D., 2003. *Geology of Millard County, Utah, Bulletin 133*. Utah Geological Survey, Salt Lake City.

Jewell, P.W., Nicoll, K., 2011. Wind regimes and aeolian transport in the Great Basin, U.S.A. *Geomorphology* 129, 1–13. doi:10.1016/j.geomorph.2011.01.005

King, J., Etyemezian, V., Sweeney, M., Buck, B.J., Nikolich, G., 2011. Dust emission variability at the Salton Sea, California, USA. *Aeolian Res., AGU Fall Meeting session on Aeolian Dust: Transport Processes, Anthropogenic Forces and Biogeochemical Cycling* 3, 67–79. doi:10.1016/j.aeolia.2011.03.005

Lawrence, C.R., Neff, J.C., 2009. The contemporary physical and chemical flux of aeolian dust: a synthesis of direct measurements of dust deposition. *Chem. Geol.* 267, 46–63. doi:10.1016/j.chemgeo.2009.02.005

Li, J., Okin, G.S., Herrick, J.E., Belnap, J., Munson, S.M., Miller, M.E., 2010. A simple method to estimate threshold friction velocity of wind erosion in the field. *Geophys. Res. Lett.* 37, L10402. doi:10.1029/2010GL043245

Marticorena, B., Bergametti, G., 1995. Modeling the atmospheric dust cycle: 1. Design of a soil-derived dust emission scheme. *J. Geophys. Res. Atmospheres* 100, 16415–16430. doi:10.1029/95JD00690

Marticorena, B., Bergametti, G., Gillette, D., Belnap, J., 1997. Factors controlling threshold friction velocity in semiarid and arid areas of the United States. *J. Geophys. Res. Atmospheres* 102, 23277–23287. doi:10.1029/97JD01303

Mazor, G., Kidron, G.J., Vonshak, A., Abeliovich, A., 1996. The role of cyanobacterial exopolysaccharides in structuring desert microbial crusts. *FEMS Microbiol. Ecol.* 21, 121–130. doi:10.1111/j.1574-6941.1996.tb00339.x

- Miller, M.E., Bowker, M.A., Reynolds, R.L., Goldstein, H.L., 2012. Post-fire land treatments and wind erosion – Lessons from the Milford Flat Fire, UT, USA. *Aeolian Res.* 7, 29-44. doi:10.1016/j.aeolia.2012.04.001
- Nguyen, L.P., Nol, E., Abraham, K.F., 2007. Using Digital Photographs to Evaluate the Effectiveness of Plover Egg Crypsis. *J. Wildl. Manag.* 71, 2084-2089.
- Okin, G., Murray, B., Schlesinger, W.H., 2001. Degradation of sandy arid shrubland environments: observations, process modelling, and management implications. *J. Arid Environ.* 47, 123–144.
- Okin, G.S., 2008. A new model of wind erosion in the presence of vegetation. *J. Geophys. Res. Earth Surf.* 113. doi:10.1029/2007JF000758
- Okin, G.S., Gillette, D.A., 2004. Modelling wind erosion and dust emission on vegetated surfaces, in: Kelly, R.E.J., Drake, N.A., Barr, S.L. (Eds.), *Spatial Modelling of the Terrestrial Environment*. John Wiley & Sons, Chichester, pp. 137–156.
- Painter, T.H., Deems, J.S., Belnap, J., Hamlet, A.F., Landry, C.C., Udall, B., 2010. Response of Colorado River runoff to dust radiative forcing in snow. *Proc. Natl. Acad. Sci.* doi:10.1073/pnas.0913139107
- Peterson, F.F., 1981. Landforms of the Basin and Range Province defined for soil survey. Nevada Agricultural Experiment Station, Max C. Fleischmann College of Agriculture, University of Nevada.
- Prospero, J.M., Ginoux, P., Torres, O., Nicholson, S.E., Gill, T.E., 2002. Environmental characterization of global sources of atmospheric soil dust identified with the nimbus 7 total ozone mapping spectrometer (TOMS) Absorbing Aerosol Product. *Rev. Geophys.* 40, 1002. doi:10.1029/2000RG000095
- R Core Team (2012). R: A language and environment for statistical computing. R Foundation for Statistical Computing, Vienna, Austria. <http://www.R-project.org/> (last accessed: 7/5/2014)
- Reynolds, R., Neff, J., Reheis, M., Lamothe, P., 2006. Atmospheric dust in modern soil on aeolian sandstone, Colorado Plateau (USA): variation with landscape position and contribution to potential plant nutrients. *Geoderma* 130, 108–123. doi:10.1016/j.geoderma.2005.01.012
- Schoeneberger, P.J., Wysocki, D.A., Benham, E.C., Broderson, W.D. (Eds.), 2003. *Field Book for Describing and Sampling Soils, Version 2.0*. Natural Resources Conservation Service. National Soil Survey Center, Lincoln.
- Shao, Y., Lu, H., 2000. A simple expression for wind erosion threshold friction velocity. *J. Geophys. Res. Atmospheres* 105, 22437–22443. doi:10.1029/2000JD900304

- Sweeney, M.R., McDonald, E.V., Etyemezian, V., 2011. Quantifying dust emissions from desert landforms, eastern Mojave Desert, USA. *Geomorphology* 135, 21–34.
doi:10.1016/j.geomorph.2011.07.022
- Tisdall, J.M., Oades, J.M., 1982. Organic matter and water-stable aggregates in soils. *J. Soil Sci.* 33, 141–163. doi:10.1111/j.1365-2389.1982.tb01755.x
- U.S. Department of Agriculture, 2014. National soil survey handbook, title 430 soil survey, part 618 (subpart B), exhibit 6.18.95 Wind Erodibility Groups (WEG) and Index.
http://www.nrcs.usda.gov/wps/portal/nrcs/detail/soils/home/?cid=nrcs142p2_054224#95 (last accessed: 7/5/2014)
- Wiggs, G.F.S., 1997. Sediment mobilisation by the wind, in: Thomas, D.S.G. (Ed.), *Arid Zone Geomorphology*. John Wiley & Sons, Ltd, pp. 351–372.
- Zhang, Z., Dong, Z., Zhao, A., Yuan, W., Han, L., 2008. The effect of restored microbiotic crusts on erosion of soil from a desert area in China. *J. Arid Environ.* 72, 710–721.
doi:10.1016/j.jaridenv.2007.09.001

Table 4-1. Threshold friction velocity of undisturbed and disturbed soil surfaces. Min. and Max. TFV are the minimum and maximum possible TFV values using 95% confidence intervals of regression parameters derived from adding and subtracting instrument error to measured pressure (Appendix A). Values with a greater than symbol (>) indicate TFV was not reached and TFVs were designated as being greater than the friction wind speed obtained from the actual velocity profile. Sediment is the amount of sediment collected in the wind tunnel at TFV. r^2 is the coefficient of determination obtained by regression of $\log z$ (height above soil surface; cm) against U (mean wind speed; cm/s).

| Surface type | Site ID | Undisturbed | | | | | Disturbed | | | | |
|-----------------|---------|-------------|-----------------|------------|-----------------|------------------------------|-----------|-----------------|------------|-----------------|------------------------------|
| | | R^2 | Min. TFV (cm/s) | TFV (cm/s) | Max. TFV (cm/s) | Sediment (g/m ²) | R^2 | Min. TFV (cm/s) | TFV (cm/s) | Max. TFV (cm/s) | Sediment (g/m ²) |
| Biological | 04 | | | >217.4 | | | 0.974 | 62.9 | 69.2 | 79.0 | 6.6 |
| Biological | 05 | | | >145.7 | | | 0.974 | 58.1 | 64.6 | 77.0 | 24.1 |
| Biological | 32 | | | >206.5 | | | 0.993 | 35.6 | 36.9 | 38.9 | 12.5 |
| Hard salt | 13 | | | >190.1 | | | 0.953 | 54.9 | 60.8 | 73.9 | 38.4 |
| Hard salt | 16 | | | >179.9 | | | 0.843 | 80.0 | 103.5 | 164.3 | 15.5 |
| Hard salt | 17 | | | >316.2 | | | 0.973 | 39.4 | 41.6 | 47.4 | 13.3 |
| Hard salt | 18 | | | >218.1 | | | 0.823 | 48.9 | 77.5 | 167.5 | 86.2 |
| Hard salt | 33 | | | >191.7 | | | 0.869 | 92.8 | 119.6 | 180.2 | 24.9 |
| Surficial rocks | 01 | 0.990 | 87.1 | 93.3 | 101.9 | 370.3 | 0.967 | 68.0 | 75.8 | 89.4 | 179.9 |
| Surficial rocks | 03 | 0.994 | 102.8 | 107.6 | 114.2 | 236.8 | 0.971 | 47.8 | 53.2 | 61.0 | 129.9 |
| Surficial rocks | 06 | 0.982 | 110.7 | 123.7 | 141.3 | 34.1 | 0.994 | 104.7 | 110.5 | 117.3 | 120.5 |
| Surficial rocks | 07 | 0.980 | 97.3 | 107.2 | 121.7 | 7.8 | 0.993 | 110.1 | 101.0 | 105.3 | 12.6 |
| Surficial rocks | 10 | | | >153.0 | | | 0.988 | 45.9 | 52.6 | 60.9 | 74.4 |
| Surficial rocks | 12 | 0.993 | 109.4 | 117.2 | 127.1 | 42.1 | 0.959 | 55.5 | 63.9 | 78.1 | 62.4 |
| Surficial rocks | 21 | 0.938 | 115.0 | 139.7 | 181.4 | 49.1 | 0.988 | 75.4 | 87.8 | 102.5 | 16.2 |
| Surficial rocks | 24 | 0.963 | 134.7 | 152.9 | 182.3 | 120.6 | 0.994 | 104.7 | 110.9 | 119.4 | 122.7 |
| Surficial rocks | 25 | | | >144.2 | | | 0.978 | 123.9 | 137.6 | 157.6 | 97.1 |
| Surficial rocks | 26 | 0.974 | 98.5 | 110.1 | 127.7 | 408.9 | 0.994 | 40.8 | 42.0 | 43.2 | 15.1 |
| Surficial rocks | 29 | | | >232.7 | | | 0.911 | 42.5 | 53.1 | 74.7 | 22.0 |
| Surficial rocks | 30 | | | >272.7 | | | 0.916 | 149.7 | 123.9 | 222.8 | 103.9 |

| | | | | | | | | | | | |
|---------------|----|-------|-------|--------|-------|-------|-------|------|-------|-------|-------|
| Hard physical | 02 | | | >146.9 | | | 0.999 | 93.8 | 103.2 | 112.2 | 6.3 |
| Hard physical | 08 | | | >155.6 | | | 0.991 | 53.3 | 57.3 | 62.9 | 7.3 |
| Hard physical | 09 | 0.954 | 104.9 | 124.0 | 154.7 | 73.6 | 0.953 | 56.9 | 76.3 | 106.8 | 4.1 |
| Hard physical | 15 | | | >146.7 | | | 0.941 | 87.6 | 105.2 | 136.2 | 19.1 |
| Hard physical | 23 | 0.951 | 80.3 | 93.6 | 116.8 | 221.1 | 0.873 | 31.6 | 51.4 | 98.9 | 87.2 |
| Hard physical | 27 | | | >172.0 | | | 0.877 | 26.7 | 35.5 | 56.1 | 7.3 |
| Hard physical | 28 | | | >175.2 | | | 0.975 | 54.2 | 61.5 | 72.3 | 11.3 |
| Hard physical | 31 | | | >214.2 | | | 0.935 | 37.3 | 44.4 | 58.4 | 2.7 |
| Weak physical | 11 | 0.931 | 81.0 | 99.1 | 163.3 | 177.3 | 0.989 | 34.7 | 36.6 | 39.1 | 54.4 |
| Weak physical | 14 | 0.970 | 102.9 | 111.0 | 123.7 | 556.9 | 0.978 | 49.9 | 51.9 | 57.3 | 29.9 |
| Weak physical | 19 | 0.943 | 59.2 | 79.8 | 130.3 | 116.4 | 0.991 | 43.2 | 52.3 | 65.6 | 10.9 |
| Weak physical | 20 | 0.962 | 82.9 | 99.8 | 126.9 | 156.5 | 0.977 | 36.0 | 31.2 | 31.8 | 586.4 |
| Weak physical | 22 | 0.965 | 123.6 | 141.0 | 168.3 | 77.9 | 0.947 | 37.2 | 43.9 | 54.4 | 136.6 |

Missing values indicate TFV not reached

Minimum and maximum TFV from 95% confidence intervals of measurements corrected for instrument error.

Table 4-2. Multiple linear regressions that best predict undisturbed TFV for soils with surficial rock fragments and weak physical crusts.

| Crust Type | Intercept | Silt (%) | Penetrometer (kg) | Rock Cover (%) | R^2 | P | RMSE (cm/s) |
|--------------------------|-----------|----------|-------------------|----------------|-------|-------|-------------|
| Surficial rock fragments | -32.21 | - | 6.338 | 1.797 | 0.92 | 0.002 | 5.02 |
| Weak physical crust | 169.20 | -1.126 | - | - | 0.93 | 0.008 | 5.26 |

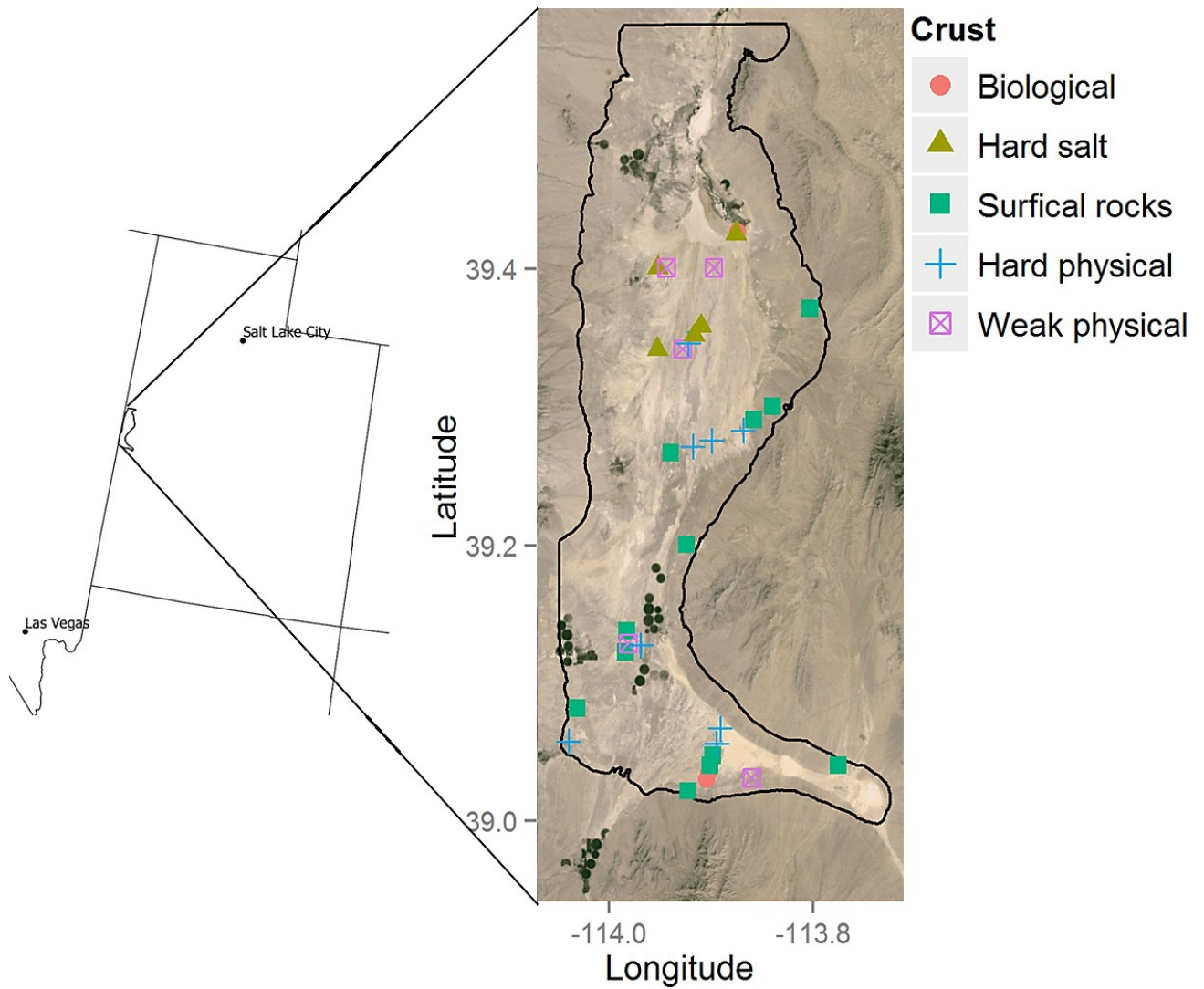


Fig. 4-1. Study area location in Snake Valley, Utah, adjacent to the Nevada border. Points overlain on air photo represent crust class locations measured for TFV.



Fig. 4-2. Clear plastic main working section of the portable wind tunnel used to measure TFV. Honeycomb flow straightener is located to the right. The expansion chamber and filter (not in photo) are located to the left. Wind travels along wind tunnel from right to left. Yellow and black tubes connect the pitot tube inside the wind tunnel to the Fluke 922 airflow meter/micromanometer.

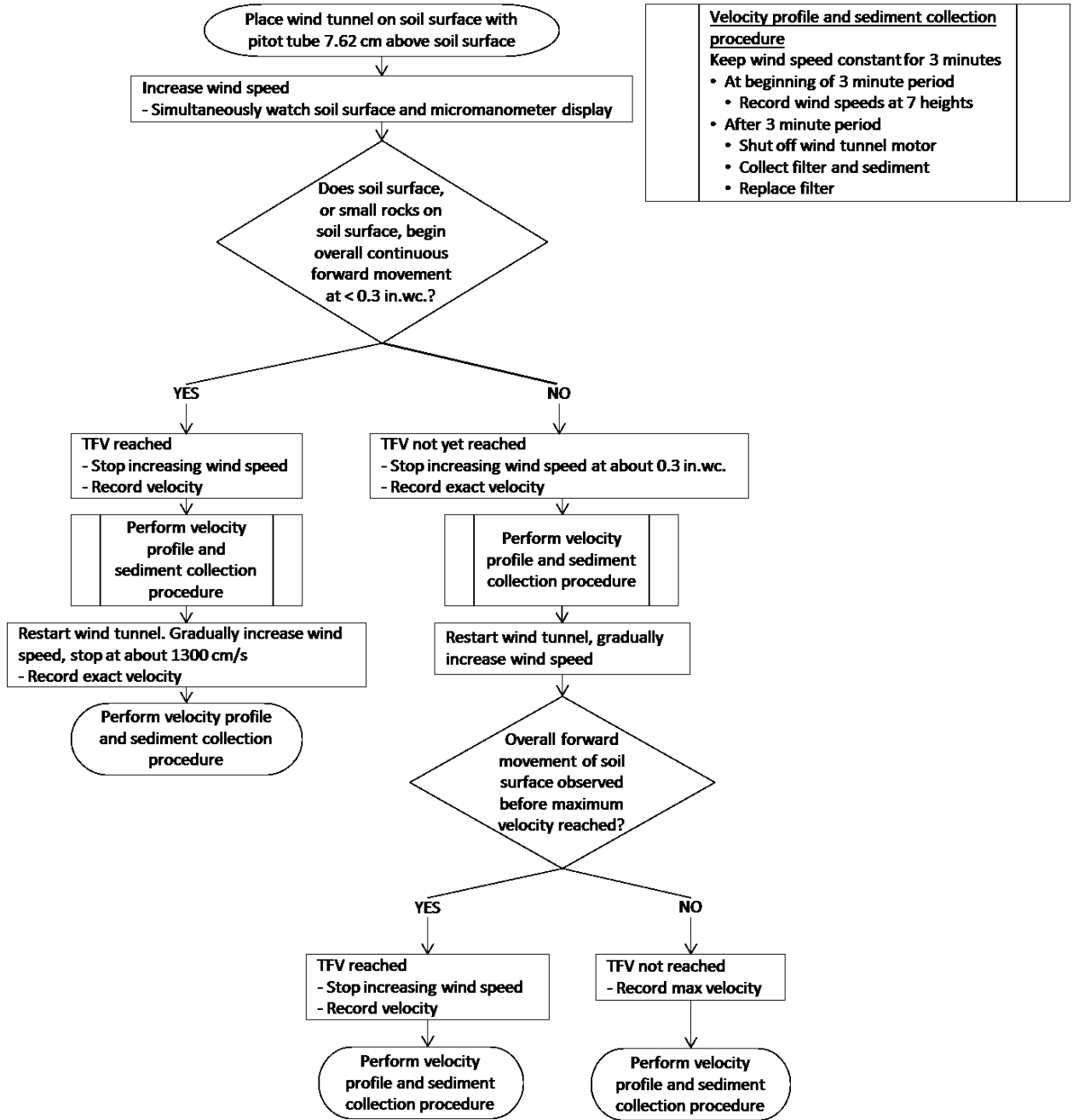


Fig. 4-3. Threshold friction velocity measurement procedure.



Fig. 4-4. Photos of representative sites from each soil surface type. From top to bottom: biological crust (A), hard salt crust (B), surficial rock fragments (C), hard physical crust (D), and weak physical crust (E). The steel frame in each photo is equal to the wind tunnel footprint.

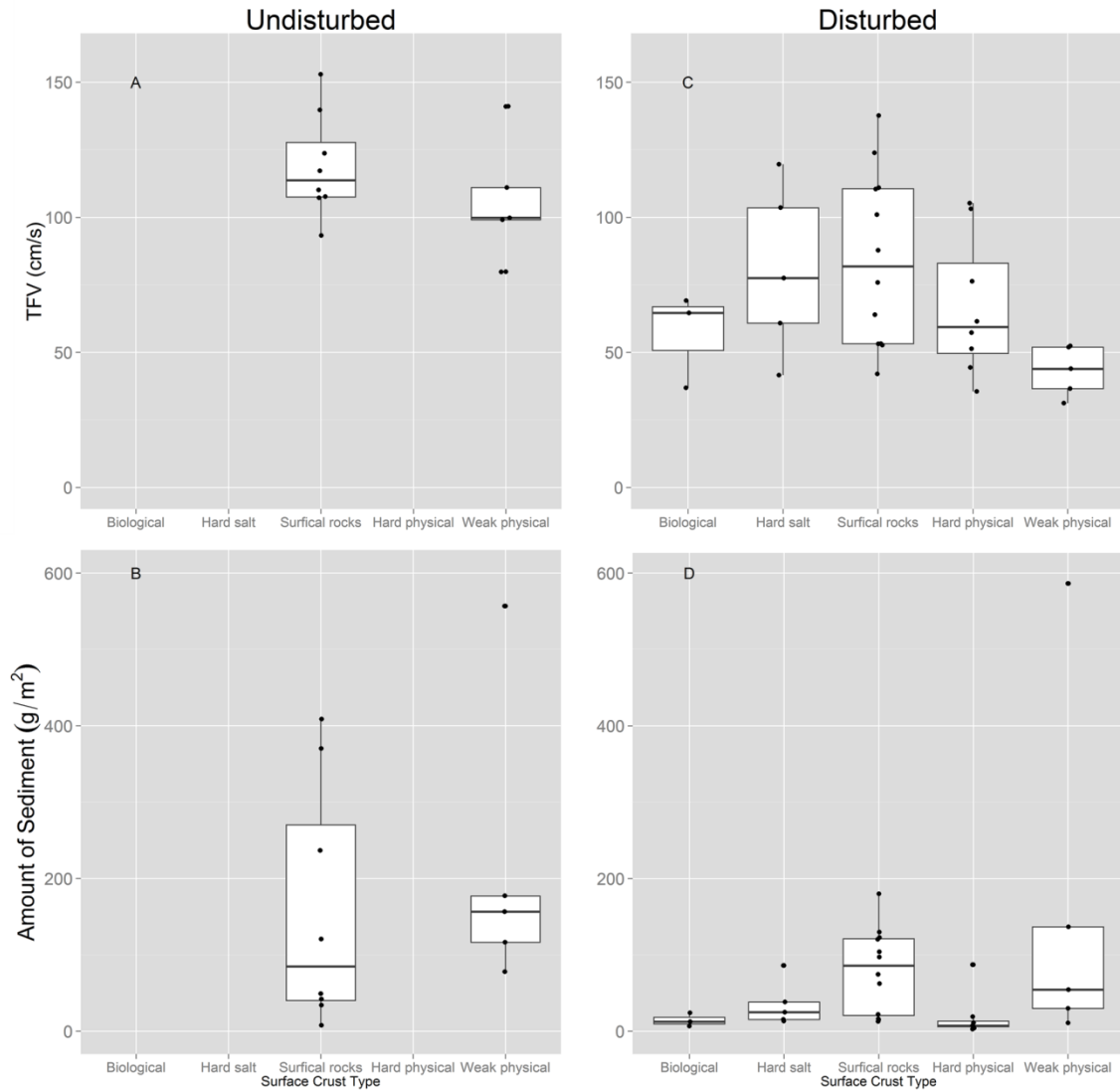


Fig. 4-5. Dot-boxplots of threshold friction velocity (TFV; top, A and C) and the amount of sediment produced (bottom, B and D) by surface type for undisturbed (left; A and B) and disturbed (right; C and D) soil surfaces. TFV for soils with undisturbed biological crusts, hard salt crusts, and hard physical crusts were not reached. Individual points are actual measurement values and have been slightly offset to avoid over plotting.

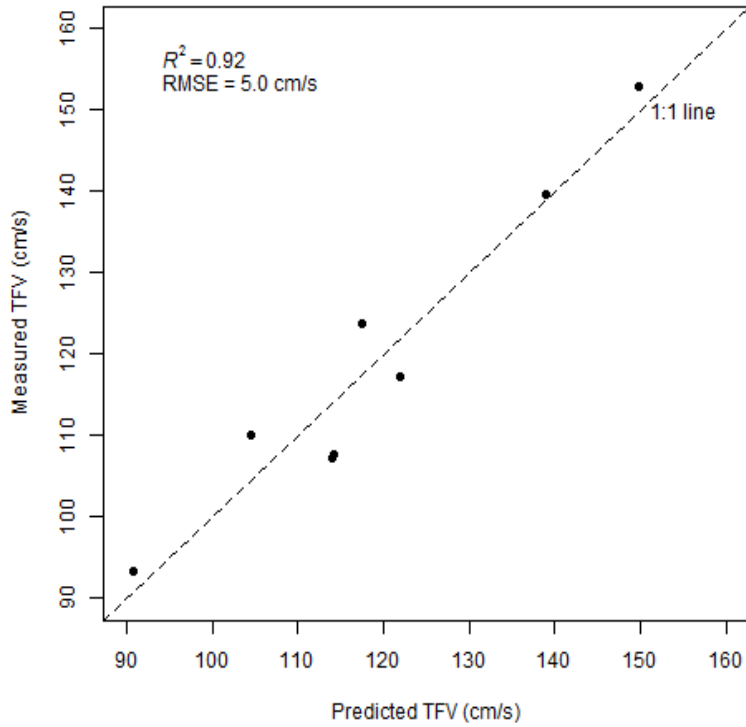


Fig. 4-6. Plot of measured vs. predicted TFV for undisturbed soils with surficial rock fragments. Threshold friction velocity was predicted using penetrometer and percent rock cover measurements. RMSE is the root mean square error of estimation (cm/s).

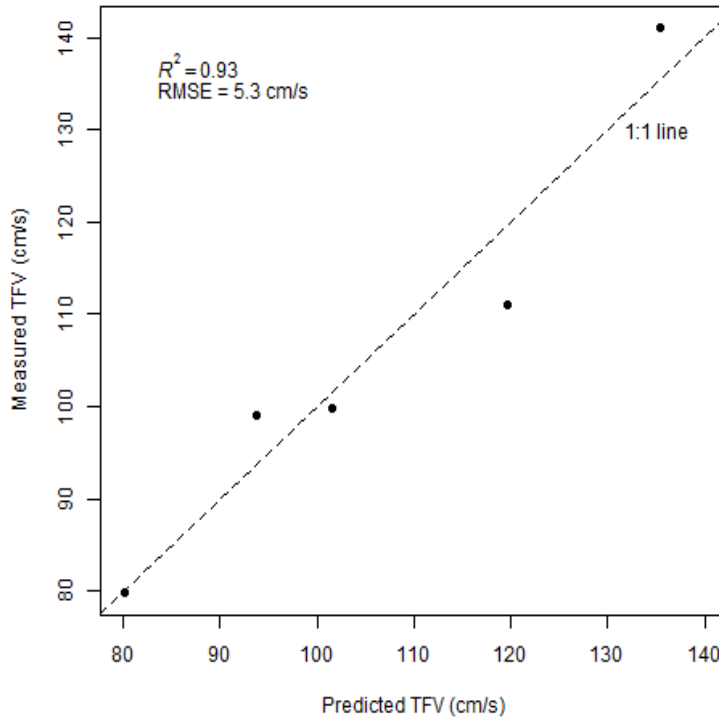


Fig. 4-7. Plot of measured vs. predicted TFV for undisturbed soils with weak physical crusts. Threshold friction velocity was predicted using silt concentration (%). RMSE is the root mean square error of estimation (cm/s).

CHAPTER 5

CONCLUSIONS

This dissertation explored the application of digital soil mapping for producing spatially explicit soil information that may be useful for arid and semi-arid land management in the western United States. Chapter 2 provided insight into the use of machine learning for digital soil mapping of soil taxonomic classes. No machine learning model was consistently the most accurate classifier; however, bagging classification trees and random forests were among the most accurate classifiers for two of the three areas, suggesting the utility of these models. Models were most accurate when built using covariates identified with a quantitative covariate selection technique. Prediction accuracy was greatest when there were few soil taxonomic classes and when the frequency distribution of soil observations was approximately equal between taxonomic classes.

Chapter 3 applied digital soil mapping to predict potential biological soil crust (BSC) level-of-development (LOD) class distribution over a large area surrounding Canyonlands National Park. Spatial predictions of moderate BSC LOD class potential were reasonably accurate. Spatial predictions of low and high BSC LOD class potential were likely not reliable. Prediction accuracy was dependent upon the relationship between each LOD class and the predictor covariates. Prediction accuracy could likely be improved through the use of additional covariates. However, some classes may be difficult to model. Spatial predictions of BSC LOD class probabilities and the final class map may be useful for assessing the impact of land use practices on BSC distribution.

Chapter 4 reported measured threshold friction velocities (TFV) and sediment production for undisturbed and disturbed lacustrine and alluvial soils in the eastern Great Basin. The nature of the soil surface was useful to explain differences in TFV and sediment production.

Undisturbed soils with surficial rock fragments and weak physical crusts had lower TFVs, and thus were more susceptible to wind erosion, than soils with biological crusts, hard salt crusts, and hard physical crusts. However, it is important to note that in this study TFV was measured with a 15-cm high wind tunnel, which physically restricted large scale (e.g., 2-km) turbulent eddies. Therefore, we cannot rule out that TFV of undisturbed soils with biological crusts, hard salt crusts, and hard physical crusts would not be reached in natural conditions.

When disturbed, soils with surficial rocks or weak physical crusts had low TFV and produced relatively large amounts of sediment. When compared with other soil surface types, soils with surficial rock fragments or weak physical crusts are likely the most susceptible to wind erosion. Threshold friction velocity in undisturbed soils with surficial rock fragments and weak physical crusts could be predicted using a combination of penetrometer force, percent surface rock cover, and silt concentration (%). Threshold friction velocity in disturbed soils could not be predicted using any of the measured soil surface properties.

Taken together, the results from Chapters 2 and 3 illustrate the utility of digital soil mapping for producing spatially explicit soil information with known error useful for the management of arid and semi-arid lands. Additionally the results from these chapters reveal the dependence of digital soil mapping prediction accuracy on the number of available observations. Digital soil mapping predictions have the lowest error when many observations are available. Because observations for digital soil mapping are dependent upon the method used to identify sampling locations, sampling strategies must be considered when applying digital soil mapping. One must also consider that some classes may be difficult to model within the study area regardless of the number of observations, such as with the high level-of-development biological soil crust class in Chapter 3.

While not directly an application of digital soil mapping, the results from Chapter 4 provide a first step towards using digital soil mapping to provide the soil information necessary to understand and manage the impacts of soil disturbance and potential groundwater withdrawal on wind erosion in arid and semi-arid areas. For example, it is likely possible to use digital soil mapping to derive soil surface types, percent rock fragment cover, or silt concentration, and to identify areas that require further field sampling, to produce spatially explicit estimates of TFV.

Ultimately, the rapid and reliable production of soil information with known error is essential for land management decisions. The results of this dissertation demonstrate that digital soil mapping can provide such information.

APPENDICES

APPENDIX A. THRESHOLD FRICTION VELOCITY MEASUREMENT ERROR ESTIMATION

A.1 Rational for estimating TFV measurement uncertainty

Threshold friction velocity was measured using the same wind tunnel as multiple previous studies (Belnap and Gillette, 1997, Belnap and Gillette, 1998, Belnap et al., 2007, Gillette et al., 1980, Gillette et al., 1982, Gillette, 1988, Li et al., 2010, and Marticorena et al., 1997), but implemented a digital micromanometer to measure wind velocities. All previous studies used a manual manometer. The use of a digital micromanometer allowed the estimation of measurement error.

A.2 TFV measurement uncertainty estimation methods

Uncertainty in threshold friction velocity measurements resulted from three sources: technician error, instrument error, and regression parameter uncertainty. Technician error was the inability of wind tunnel technicians to visually estimate the exact moment when TFV occurred, and to record a wind velocity profile at that instant. This was particularly noticeable when TFV occurred at very low wind velocities. We were unable to quantify this source of error, but it is likely minimal.

Instrument error was the inherent micromanometer measurement error and was a function of measurement magnitude (lower pressures had greater error) and temperature (Fluke 922 user's manual, http://assets.fluke.com/manuals/922_umeng0100.pdf). Because instrument error was not constant, adding and subtracting instrument error from each measurement resulted in two different regression coefficients and thus two different TFV estimates. Regression parameter uncertainty was the uncertainty associated with each regression coefficient used to calculate TFV (Equations 4-4 and 4-5, Chapter 4, section 2.2). Plots of measured wind speed profiles with corrections for measurement error and regression uncertainty for undisturbed and disturbed soil surfaces at TFV are presented in Figs A-1 to A-9, and A-10 to A-18, respectively.

To quantify the relative influence of instrument error and regression parameter uncertainty on the estimation of threshold friction velocity, TFV was calculated using two inputs to Equation 4-4 (Chapter 4, section 2.2). These inputs were: 1) regression coefficients from measurements corrected for \pm instrument error, and 2) upper and lower 95% confidence interval bounds of the regression coefficient using the initial measurements. The input that resulted in the widest range of TFV values was considered the largest source of uncertainty.

A.3 TFV measurement uncertainty

Regression coefficient uncertainty was the largest overall source of TFV uncertainty (Fig. A-19). Regression coefficient uncertainty, measured as confidence interval width, is a function of both the linearity of the regression and the number of observations used in the regression. Regression coefficient uncertainty is greatest when the regression deviates from linear and there are relatively few observations.

In addition to increasing TFV uncertainty, deviance from linearity (measured with the coefficient of determination, r^2) impacts the validity of TFV estimates. The law-of-wall is valid only when a log-linear relationship between height and velocity exists. When the regression is not log-linear, TFV is not valid.

Based on our observations, deviance from linearity was largely the result of convection. Mitigating convection could be done by operating the wind tunnel when environmental conditions reduce convection from soil surface heating, such as in the spring and autumn or during the morning and evening. If the wind tunnel is operated when convection is likely, shading the wind tunnel and micromanometer is necessary (optimal micromanometer temperature is < 28 °C). Shading the wind tunnel would have the additional benefit of increasing operator comfort, thereby helping to minimize operator error.

In addition to mitigating convection, a practical way to ensure high linearity could be through the use of a pre-programmed spreadsheet designed to automatically calculate TFV and uncertainty. If used on a laptop or tablet computer, uncertainty could be assessed at the time the wind profile is measured and if non-linear, another wind profile collected. If this is not possible, multiple wind profiles should be recorded at TFV.

Regression parameter uncertainty is also influenced by the number of observations used in the regression; more observations result in narrower confidence intervals. To investigate the impact of adding additional observations on TFV uncertainty, we simulated five additional observations for a highly log-linear wind profile (Table 4-1, Chapter 4, undisturbed site 3, $r^2 = 0.994$). Simulated pitot tube heights were taken midway between existing heights (e.g. 5.08 cm between 2.54 and 7.62 cm). Simulated wind velocities at these heights were derived using the regression equation for this wind profile with random error added to each observation. Random error was constrained to the interval of the regression residual standard deviation.

Adding additional observations reduced TFV uncertainty up to 46.5% (Fig. A-20). As additional observations require very little additional time to measure, and as it is difficult to collect more than five additional measurements at set heights within the wind tunnel, we recommend that wind speeds be recorded at twelve pitot tube heights (the original seven, plus an additional five) for every wind profile.

Although not as significant as regression parameter uncertainty, instrument error does influence TFV uncertainty, particularly for wind profiles that have low regression parameter uncertainty (e.g. disturbed sites 7 and 20, Fig. A-19). Uncertainty in TFV resulting from instrument error could be reduced by measuring wind profiles in units of velocity (cm/s) instead of units of pressure (inches of water column), even though instrument error is greater for units of velocity. This reduction in TFV uncertainty when using units of velocity is because required

velocity measurement correction changes regression parameters relatively little compared to required pressure measurement corrections. This is particularly noticeable for low wind velocities.

The lowest absolute TFV uncertainty using Equation 4-4 was 12.9 cm/s (disturbed site 32, $r^2 = 0.993$, Table 4-1, Fig. A-19) which may approximate the lower boundary of achievable TFV accuracy under common field conditions using the Fluke 922 airflowmeter/micromanometer. Uncertainties in previously published TFV values using this wind tunnel and a manual manometer (Belnap and Gillette, 1997, Belnap and Gillette, 1998, Belnap et al., 2007, Gillette et al., 1980, Gillette et al., 1982, Gillette, 1988, Li et al., 2010, and Marticorena et al., 1997) are likely not less than this value.

A.4 TFV measurement uncertainty conclusions.

Threshold friction velocity measurement uncertainty is mostly a function of regression parameter uncertainty. Future users of this micromanometer and wind tunnel should ensure that all measured velocity profiles are highly log-linear (generally $r^2 > 0.98$), should take wind speed readings at twelve pitot tube heights, and should measure wind profiles in units of velocity.

A.5 References

- Belnap, J., Gillette, D.A., 1997. Disturbance of biological soil crusts: impacts on potential wind erodibility of sandy desert soils in southeastern Utah. *Land Degrad. Dev.* 8, 355–362. doi:10.1002/(SICI)1099-145X(199712)8:4<355::AID-LDR266>3.0.CO;2-H
- Belnap, J., Gillette, D.A., 1998. Vulnerability of desert biological soil crusts to wind erosion: the influences of crust development, soil texture, and disturbance. *J. Arid Environ.* 39, 133–142. doi:10.1006/jare.1998.0388
- Belnap, J., Phillips, S.L., Herrick, J.E., Johansen, J.R., 2007. Wind erodibility of soils at Fort Irwin, California (Mojave Desert), USA, before and after trampling disturbance: implications for land management. *Earth Surf. Process. Landf.* 32, 75–84. doi:10.1002/esp.1372

- Gillette, D., Adams, J., Endo, A., Smith, D., Kihl, R., 1980. Threshold Velocities for Input of Soil Particles into the Air by Desert Soils. *J. Geophys. Res.-Oceans Atmospheres* 85, 5621–5630. doi:10.1029/JC085iC10p05621
- Gillette, D.A., 1988. Threshold friction velocities for dust production for agricultural soils. *J. Geophys. Res. Atmospheres* 93, 12645–12662. doi:10.1029/JD093iD10p12645
- Gillette, D.A., Adams, J., Muhs, D., Kihl, R., 1982. Threshold friction velocities and rupture moduli for crusted desert soils for the input of soil particles into the air. *J. Geophys. Res. Oceans* 87, 9003–9015. doi:10.1029/JC087iC11p09003
- Li, J., Okin, G.S., Herrick, J.E., Belnap, J., Munson, S.M., Miller, M.E., 2010. A simple method to estimate threshold friction velocity of wind erosion in the field. *Geophys. Res. Lett.* 37, L10402. doi:10.1029/2010GL043245
- Marticorena, B., Bergametti, G., Gillette, D., Belnap, J., 1997. Factors controlling threshold friction velocity in semiarid and arid areas of the United States. *J. Geophys. Res. Atmospheres* 102, 23277–23287. doi:10.1029/97JD01303

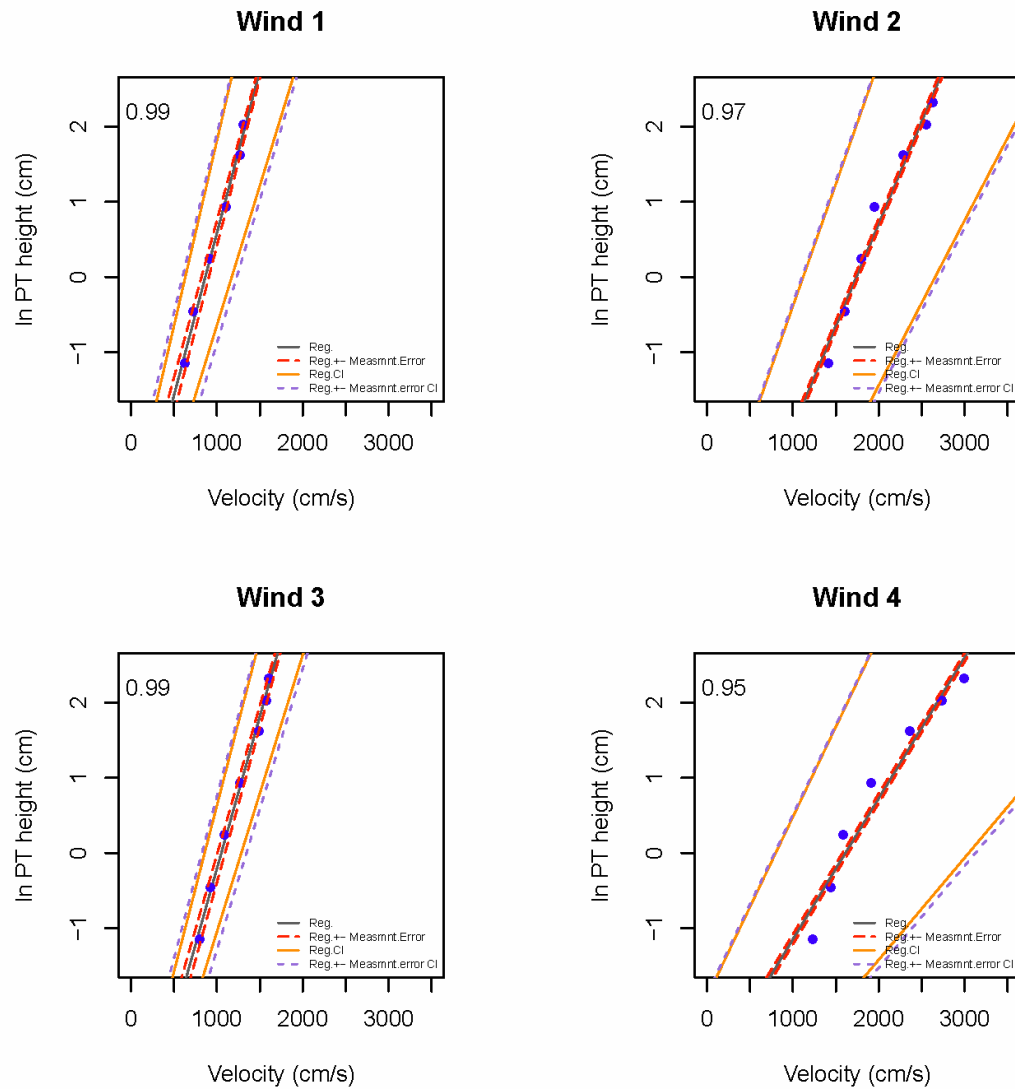


Fig. A-1. Measured wind speed profiles of the undisturbed soil surfaces at TFV for sampling sites 1-4. Blue dots represent measured values. Lines represent regressions and estimated error using Equation 4-4. Text in upper left corners are the coefficient of determination (r^2) for each regression.

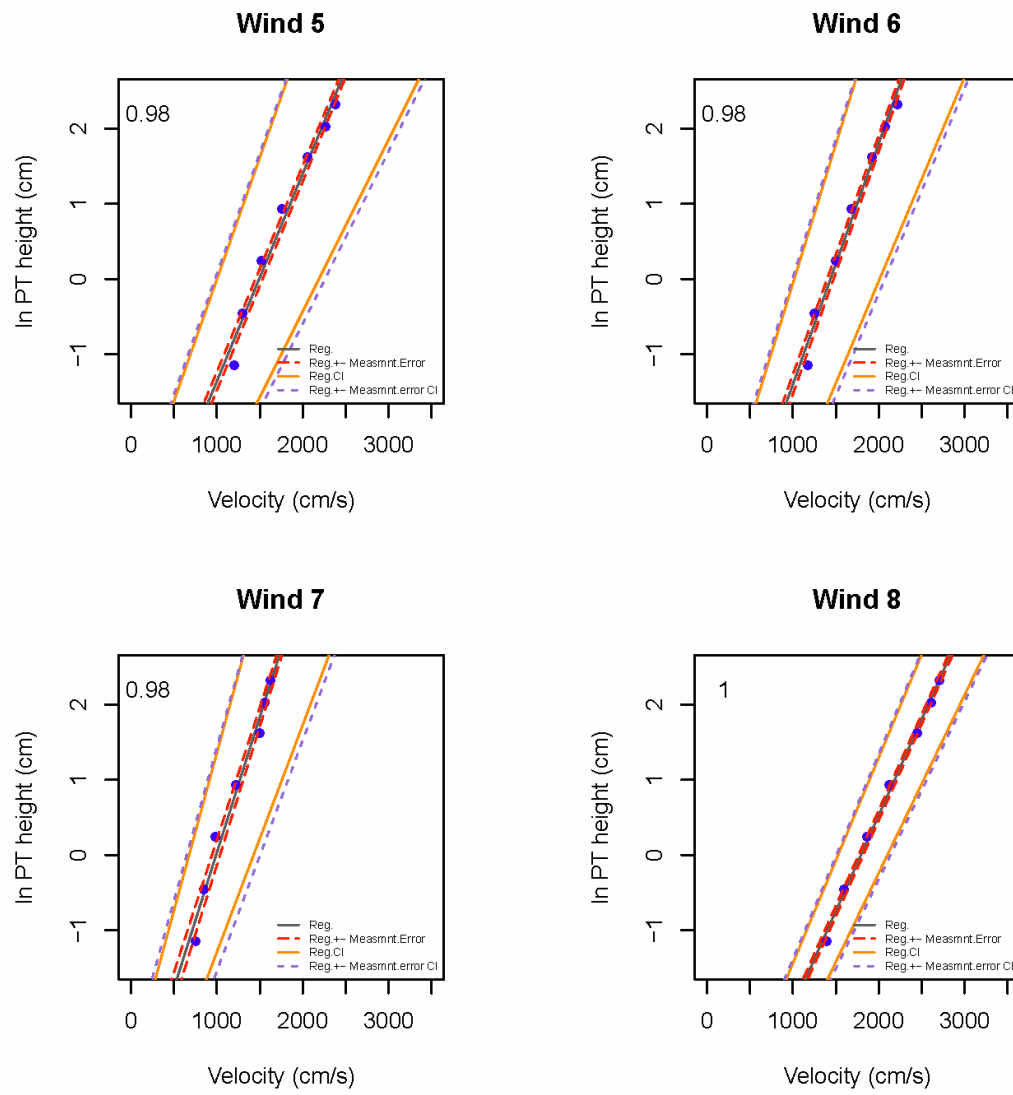


Fig. A-2. Measured wind speed profiles of the undisturbed soil surfaces at TFV for sampling sites 5-8. Blue dots represent measured values. Lines represent regressions and estimated error using Equation 4-4. Text in upper left corners are the coefficient of determination (r^2) for each regression.

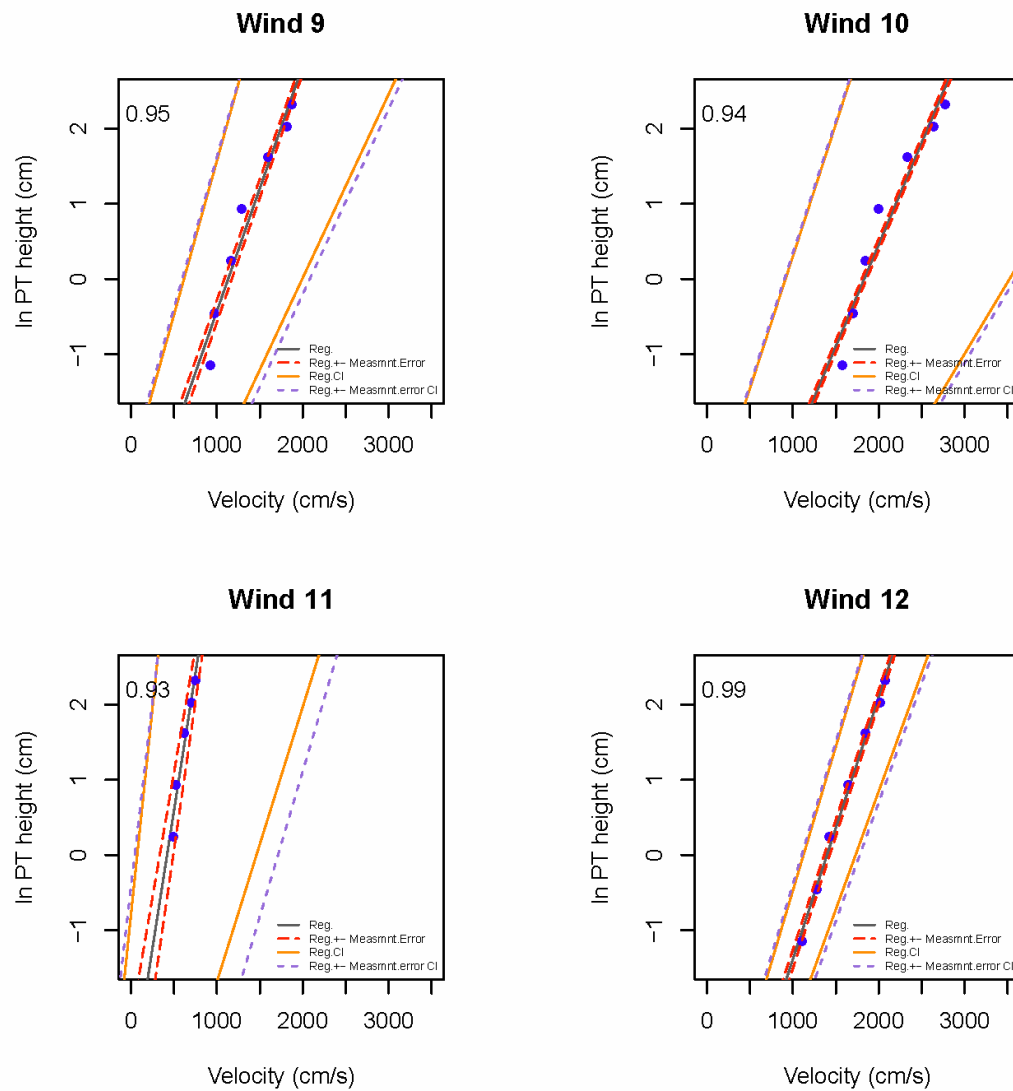


Fig. A-3. Measured wind speed profiles of the undisturbed soil surfaces at TFV for sampling sites 9-12. Blue dots represent measured values. Lines represent regressions and estimated error using Equation 4-4. Text in upper left corners are the coefficient of determination (r^2) for each regression.

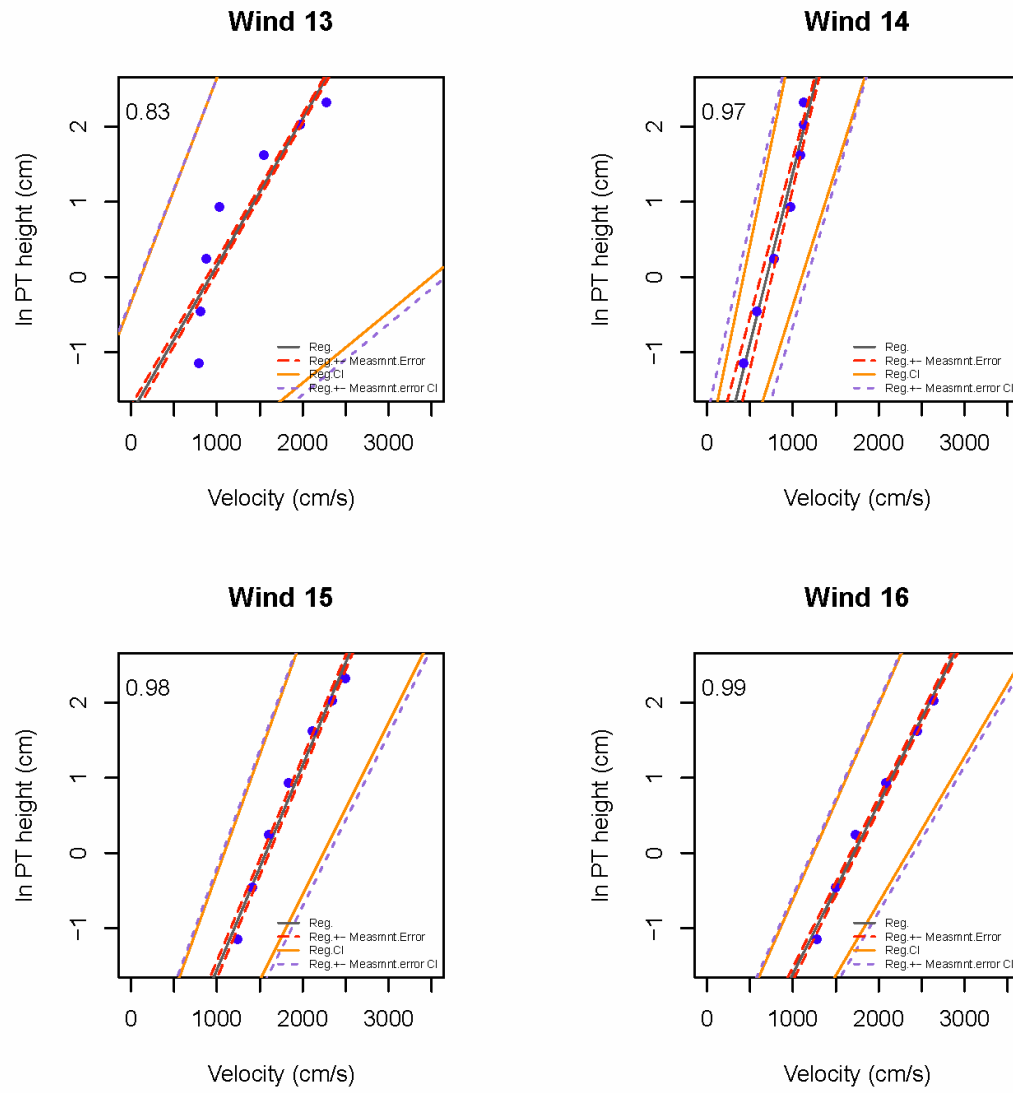


Fig. A-4. Measured wind speed profiles of the undisturbed soil surfaces at TFV for sampling sites 13-16. Blue dots represent measured values. Lines represent regressions and estimated error using Equation 4-4. Text in upper left corners are the coefficient of determination (r^2) for each regression.

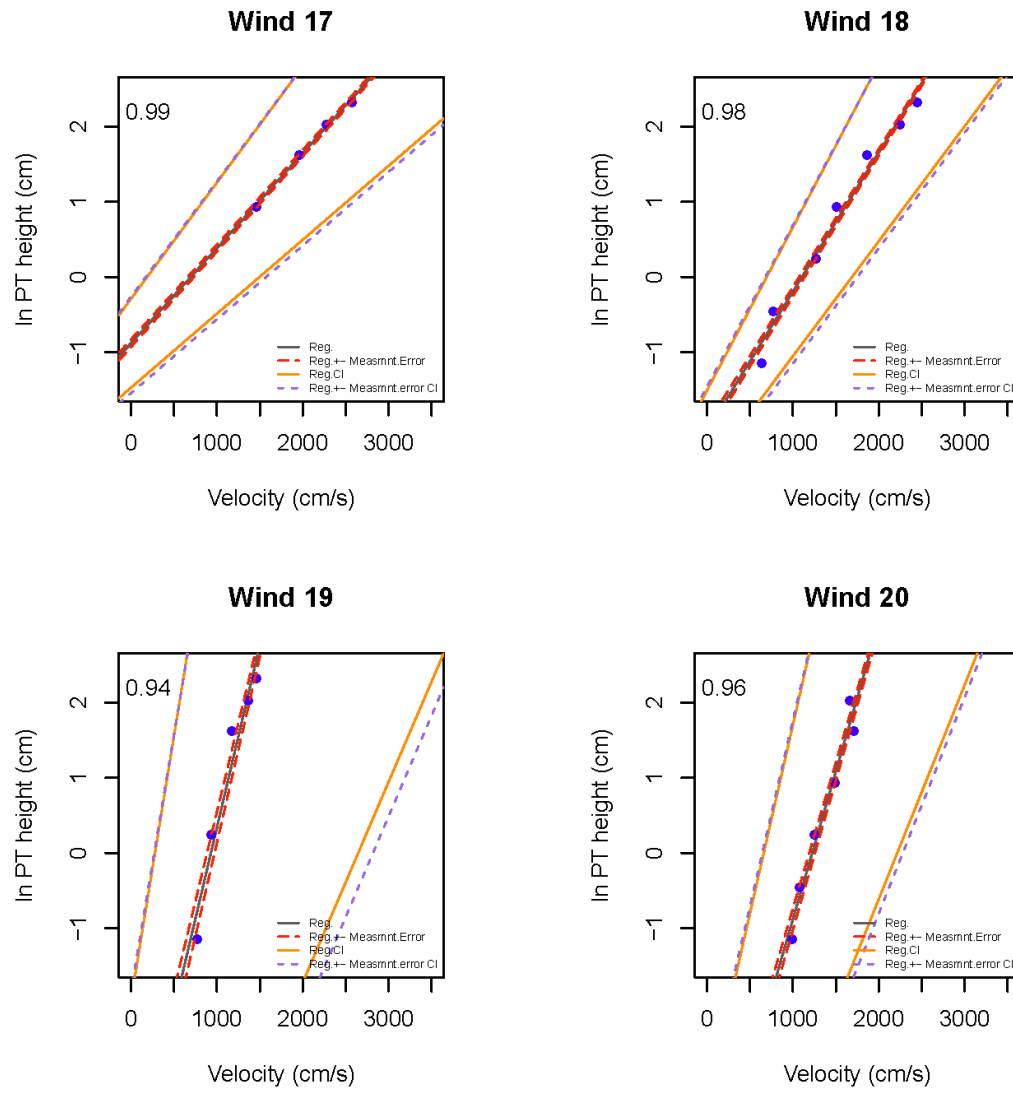


Fig. A-5. Measured wind speed profiles of the undisturbed soil surfaces at TFV for sampling sites 17-20. Blue dots represent measured values. Lines represent regressions and estimated error using Equation 4-4. Text in upper left corners are the coefficient of determination (r^2) for each regression.

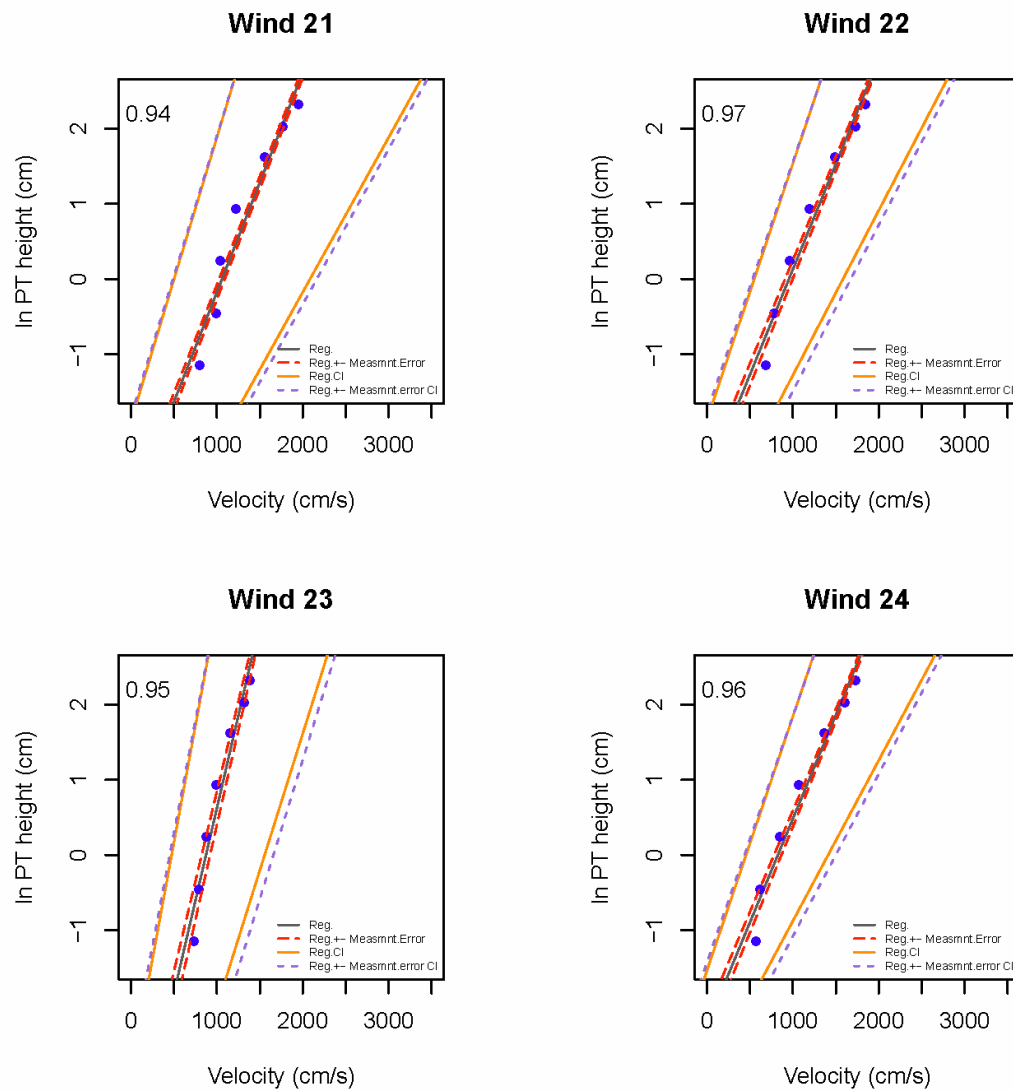


Fig. A-6. Measured wind speed profiles of the undisturbed soil surfaces at TFV for sampling sites 21-24. Blue dots represent measured values. Lines represent regressions and estimated error using Equation 4-4. Text in upper left corners are the coefficient of determination (r^2) for each regression.

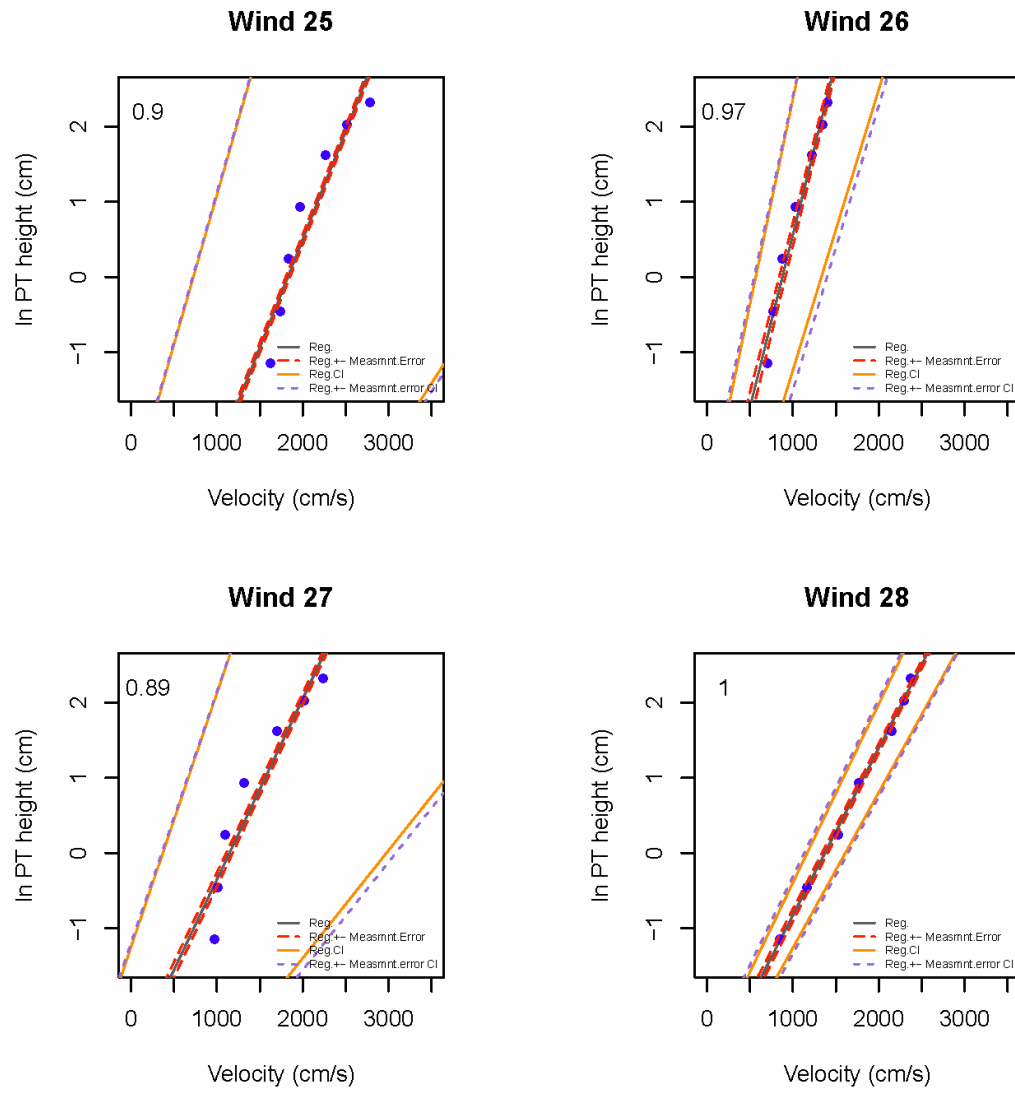


Fig. A-7. Measured wind speed profiles of the undisturbed soil surfaces at TFV for sampling sites 25-28. Blue dots represent measured values. Lines represent regressions and estimated error using Equation 4-4. Text in upper left corners are the coefficient of determination (r^2) for each regression.

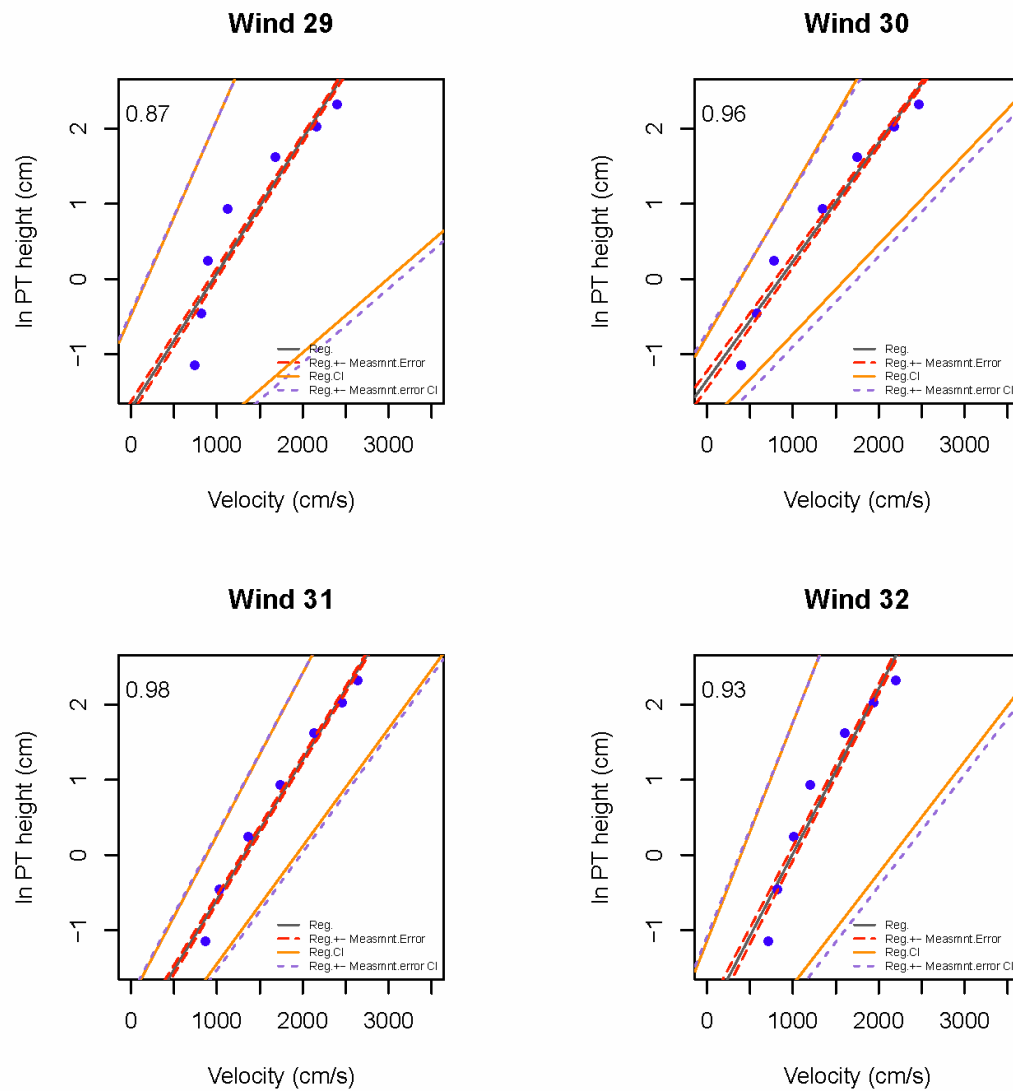


Fig. A-8. Measured wind speed profiles of the undisturbed soil surfaces at TFV for sampling sites 29-32. Blue dots represent measured values. Lines represent regressions and estimated error using Equation 4-4. Text in upper left corners are the coefficient of determination (r^2) for each regression.

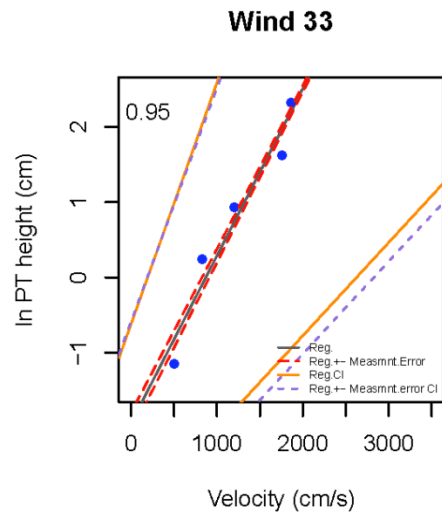


Fig. A-9. The measured wind speed profile of the undisturbed soil surface at TFV for sampling site 33. Blue dots represent measured values. Lines represent regressions and estimated error using Equation 4-4. Text in upper left corners are the coefficient of determination (r^2) for each regression.

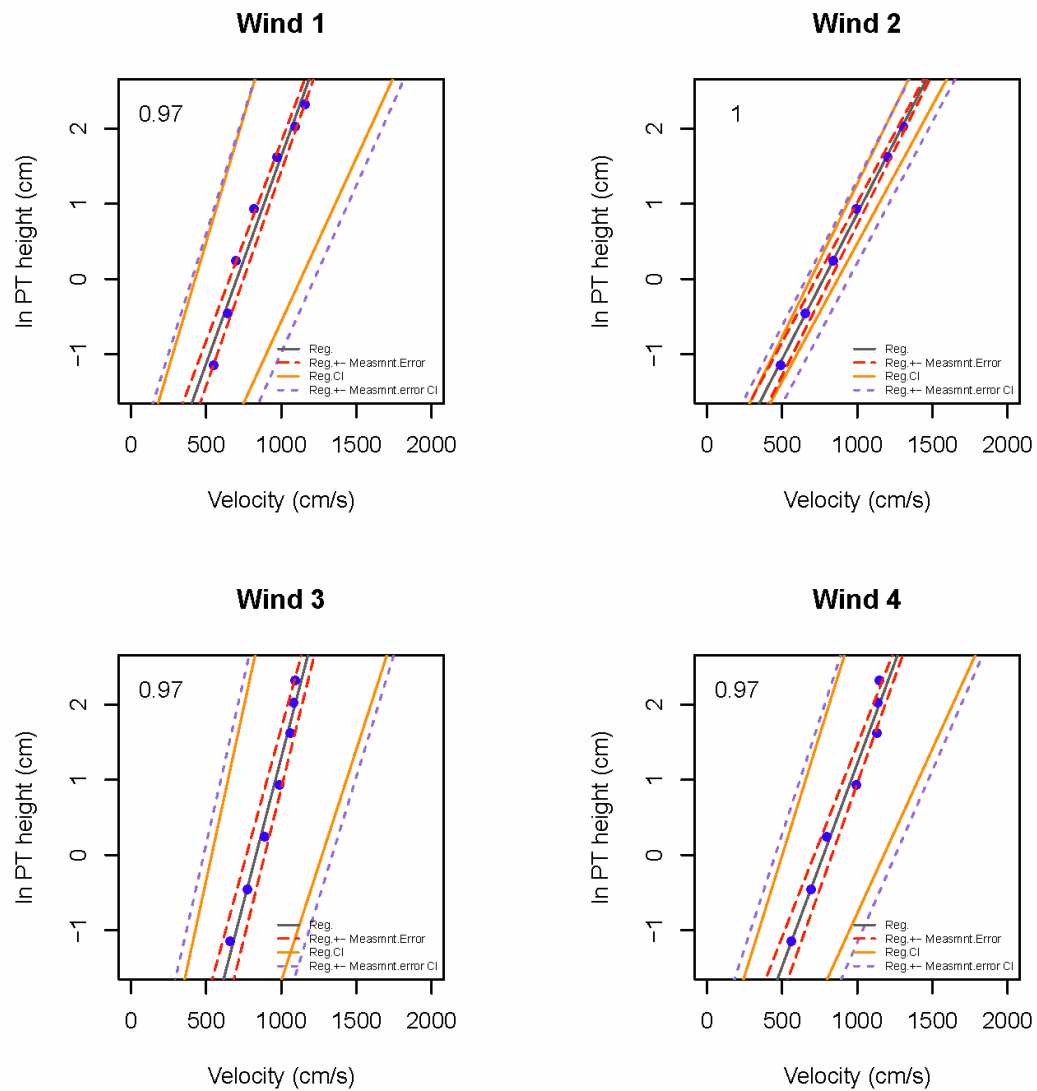


Fig. A-10. Measured wind speed profiles of the disturbed soil surfaces at TFV for sampling sites 1-4. Blue dots represent measured values. Lines represent regressions and estimated error using Equation 4-4. Text in upper left corners are the coefficient of determination (r^2) for each regression.

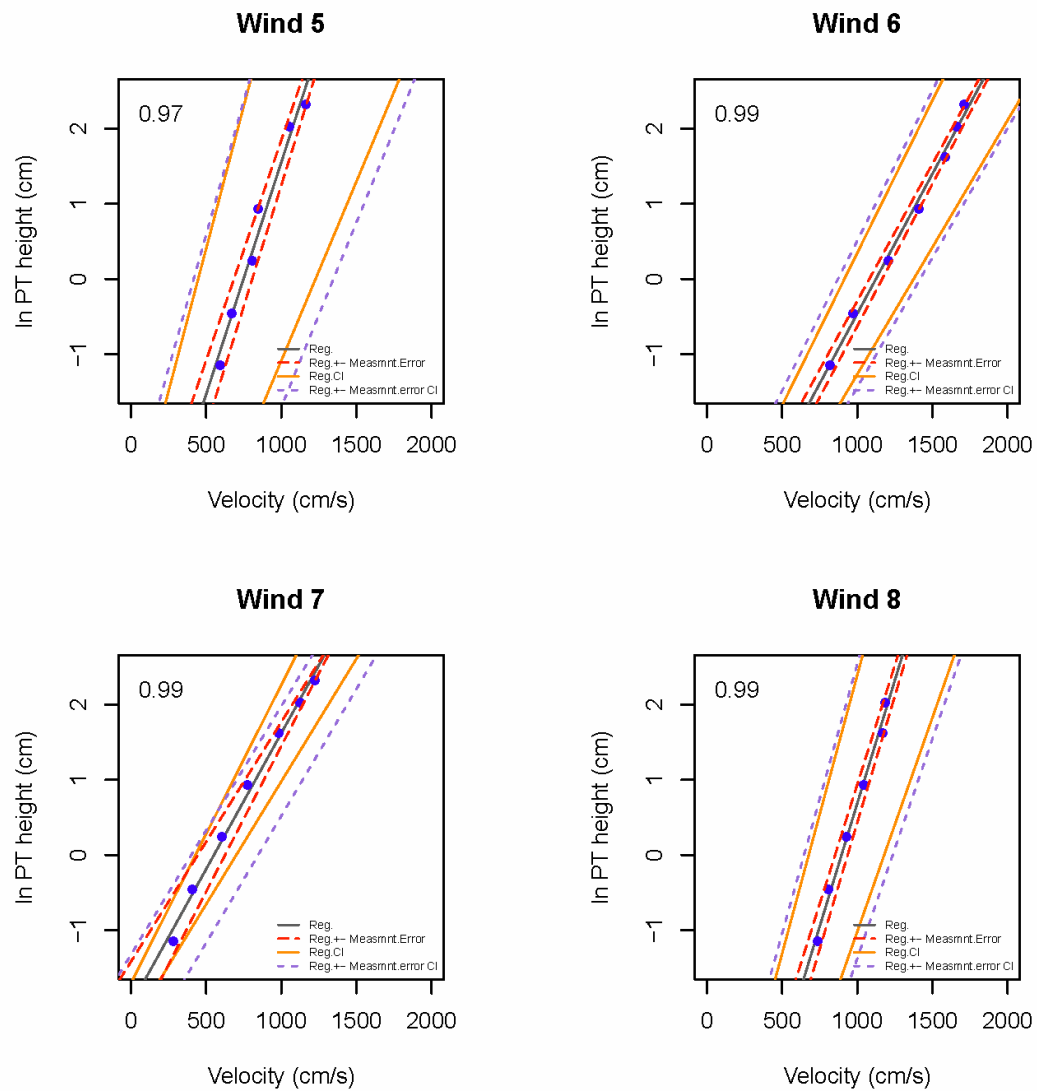


Fig. A-11. Measured wind speed profiles of the disturbed soil surfaces at TFV for sampling sites 5-8. Blue dots represent measured values. Lines represent regressions and estimated error using Equation 4-4. Text in upper left corners are the coefficient of determination (r^2) for each regression.

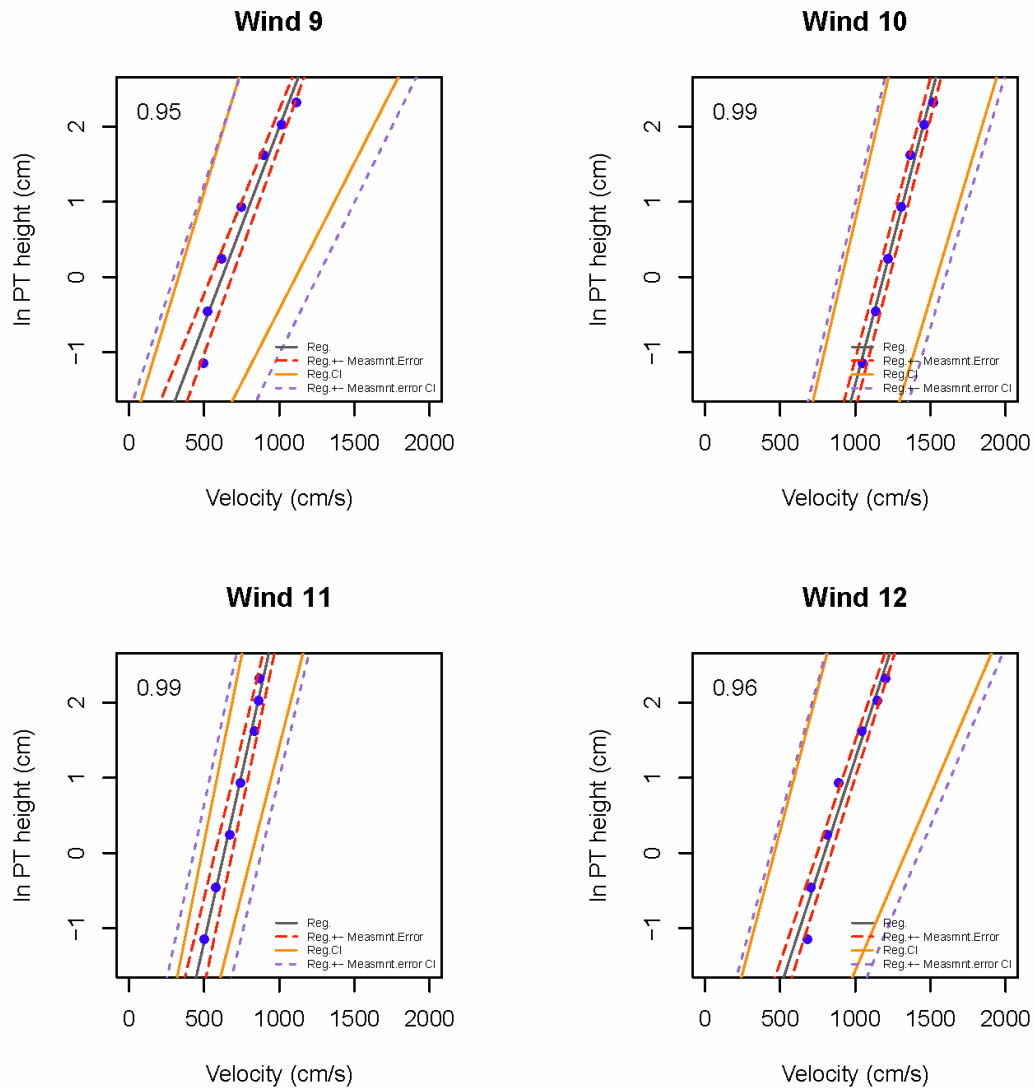


Fig. A-12. Measured wind speed profiles of the disturbed soil surfaces at TFV for sampling sites 9-12. Blue dots represent measured values. Lines represent regressions and estimated error using Equation 4-4. Text in upper left corners are the coefficient of determination (r^2) for each regression.

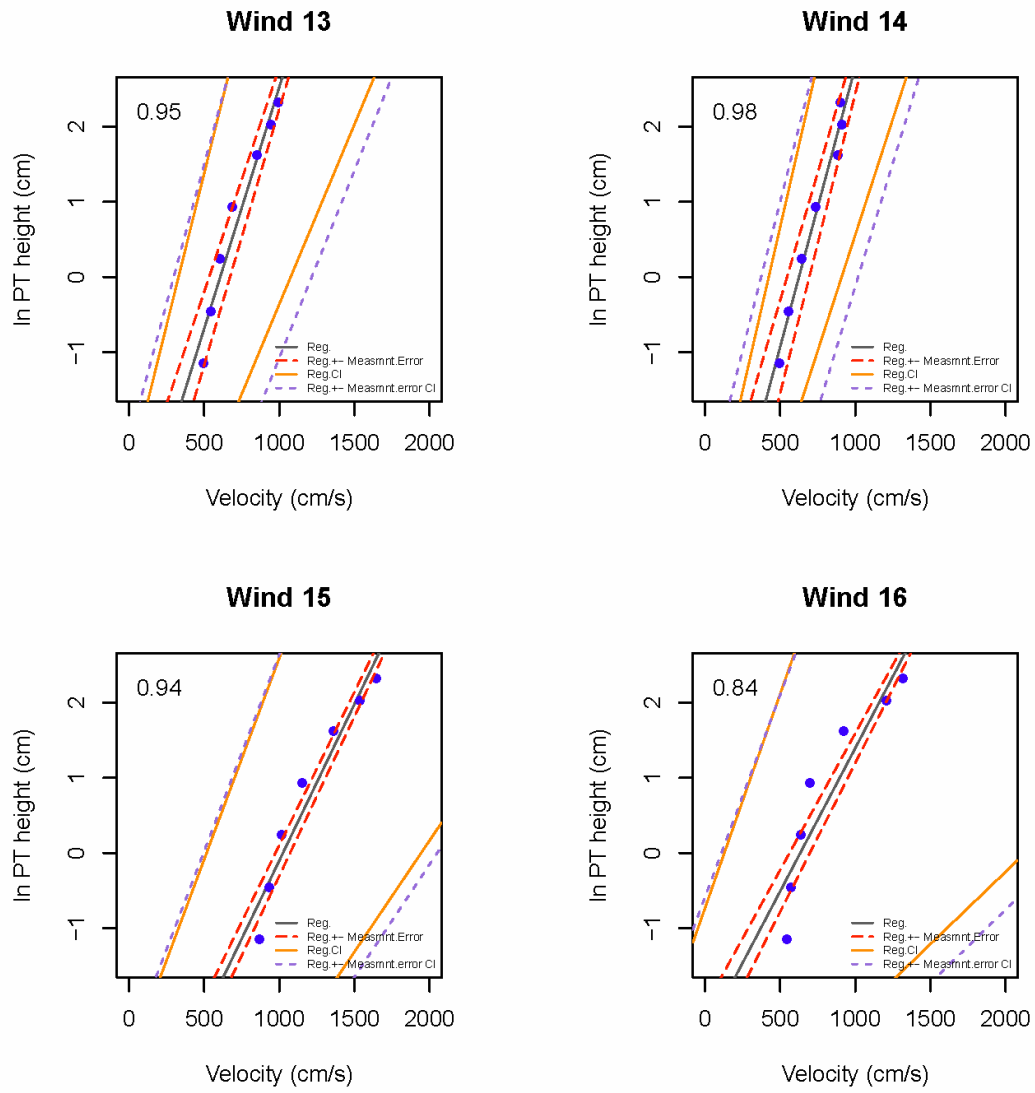


Fig. A-13. Measured wind speed profiles of the disturbed soil surfaces at TFV for sampling sites 13-16. Blue dots represent measured values. Lines represent regressions and estimated error using Equation 4-4. Text in upper left corners are the coefficient of determination (r^2) for each regression.

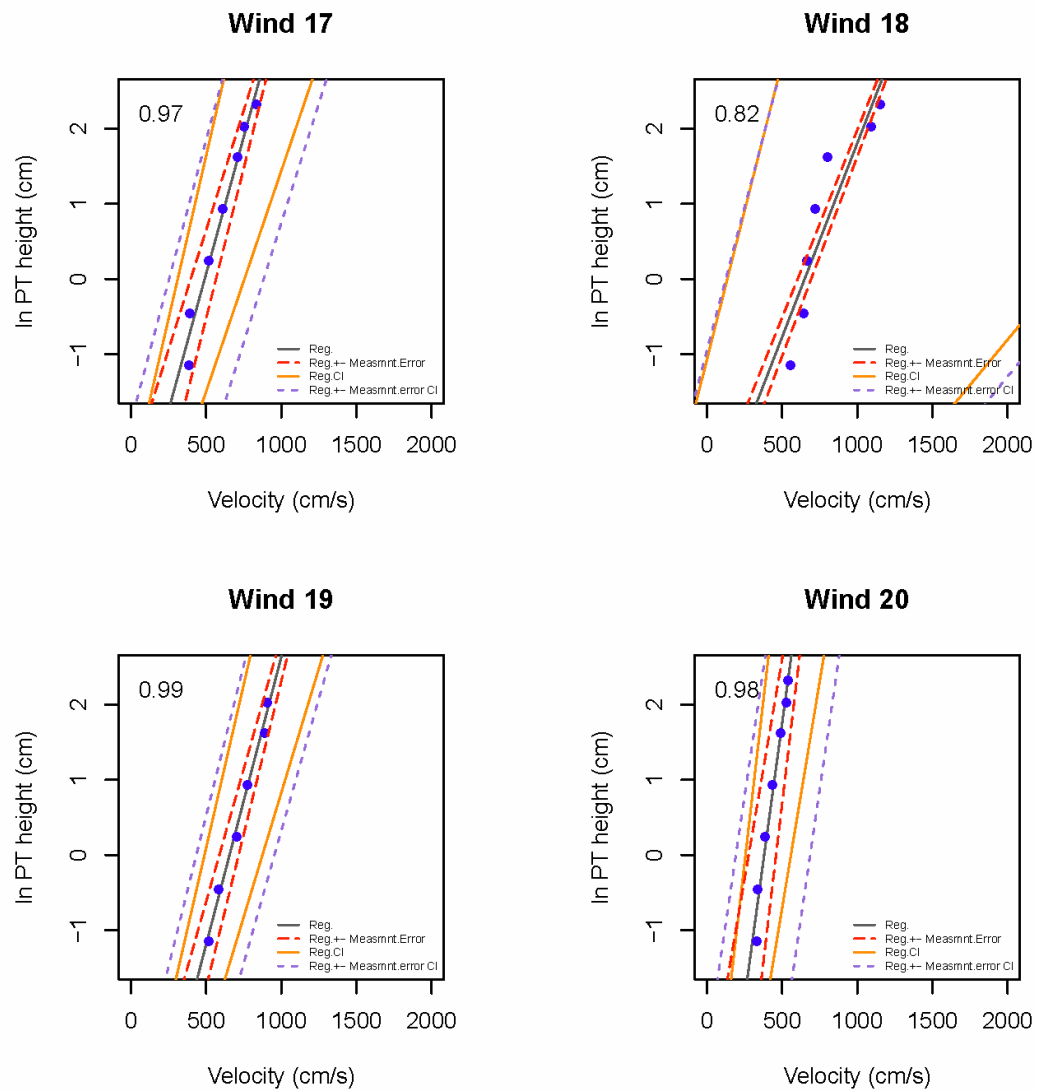


Fig. A-14. Measured wind speed profiles of the disturbed soil surfaces at TFV for sampling sites 17-20. Blue dots represent measured values. Lines represent regressions and estimated error using Equation 4-4. Text in upper left corners are the coefficient of determination (r^2) for each regression.

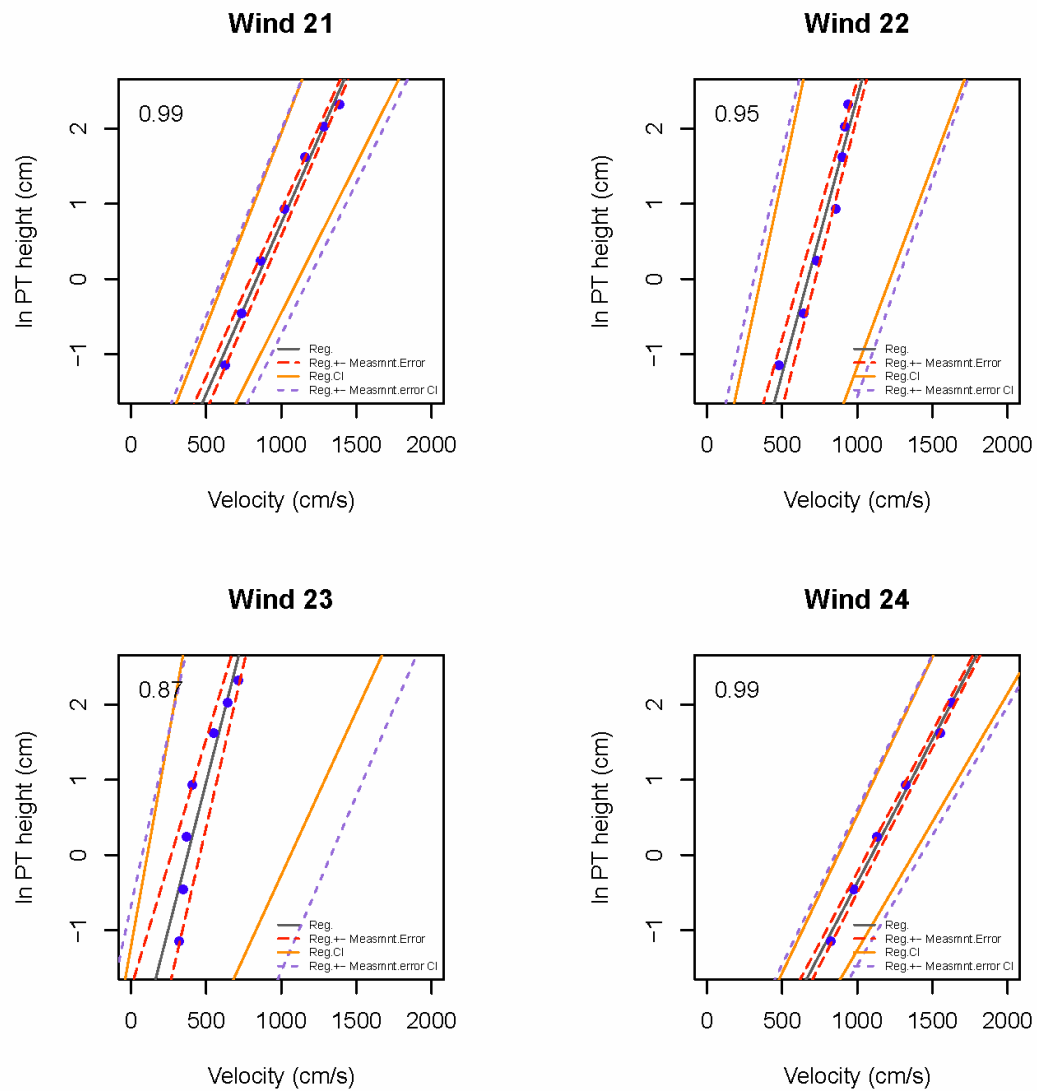


Fig. A-15. Measured wind speed profiles of the disturbed soil surfaces at TFV for sampling sites 21-24. Blue dots represent measured values. Lines represent regressions and estimated error using Equation 4-4. Text in upper left corners are the coefficient of determination (r^2) for each regression.

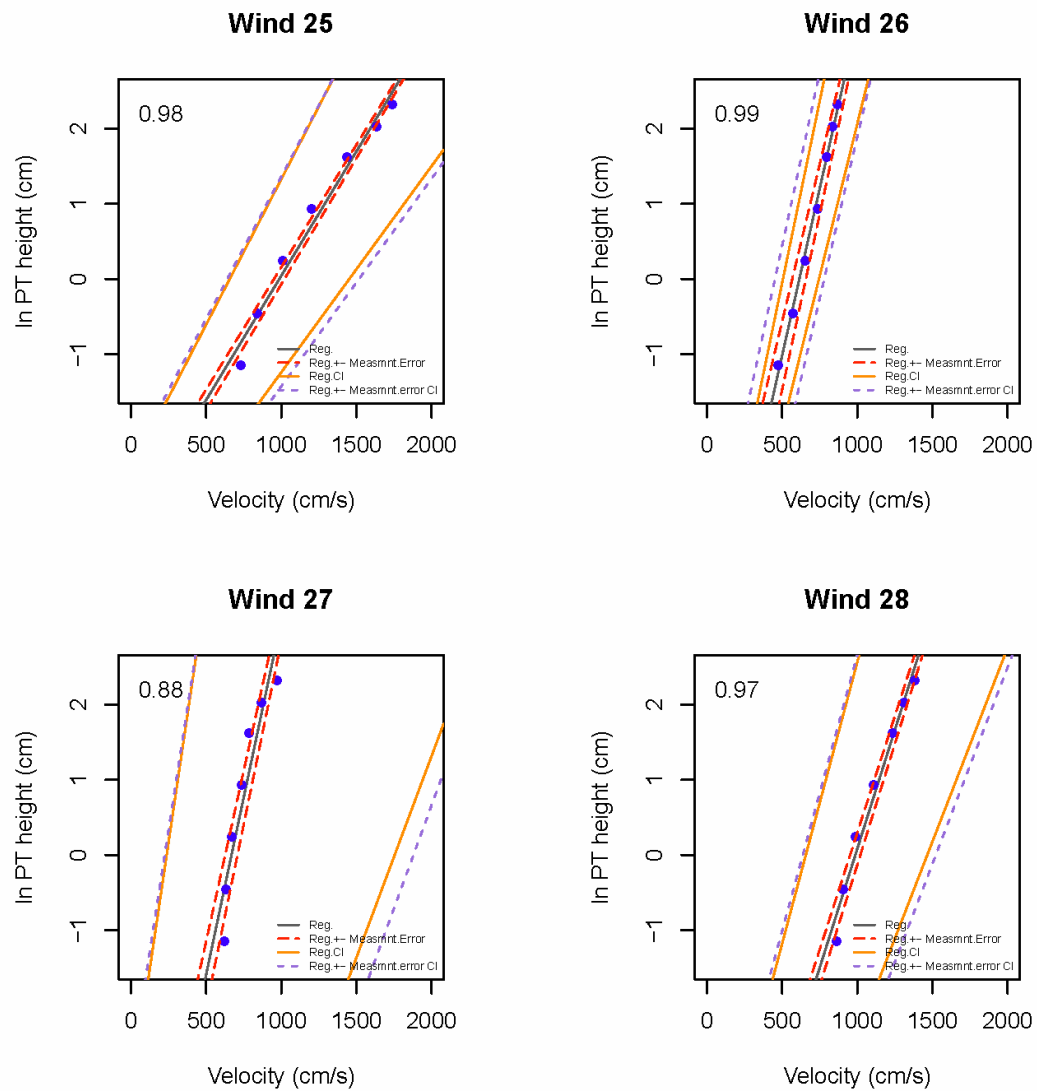


Fig. A-16. Measured wind speed profiles of the disturbed soil surfaces at TFV for sampling sites 25-28. Blue dots represent measured values. Lines represent regressions and estimated error using Equation 4-4. Text in upper left corners are the coefficient of determination (r^2) for each regression.

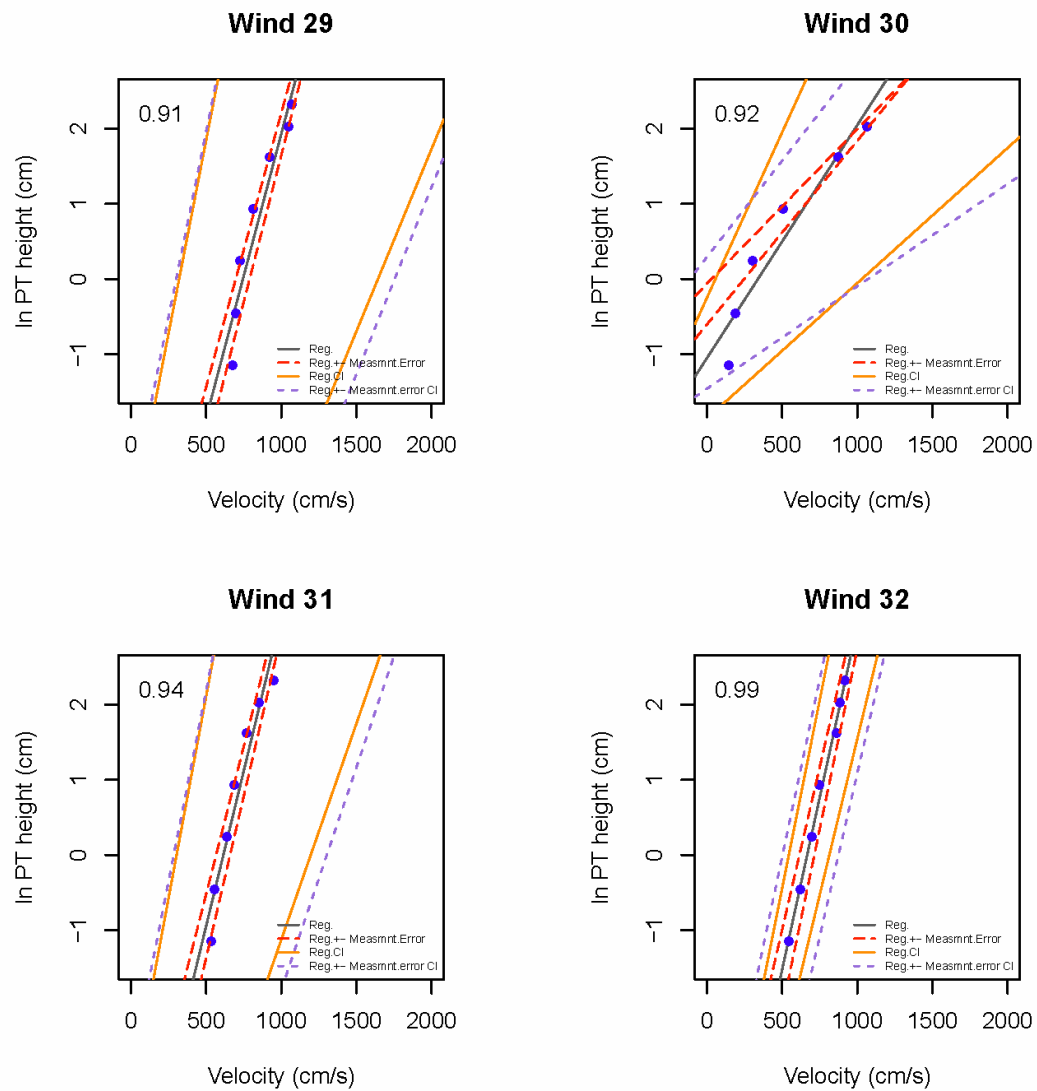


Fig. A-17. Measured wind speed profiles of the disturbed soil surfaces at TFV for sampling sites 29-32. Blue dots represent measured values. Lines represent regressions and estimated error using Equation 4-4. Text in upper left corners are the coefficient of determination (r^2) for each regression.

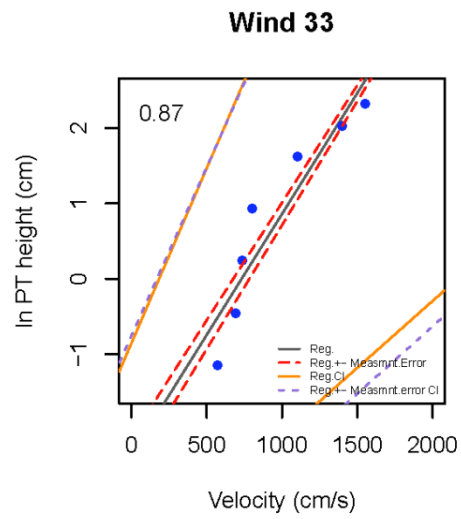


Fig. A-18. The measured wind speed profile of the disturbed soil surface at TFV for sampling site 33. Blue dots represent measured values. Lines represent regressions and estimated error using Equation 4-4. Text in upper left corners are the coefficient of determination (r^2) for each regression.

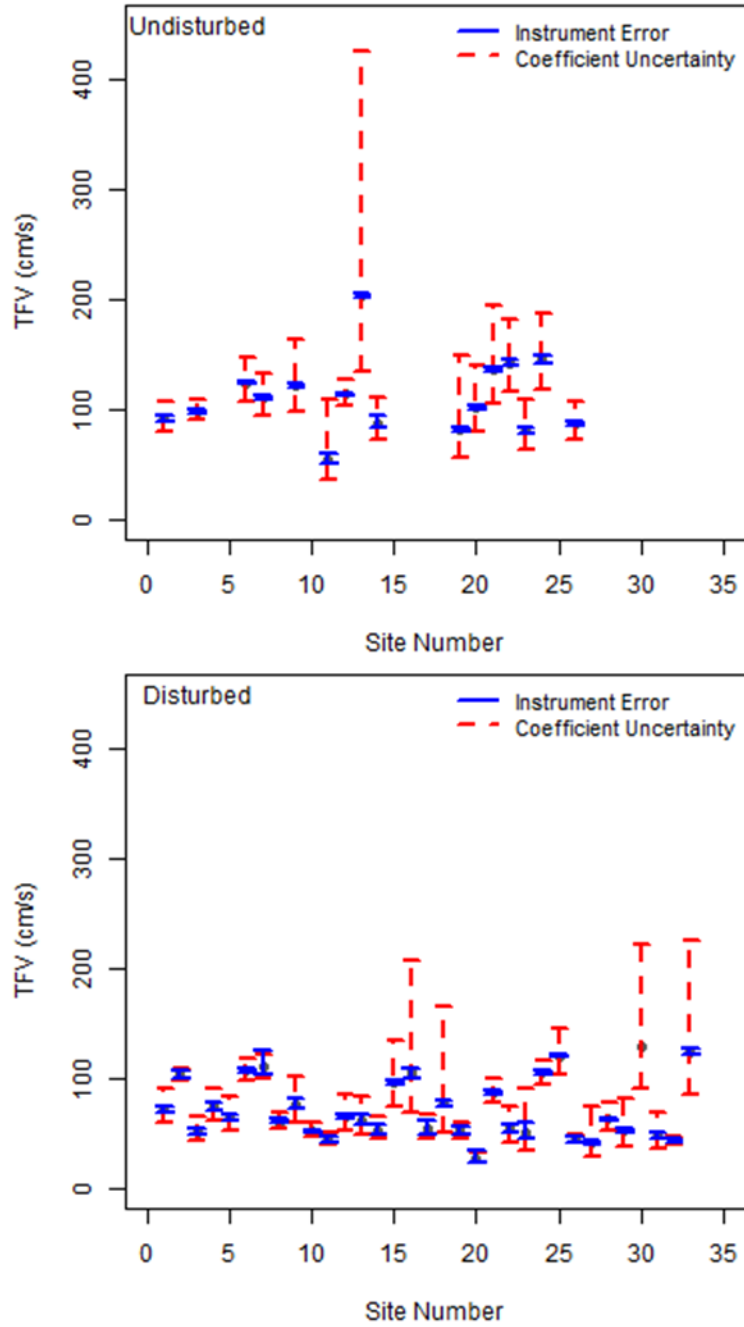


Fig. A-19. Sources of uncertainty in TFV measurement for undisturbed and disturbed soils. Only undisturbed sites that reached TFV are shown in the upper figure.

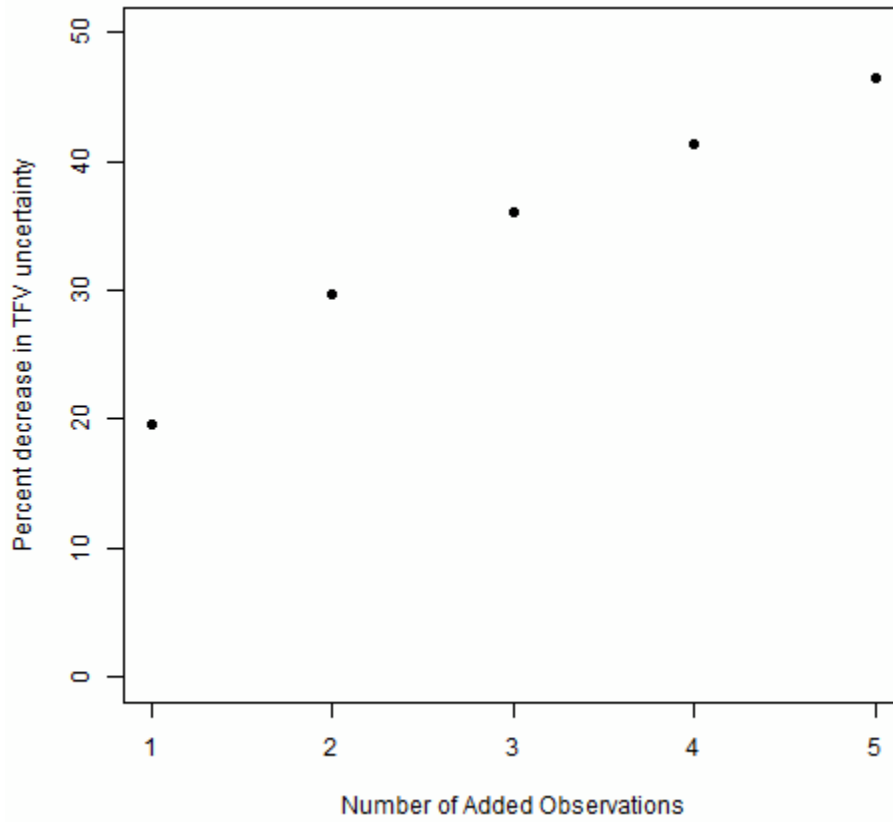


Fig. A-20. Percent decrease in TFV uncertainty with added simulated observations.

APPENDIX B. PERMISSION AND RELEASE LETTERS

5th July 5, 2014

Michael C. Duniway
2282 2290 S W Resource Blvd
Moab, UT 84532
mduniway@usgs.gov
435-719-2330

Dear Michael:

I am in the process of preparing my dissertation in the Departments of Plants, Soils and Climate, at Utah State University. I hope to complete in the summer of 2014.

I am requesting your permission to include in my dissertation the manuscript "Machine learning for predicting soil classes in three semi-arid landscapes", that you coauthored.

Please indicate your consent to this request by signing in the space provided. If you have any questions, please call me at the number below. I hope you will be able to reply immediately.

Thank you for your cooperation,
Colby Brungard



4820 Old Main Hill
Logan, UT. 84321
435-797-3404 c.w.b@aggiemail.usu.edu

I hereby give permission to Colby Brungard to reprint the manuscript "Machine learning for predicting soil classes in three semi-arid landscapes", that I coauthored in his dissertation.

Signed



5th July 5, 2014

Skye A. Wills
National Soil Survey Center
100 Centennial Mall North
Lincoln, NE 68508
Skye.wills@lin.usda.gov
402-437-5310

Dear Skye:

I am in the process of preparing my dissertation in the Departments of Plants, Soils and Climate, at Utah State University. I hope to complete in the summer of 2014.

I am requesting your permission to include in my dissertation the manuscript "Machine learning for predicting soil classes in three semi-arid landscapes", that you coauthored.

Please indicate your consent to this request by signing in the space provided. If you have any questions, please call me at the number below. I hope you will be able to reply immediately.

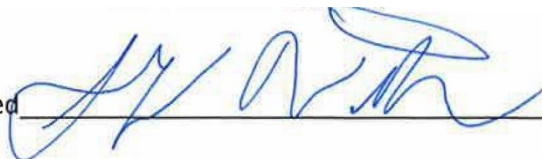
Thank you for your cooperation,
Colby Brungard



4820 Old Main Hill
Logan, UT. 84321
435-797-3404 c.w.b@aggiemail.usu.edu

I hereby give permission to Colby Brungard to reprint the manuscript "Machine learning for predicting soil classes in three semi-arid landscapes", that I coauthored in his dissertation.

Signed _____



CURRICULUM VITAE

Colby W. Brungard

| | | |
|---------------------------------|--|---|
| CONTACT INFORMATION | Utah State University Department of Plants, Soils, and Climate 4820 Old Main Hill Logan, UT 84322-4820 USA | <i>Work:</i> (435) 797-3404 <i>Home:</i> (435) 752-4185 c.w.b@aggiemail.usu.edu |
| EDUCATION | Utah State University, Ph.D, Soil Science, (Expected Graduation: July 2014) <ul style="list-style-type: none"> • Dissertation Title: Advancing Digital Soil Mapping and Assessment in Arid Landscapes • Advisor: Dr. Janis L. Boettinger • Area of Study: Digital Soil Mapping M.S., Soil Science, October, 2009 <ul style="list-style-type: none"> • Thesis Title: Alternative Sampling and Analysis Methods for Digital Soil Mapping in Arid Rangelands of Southwestern Utah, USA. • Advisor: Dr. Janis L. Boettinger • Area of Study: Pedology, Taxonomy and Digital Soil Mapping B.S., Physical Geography, December 2006 <ul style="list-style-type: none"> • <i>Valedictorian, College of Natural Resources</i> • <i>Magna cum Laude</i> | Logan, Utah, USA |
| OTHER ACADEMIC EXPERIENCE | Undergraduate Student Utah State University, Logan, Utah USA <ul style="list-style-type: none"> • Full complement of earth science classes. • Development of essential mapping skills including GIS, remote sensing, photo interpretation, projections, coordinates, cartography and databases. • International development and international comparative politics classes. | Jun 2001 Dec 2007 |
| PUBLICATIONS | Brungard, C.W., Boettinger, J.L., Duniway, M.C., Wills, S.A., Edwards Jr., T.C. Machine learning for predicting soil classes in three arid landscapes. <i>Geoderma</i> , 2014 (GEODER9018, submitted). Pahlavan Rad, M.R., Toomanian, N., Khormali, F., Brungard, C.W., Komaki, C.B., Bogaert, P., 2014. Updating soil survey maps using random forest and conditioned Latin hypercube sampling in the loess derived soils of northern Iran. <i>Geoderma</i> , 232–234, pp.97–106. | |

Brungard, C.W., Boettinger, J.L., 2012. Spatial prediction of biological soil crust classes; value added DSM from soil survey, in: Minasny, B., Malone, B.P., McBratney, A. (Eds.), *Digital Soil Assessments and Beyond: Proceedings of the 5th Global Workshop on Digital Soil Mapping*. CRC Press, Sydney Australia, pp. 57-60.

Brungard, C.W., Boettinger, J.L., 2010. Application of Conditioned Latin Hypercube Sampling for Digital Soil Mapping of Arid Rangelands in Utah, USA, in: Boettinger, J.L., Howell, D.W., Moore, A.C., Hartemink, A.E., Kienast-Brown, S. (Eds.), *Digital Soil Mapping: Bridging Research, Production, and Environmental Application, and Operation*. Springer, Dordrecht, pp. 67-78.

(In-preparation) Brungard, C.W., Boettinger, J.L., What soil properties control threshold friction velocity in the Great Basin, USA? For submission to *Aeolian Research*.

(In-preparation) Brungard, C.W., Boettinger, J.L., Modeling biological soil crust classes at macro- and meso- scales. For submission to *Journal of Arid Environments*.

PROFESSIONAL
EXPERIENCE

Graduate Research Assistant

Dept. of Plants, Soils and Climate, Utah State University Jan 2007–present

Digital Soil Mapping

- Compared 20 machine learning models using three different covariate sets for predicting soil taxonomic classes at three geographically distinct locations in the semi-arid western United States of America
- Modeled soil attributes, biological soil crust classes and ecological site classes from recent soil survey data for 1365 km².
- Modeled biological soil crust potential over 8275 km²
- Modeled soil taxonomy subgroup classes and estimated uncertainty for an unmapped 280 km² area with complex geology and terrain.
- Currently modeling soil properties to understand the factors controlling vegetation distribution over 210 km².
- Developed environmental covariate data from remote sensing and digital elevation models.
- Applied conditioned latin hypercube sampling for field sampling site identification and estimated optimal sample size for an area of complex environmental covariates.
- Described and classified approximately 380 pedons.
- Coordinated and directed 7 field assistants throughout two field seasons.

Remote Sensing

- Acquired, pre-processed, analyzed and used remotely sensed imagery (Landsat 5, Landsat 7, Landsat 8) to develop environmental covariates for 5 different digital soil mapping studies.

- Familiar with atmospheric correction for Landsat imagery.
- Tested WorldView-2 imagery for predicting soil carbon in a wetland ecosystem.

Soil Map Update and Refinement

- Currently classifying pedons based on laboratory analysis to refine an existing soil survey for 770km².
- Currently preparing to use geostatistical analysis to understand the spatial distribution of surface soil properties.
- Currently assessing soil properties for modeling wind erosion.
- Preparing to use VNIR spectrometry to predict carbon in ~400 soil samples

Laboratory Analysis

- Developed standard laboratory operating procedures and supervised 7 research technicians for performing physical and chemical lab tests of ~1000 soil samples. Tests included total, inorganic and organic C, total N, available P, exchangeable cations, electrical conductivity, pH, texture and VNIR scans.

Cooperative Soil Survey

- Trained land managers in field soil description methods and practices.
- Trained 3 geologists in wetland field soil description methods and practices.
- Coordinated mapping progress and accuracy with soil survey staff, land managers and researchers.

Instructor

Dept. of Plants, Soils and Climate, Utah State University Sept 2007–Dec 2007
Soil Genesis, Morphology and Classification (Soils 5130)

- Lectured 3 hours/week on soil formation theory, morphology, some biogeochemical soil properties, major soil orders, and classification.
- Led weekly outdoor field lab in soil description and classification.
- Revised, created and graded exams and lab assignments.

Graduate Teaching Assistant

Dept. of Plants, Soils and Climate, Utah State University
Soil Genesis, Morphology and Classification (Soils 5130) Sept 2012–Dec 2012

- Prepared field kits and assisted with weekly outdoor field lab in soil description and classification.

Soils, Water and the Environment (Soils 2000) Sept 2008–Dec 2008

- Assisted with introductory undergraduate soils class.
- Proctored exams, delivered occasional lecture and graded assignments.

Undergraduate Research Assistant

Dept. of Plants, Soils and Climate, Utah State University Nov 2005–Jan 2007
Soil Genesis Lab

- Assisted graduate student with excavation, field description and classification of approximately 200 pedons.

GIS Technician

USDI Bureau of Land Management, Shoshone, Idaho USA Jun 2005–Aug 2005

- Developed procedures for creation and maintenance of cave inventory spatial database.
- Developed and maintained Off-Highway-Vehicle trail spatial database.
- Professionally assisted staff of 30 with map creation and data management.

Assistant Manager

Geospatial Teaching Lab, Utah State University Nov 2004–Feb 2005

- Assisted students with data management and general GIS instruction.
- Assisted with site licensing for GIS and Remote Sensing software.

PROFESSIONAL PRESENTATIONS

Invited Presentations

Brungard C.W. and J.L. Boettinger. 2010. "Digital Soil Mapping of Soil Attribute and Taxonomic Classes with Random Forests in Arid Rangelands, Utah, USA." National Soil Survey Center, 20-22 July, 2010, Lincoln, Nebraska.

Volunteered Presentations

Brungard, C.W., Boettinger, J.L., Edwards, T.C. 2013. "The limitations of data mining for digital soil mapping: implications for soil survey programs". Pedometrics 2013, 28-30 August, 2013. Nairobi, Kenya.

Brungard, C.W. 2012. "Spatial Prediction of Ecological Site and Biological Soil Crust Classes in Canyonlands National Park." Society for Range Management Workshop on Ecological Site Description and State-and-Transition Model Development, 28 January, Spokane, Washington.

Brungard, C.W. and J.L. Boettinger. 2011. "Spatial Prediction of Potential Biological Soil Crust Classes in and Around Canyonlands National Park: Implications for Management." 11th Biennial Conference of Research on the Colorado Plateau, 24-27 October, Flagstaff, Arizona.

Brungard, C.W. and J.L. Boettinger. 2011. "Spatial Prediction of Ecological Site and Biological Soil Crust Classes in Canyonlands National Park." Soil Science Society of America International Annual Meeting, 16-19 October, 2011, San Antonio, Texas.

Brungard, C.W. 2011. "Spatial Prediction of Soil Carbon Using WorldView-2 Imagery and Elevation Data for a Desert Wetland Ecosystem, Utah, USA." Soil Science Society of America International Annual Meeting, 16-19 October, 2011, San Antonio, Texas.

Brungard, C.W. and J.L. Boettinger. 2011. "Predicting Biological Soil Crust

and Ecological Site Classes Using Polygon, Topographic, and Spectral Data. National Cooperative Soil Survey Conference, 22-26 May, 2011, Asheville, North Carolina.

Brungard, C.W. 2011. "Spatial Prediction of Soil Carbon in a Desert Wetland using WorldView-2 and LiDAR." 2011 Intermountain Graduate Student Symposium, 30 March - 1 April, 2011, Logan, Utah.

Brungard, C.W. and J.L. Boettinger. 2010. "Predicting Soil Attribute and Taxonomic Classes Using Random Forests in Arid Rangelands, Utah, USA." 4th Global Workshop on Digital Soil Mapping, 24-26 May, 2010, Rome, Italy.

Brungard, C.W. 2010. "Digital Soil Mapping for Soil Survey." 2010 Intermountain Graduate Student Symposium, 26 March, 2010, Logan, Utah.

Brungard, C.W. and J.L. Boettinger. 2009. "From Pedon to Prediction: Innovative Methods for Predicting Soil Distribution on the Landscape." Soil Science Society of America International Annual Meeting, 1-5 November, 2009, Pittsburgh, Pennsylvania.

Brungard, C.W. 2009. "Conditioned Latin Hypercube Sampling (cLHS); A Digital Soil Mapping Example." 27 March, 2009 Intermountain Graduate Student Symposium, 2009, Logan, Utah.

Brungard, C.W. and J.L. Boettinger. 2008. "Application of Conditioned Latin Hypercube Sampling for Digital Soil Mapping of Arid Rangelands in Utah, USA." 3rd Global Workshop on Digital Soil Mapping, 30 September - 3 October 2008, Utah State University, Logan, Utah.

Brungard C.W. and J.L. Boettinger. 2008. "Conditioned Latin Hypercube Sampling (cLHS): A digital soil mapping example." NRCS Western States Remote Sensing Workshop, 30 April - 1 May, 2008, Phoenix, Arizona.

EXTERNAL
FUNDING

2012-2014 Co-PI. USDA Natural Resources Conservation Service. Digital soil mapping of soil properties and historical aerial photo analysis as tools for developing and testing ecological site concepts \$39,426.

2010-2011 USDA Natural Resources Conservation Service, National Soil Survey Center. Loan of \$50,000 VNIR Spectrometer.

2010 PI. DigitalGlobe: 8-Band Research Challenge. 106 km² Worldview-2 satellite image.

AWARDS

Utah State University

Logan, Utah, USA

- 2011 Graduate Researcher of the Year. College of Agriculture. Utah State University
- 2010 First place, Dept. of Plants, Soils and Climate, 13th Intermountain Graduate Research Symposium
- 2009 Utah State University Graduate Student Senate Stipend Enhancement Award
- 2009 Academic merit tuition waiver
- 2008 First place, College of Agriculture, 11th Intermountain Graduate Research Symposium
- 2008 Academic merit tuition waiver
- 2006 Selected to deliver Commencement address, Utah State University Winter Commencement
- 2006 Fall Valedictorian, College of Natural Resources, Utah State University
- 2006 Inducted into Phi Kappa Phi honor society
- 2006 Outstanding senior, College of Natural Resources, Utah State University
- 2006 Geospatial information and technology (GITA) scholarship
- 2006 Geography faculty scholarship for academic excellence
- 2006 Environment and Society faculty scholarship
- 2005 Alsop Athenaeum Award

Boy Scouts of America Longmont, Colorado USA
 • Eagle Scout (1998)

SERVICE

Professional Service

- Member of Utah Organizing Committee, 3rd Global Workshop on Digital Soil Mapping, Sept. 30–Oct. 3, 2008, Logan, Utah.

**TECHNICAL
KNOWLEDGE
AND SKILLS**

Mapping software: ArcGIS 9.1 – 10.0, ERDAS Imagine 9.2 – 11.0
 Open Source GIS: GRASS 6.0.1, QGIS 1.6.0, SAGA 2.0.8, Introductory python programming knowledge.
 Statistical Analysis Software: R (highly proficient)
 Applications: Microsoft Office, and other common productivity packages for Windows, L^AT_EX.

**INTERNATIONAL
EXPERIENCE**

David M. Kennedy Center for International Studies
 Manila, Philippines

Employment Services Intern Jan 2002–Apr 2002

- Instructor for bi-weekly career development class.
- Studied informal market economy.
- Traveled extensively throughout Philippines, lived with native Filipinos.

The Church of Jesus Christ of Latter day Saints
Naga City, Philippines

Missionary

Dec 1998–Dec 2000

- Lived and worked among rural Filipino population.
- Developed cross-cultural communication skills.
- Supervised groups of 5, 15, and 200 missionaries.

RESEARCH
INTERESTS

Pedology, Geomorphology and Landscape Evolution

Sampling strategies for Digital Soil Mapping

Statistical, Geostatistical and Data Mining methods for Digital Soil Mapping, Modeling and Assessment.

Sustainable International Agricultural Development

Field collection of soil data